Total Dissolved Gas Generation at Hugh L. Keenleyside Dam, B.C., Canada

by

Graeme James Billay

A thesis submitted in partial fulfillment of the requirements for the degree of

Master of Science

in

Water Resources Engineering

Department of Civil and Environmental Engineering
University of Alberta

Abstract

Total dissolved gases generated downstream of hydropower dams pose an environmental risk to fish species. The objective of this study was to understand total dissolved gas generation mechanisms at Hugh L. Keenleyside Dam along the Columbia River near Castlegar, BC. This was in an effort to produce a predictive model for dam operations. Two types of spill structures were studied, spillways, and low-level outlets. Several predictive models from the literature were modified and tested for the structures at the dam to better understand their wider applicability and to bring insight into this dam's unique ability to dissolve gas. It was found that the southern set of low-level outlets can generate a significant amount of total dissolved gas relative to the northern set of low-level outlets, primarily as a result of greater turbulence in the stilling basin, and as a result, a higher gas-transfer rate. In 2016, for similar flow rates, the operation of three south low-level outlets generated 124% total dissolved gas supersaturation versus 112% total dissolved gas supersaturation generated by three northern low-level outlets. The spillway stilling basins at Hugh L. Keenleyside Dam are very unique relative to most other basins found in the literature, as a result, many models also found in the literature failed to adequately present acceptable total dissolved gas predictions. This was remedied in part by separately considering the stilling basin region's and river region's contribution to total dissolved gas generation. Of the models tested for the spillway dataset, only one achieved a root-mean-square-error within instrument uncertainty, the error was 1.5%. The best results were found using a similar approach for the low-level outlets, where the lowest root-mean-square-error was 1.14%. The

dynamic nature of the flow within the stilling basin regions of the dam and difference in flow patterns in the downstream river region underscores the importance of numerical modelling and the challenges simpler analytical models have at predicting total dissolved gas generation.

Acknowledgements

I would like to thank my supervisor, Dr. David Zhu for his guidance and encouragement to complete this work and to always keep testing assumptions to better enforce understanding of the topic.

Thanks to Rajib Kamal and Pengcheng Li, my research partners, for their effort in helping prepare for field trips and with executing the collection of field measurements, preparing BC Hydro reports, and general discussion that greatly aided the completion of this work.

Thank you to Alf Leake, James Crossman, and others at BC Hydro for facilitating field work operations and for lending us their equipment.

Thank you to James Bruce at Creekside Aquatic Sciencs Ltd. for his help during the field work.

The author would also like to acknowledge Perry Fedun for helping myself and the research team prepare for field work and particularly for building the floating platforms from which a lot of measurements were taken.

A very special thank you to my mother and father for their unending confidence and encouragement throughout my program.

Table of Contents

List of Tables

List of Figures

List of Symbols

a	Specific area
A	Area available for gas-transfer
A_b	Surface area of a bubble
A_i	Conversion constant for dissolved gas concentration
C	Concentration
$\Delta C,_B$	Change in concentration in the stilling basin
C_d	Concentration of dissolved gas
C_i	Concentration of ith dissolved gas
$C_{o,i}$	Saturation concentration of ith gas at standard temperature pressure
C_s	Saturation concentration
C_{se}	Effective saturation concentration
C_u	Upstream concentration
dP_{TW}	Difference between forebay TDG pressure and barometric pressure
dP_{TW}	Difference between tailwater TDG pressure and barometric pressure
d_b	Bubble diameter
d_{eff}	Effective depth
d_g	Gate opening height
d_j	Depth of the water jet
d_{TW}	Depth of water jet at tailwater surface
D	Diffusivity of air in water
E	Energy loss rate
F	Flux rate per unit surface area
FB_{elev}	Forebay elevation
F_r	Froude number
$F_{r,G}$	Foude number calculated at low-level outlet gate in Bruce (2016)
$F_{r,TW}$	Froude number at the tailwater surface
F_t	Turbulent Froude number

g	Acceleration due to gravity
h	Depth over which gas-transfer takes place
h_{c1}	Bubble centroid of basin region (Geldert et al, 1998)
h_{c2}	Bubble centroid of river region (Geldert et al, 1998)
h_e	Height of end sill
H	Henry's law constant
ΔH	Differential head (forebay elevation minus tailwater elevation)
H_g	Head above the center of the gate opening
H_s	Hydraulic head immediately upstream of gate sill
H_0	Total head loss (forebay elevation minus stilling basin floor)
k	Turbulent kinetic energy per unit mass
K	Bulk transfer coefficient
K_e	Bubble entrainment coefficient
K_g	Gas-film coefficient
K_L	Liquid-film coefficient
K'	Constant of proportionality
$K_L a t_b$	Bubble mass-transfer over time
$K_L a t_{b,B}$	Bubble mass-transfer over time in the stilling basin
$K_L a t_s$	Surface mass-transfer over time
$K_L a t_{s,R}$	Surface mass-transfer over time in the river
K_{20}	Temperature corrected mass-transfer coefficient
l	Constant
L	Length
L_r	Representative scale of turbulent eddies
m	Constant
n	Constant
P_{atm}	Barometric pressure
P_{avg}	Average hydrostatic pressure in the stilling basin
P_d	Total gas pressure
P_i^l	Partial pressure of the ith gas in the liquid phase
P_t	Total pressure

P_{wv}	Water vapour pressure
q_a	Specific air flow rate
q_w	Specific water flow rate
Q_a	Air flow rate
Q_w	Water flow rate
Q_s	Spillway discharge
R	Reynold's number
R_r	Reynold's rise velocity
S_c	Schmidt number
t	Time
t_b	Time of gas-transfer between the bubble and water
t_s	Time of gas-transfer between water and the atmosphere
T	Temperature
TW_{elev}	Tailwater elevation
v_{avg}	Average velocity in the stilling basin
v_b	Rise velocity of a bubble
v_e	Water velocity at end sill
v_j	Velocity of the water jet
v_R	Velocity in the river region
v_{TW}	Velocity of jet at tailwater surface
V	Control volume
V_b	Volume of a bubble
W	Width
W_e	Weber number
$X_{1/2}$	Bubble half-life
y_e	Water depth over end sill
y_e'	Water depth over end sill (using approximate end sill height of 13m)
y_p	Bubble penetration depth
y_t	Tailwater depth
α	Mass-transfer coefficient

α_0	Specific gravity of the roller
α_1	Angle of outer jet spread
β	Fraction of y_p that is the distance from the water surface to the centroid of a bubble swarm, or correction factor between effective depths in Geldert et al, 1998.
β_i	Bunsen coefficient of the ith gas
β'	Conversion factor from pressure to concentration
β_{1-4}	Constant
Δ	Differential pressure factor
λ	Air layer thickness
η	Coefficient
ϕ	Air-void fraction
θ	Slope
ρ_w	Density of water
σ	Surface tension of water
ν	Kinematic viscosity
χ_i	Gas fraction of the ith gas
γ	Unit weight of water

Chapter 1: Introduction

1.1 Total Dissolved Gases

Surrounding the design and construction of dams and hydropower facilities are a multitude of environmental concerns. However, one such environmental impact is not widely considered during the design of dams; this is the issue of total dissolved gases (TDG). Total dissolved gases are the amount of air that is residing within the river or another water body. Aquatic species like fish require the dissolved oxygen (one component of the gases dissolved) to survive. Typically, this gas is dissolved through the surface of the water from the atmosphere, but with the construction of dams or other hydraulic structures, facility spill operations may increase the level of dissolved gases within the downstream river by creating a large amount of turbulent mixing at the bottom of their spillways or other outlet structures. What this does is introduce a significant number of bubbles into the water that can be dragged down deep into the stilling basins, increasing the potential for dissolved gas generation to occur. In some cases, an increase in dissolved gases may also increase the overall quality of the water. Unfortunately, in most hydropower cases the high flows that spill over the dams create such a turbulent condition that a significant amount of dissolved gas is generated. This type of condition can actually lead to very adverse impacts on the fish living downstream, in some cases, causing mortality. This issue is difficult to address in dams already in operation, but efforts have been made to propose structural and operational changes to the facilities in an effort to reduce the risk of high dissolved gas generation.

Total dissolved gas is generated at hydropower facilities primarily by the entrainment of air in the form of bubbles that are plunged deep into the stilling basins. Under the hydrostatic pressure of the stilling basin, the gases within these bubbles are forced into solution. Since most water bodies are already saturated with air, this increase in dissolved gas leads to a "supersaturated" condition. The severity of supersaturation is of particular interest with regard to fish mortality. To prevent this the Canadian Council of Ministers of the Environment (1999) suggests a limit

of 110% supersaturation. This relative value is typically comparing the sum of the partial pressures of all gases dissolved within the water body to the local atmospheric pressure and follows similar guidelines found in the United States. A supersaturated condition of 110% would indicate the dissolved gases in the water have a total measured pressure of 110% that of the barometric pressure, or that the concentration of dissolved gas is 110% that of the saturation concentration of the local atmosphere.

High levels of dissolved gas in the water can cause gas bubble trauma (GBT) in fish. Gas bubble trauma occurs when the dissolved gases come out of solution to form bubbles. These bubbles may form in a fish beneath the skin, tails, fins, and eyes (Weitkamp and Katz, 1980). This puts the fish in a critical condition that can lead to mortality. Limiting this threat to aquatic environments downstream of hydropower dams is of great ecological importance and illustrates the need for the current study.

Since there are many factors specific to each structure or facility that influence the generation of dissolved gas, determining a predictive equation that applies to all dams has been challenging. However, there have been models developed to predict downstream dissolved gas for several lower Columbia River dams in the United States (University of Washington, 2000). These models rely on coefficients determined for each of the dams the model is to be applied to, and in many cases, this requires a huge amount of effort in the way of field observations. Studies conducted by the United States Army Corps of Engineers have looked into various solutions to the problem of increased dissolved gas levels with some success via the construction of spillway flow deflectors (USACE, 1996). However, the most significant decrease in dissolved gas generation occurred by changing the operational procedures of the dam. Most of this work has been focused primarily on dam spillways. Very little has been done on low-level outlets or closed conduits and the research that has been applied produced no decent results (Gulliver et al., 1998). Bruce (2016) has developed a regression-based model to predict dissolved

gas generation at Hugh L. Keenleyside Dam (HLK), however, it does not necessarily add to the academic understanding of the hydraulic mechanisms that cause this. Since HLK utilizes 6 of 8 low-level outlets on a routine basis it is possible to further the research of dissolved gas generation as a result of using these specific structures.

The Columbia River Basin extends from the headwaters of the British Columbian Rocky Mountains into the United States (see Figure 1 and Figure 2). The basin is of significant ecological and economic concern to both countries, and in an attempt to increase the potential for hydropower electricity generation and flood protection, the Columbia River Treaty was enacted in 1964. This agreement identified three dams on the Canadian side of the border to be designated Treaty Dams and whose outflow must meet the downstream requirements for hydropower generation and flood protection. Hugh L. Keenleyside Dam is one of these Treaty Dams. Since operational parameters at this dam are partly regulated by the treaty, it imposes certain restrictions on adjusting its operations to minimize TDG generation. As a result, identifying the specific conditions under which TDG is most likely to be generated is important in order to develop a plan for optimizing spill operations.

Upstream of HLK dam is the Arrow Lakes Reservoir, Revelstoke Dam, and Mica Dam (which is another Treaty Dam). The discharge of these upstream dams may also play a role in the TDG present in the forebay of HLK dam. The present scope of work includes measurements of TDG within the forebay of HLK dam, the tailwater, and the downstream river.

1.2 Objectives and Scope of the Research

The research objective is to study the hydraulic conditions that are conducive to generating high levels of dissolved gas using the Hugh L. Keenleyside Dam on the Columbia River near Castlegar, British Columbia as a case study. Particular attention will be paid to the low-level outlets since they represent a situation that

has not undergone rigorous study in the literature and currently presents a challenge for reducing TDG at HLK in particular.

The research consists of two components, the first component is the acquisition of past and present TDG data from HLK collected by third parties and by field work conducted by the University of Alberta research team. The second component is the analysis of this data and subsequent model creation for the prediction of TDG and explanation of the present mechanisms of TDG generation at HLK.

Chapter 2 of this thesis discusses the physical mechanisms of TDG generation, one-dimensional models of TDG prediction at hydropower facilities, and previous investigations at Hugh L. Keenleyside Dam. Chapter 3 discusses HLK in particular and the field work that was conducted for the purpose of quantifying the structures ability to generate TDG. Chapters 4 and 5 test models from the literature and illustrate the development of new, modified models to predict and explain TDG generation at the dam. Conclusions drawn from this work are presented in Chapter 6 with a brief discussion on the limitations of the current work and the potential next steps that could be taken in this field.

Ultimately, it is hoped that a more adequate and quantitative explanation of the TDG generation mechanisms can be summarized for structures at Hugh L. Keenleyside Dam (particularly for the low-level outlets) and may aid in the future operations of these structures.

Chapter 2: Literature Review

2.1 Dissolved Gas Calculations

The primary gases that comprise the atmosphere, oxygen (O_2), nitrogen (N_2), argon (Ar), and carbon dioxide (CO_2), are also present in a dissolved phase in water. The total concentration of these gases in the liquid phase is known as total dissolved gas (TDG). Total dissolved gas may be measured a number of ways but the primary metric of dissolved gas is to compare the summation of the partial pressures of the four primary gases to the local barometric pressure and express it as a percent. Levels of TDG >100% are considered supersaturated and TDG <100% are undersaturated.

$$TDG = \frac{P_d}{P_{atm}} \times 100\% \qquad \text{Eq. 1}$$

where P_{atm} is the barometric pressure (mmHg), and P_d is the total gas pressure in the liquid phase (mmHg) calculated as in Colt (2012),

$$P_d = \sum P_i^l + P_{wv} \qquad \text{Eq. 2}$$

where P_i^l is the partial pressure of the ith gas in the liquid phase, or gas tension (mmHg), and P_{wv} is the water vapour pressure (mmHg). The partial pressure of a gas can be calculated by,

$$P_i^l = \frac{A_i}{\beta_i} C_i \qquad \text{Eq. 3}$$

where C_i is the concentration of the dissolved gas (mg/L), A_i is the ratio of molecular weight to volume corrected for pressure, and β_i is the Bunsen coefficient (L/(L atm)). The term A_i/β_i is the conversion factor from dissolved gas concentration (mg/L) to dissolved gas pressure (mmHg).

The preceding equations can be used to determine the total gas pressure given a concentration of dissolved gas, or if given a measured value for TDG as a percent of barometric pressure (and the barometric pressure is known), be used to back-calculate the TDG as an absolute concentration (mg/L). To calculate the saturation concentration of atmospheric gases the following equation may be used,

$$C_s = \sum C_{o,i} \left(\frac{P_{atm} - P_{wv}}{760 - P_{wv}} \right) \quad \text{Eq. 4}$$

where, $C_{o,i}$ is the saturation concentration (mg/L) of the *i*th gas at standard temperature and pressure (STP), that is, the concentration of gas at sea level at 0°C.

Finally, the total dissolved gas concentration (mg/L) calculated from measured values of total gas pressure (mmHg) is,

$$C_d = \sum \chi_i \left(P_d - P_{wv} \right) \left(\frac{\beta_i}{A_i} \right) \quad \text{Eq. 5}$$

where C_d is the dissolved gas concentration in mg/L (this may also be expressed as a percent saturation relative to barometric pressure), χ_i is the gas fraction of the *i*th gas in the atmosphere.

The above variables for several temperatures are given in Colt (2012).

2.2 Physics of Gas-Transfer

Gas-transfer in turbulent flow is typically characterized by a first-order process where the rate of mass-transfer is dependent on the difference between the local concentration of the gas and the atmosphere (Gulliver et al., 1997) and can be described by,

$$F = V \frac{dC}{dt} = KA(C_s - C) \quad \text{Eq. 6}$$

where F is the total flux, V is the control volume, A is the area available for gas-transfer, C is the dissolved gas concentration, C_s is the saturation concentration in the gas phase, t is the time over which gas-transfer takes place, and K is the bulk transfer coefficient (m/s), this value is often not explicitly given dimensions in the literature but must be m/s to maintain dimensional homogeneity.

The inverse of the mass-transfer coefficient is the resistance to mass-transfer and has a liquid component and a gas component,

$$\frac{1}{K} = \frac{1}{K_L} + \frac{1}{HK_g} \quad \text{Eq. 7}$$

where K_L is the liquid-film coefficient, K_g is the gas-film coefficient, and H is the Henry's law constant. Atmospheric gases have large Henry's law constants making the dominant factor in mass-transfer between air and water the liquid-film resistance, thus, $K = K_L$. The surface area of the air-water interface divided by the control volume (A/V) is the specific area a. Eq. 6 can now be rewritten as,

$$\frac{dC}{dt} = K_L a(C_s - C) \quad \text{Eq. 8}$$

Henry's law states that the saturation concentration of a gas in a liquid is directly proportional to the partial pressure of that gas, therefore the saturation concentration of air will increase as air in the gaseous form (bubbles) are subjected to greater hydrostatic pressure. It becomes important to account for this increase in saturation concentration when deriving predictive equations of dissolved gas.

The mass-transfer coefficient K_L that describes the dissolution of gas from within a bubble to the surrounding water has been studied extensively and many researchers have proposed varying estimates for this variable (Lamont and Scott, 1970; Kawase et al., 1992). Based on the work of Takemura and Yabe (1998), researchers have adopted these models for bubble mass-transfer and applied them to dissolved gas generation downstream of hydropower dams (Politano et al., 2017; Yang et al., 2017). Because of the scaling up of the situation (prototype dam vs lab experiments) and the great degree of turbulence and bubble size distribution, these equations are often applied with some sort of coefficient to correct for uncertainties. Some models have turbulence like characteristics built into them, such as the use of representative eddy scales, or turbulent kinetic energy terms, these can only be applied to numerical models where turbulence models can be used to solve for them. Therefore, solving for the bubble mass-transfer term at the prototype scale without employing a numerical model leaves the need for some correction factors to be implemented, either within the solution for K_L itself (Yang et al., 2017) or within

the broader TDG predictive model (Geldert et al., 1998; Urban et al., 2008; Li et al., 2009).

Gulliver et al. (1997) developed a method for estimating the effective saturation concentration of gases. Since methane is a naturally occurring gas in rivers but makes up an extremely small percentage of atmospheric gases, the increase in partial pressure as a result of depth is almost insignificant. Thus, the difference between measured oxygen and methane transfer efficiencies can be attributed to the increase in saturation concentration of oxygen as a result of depth in the stilling basins of dam outlet works. The use of methane as a tracer gas and an indexing relationship derived by Gulliver et al. (1990) provides an equation for determining the effective depth, which is the depth in the plunge pool that the hydrostatic pressure acting on a bubble would bring it into equilibrium with the saturation concentration.

$$d_{eff} = \frac{P_{atm}}{\gamma}\left(\frac{C_{se}}{C_s} - 1\right) \qquad \text{Eq. 9}$$

where C_{se} is the percent effective saturation concentration, C_s is the saturation concentration (100%), and γ is the unit weight of water (kN/m^3). Field measurements showed an increase in effective depth with discharge where at low discharges the effective saturation concentration would be close to what is estimated from the local barometric pressure and at high discharges would be significantly higher due to the depths to which bubbles are plunged in the stilling basin, approaching 0.7 times the tailwater depth. Johnson and King (1975) calculated the effective bubble depth to be 2/3 of the tailwater depth based on field measurements and assumed a triangular-shaped bubble swarm.

An equation for the maximum bubble penetration depth was also derived by Hibbs and Gulliver (1997) and illustrated that depending on spillway discharge, one of two scenarios are likely to occur and with the estimation of the maximum bubble depth and shape of the bubble swarm in the stilling basin, the following equation could be used to determine the effective bubble depth.

$$\frac{1}{\left(\frac{d_{eff}}{y_t}\right)} = \frac{1}{\beta\left(\frac{y_p}{y_t}\right)} + \frac{1}{\left(\frac{d_{eff}}{y_t}\right)_{max}} \quad \text{Eq. 10}$$

where y_t is the tailwater depth (m), $(d_{eff}/y_t)_{max}$ is 2/3 the tailwater depth, y_p is the maximum bubble penetration depth (m) given by Eq. 11, and β is the fraction of y_p that is the distance from the water surface to the centroid of the bubble swarm and is approximately 0.32 based on an empirical fit of field observations at one spillway (Hibbs and Gulliver, 1997).

$$\frac{y_p}{d_j} = \left[\frac{\frac{v_j}{v_b} + \sqrt{\left(\frac{v_j}{v_b}\right)^2 - \frac{41.73tan\alpha_1}{sin^2\theta}}}{\frac{6.46tan\alpha_1}{sin^{3/2}\theta}}\right]^2 \quad \text{Eq. 11}$$

Here, d_j and v_j are the jet thickness and velocity at the basin plunge point respectively, θ is the slope of the spillway from the horizontal, v_b is the bubble rise velocity (~0.25 m/s), and α_1 is the angle of outer jet spread (~14˚). Solving Eq. 10 and Eq. 11, allows the effective depth to be estimated under both low and high discharge conditions. Since this equation is based on the predicted penetration depth of bubbles entrained by a circular jet in an unconfined pool, the value for the maximum plunging depth of a bubble using Eq. 11 is always much greater than the stilling basin depth at HLK dam and in other dams described by Hibbs and Gulliver (1997). The larger this value, the closer the effective depth approaches 2/3 of the tailwater depth.

Eq. 9 can be rearranged for an estimation of the effective saturation concentration.

$$C_{se} = C_s\left(1 + \frac{d_{eff}\gamma}{P_{atm}}\right) \quad \text{Eq. 12}$$

At high spillway discharges, C_{se} is dependent only on tailwater depth, in which the approximation of the effective depth is equal to 2/3 of the tailwater depth and is the same calculation suggested by Johnson and King (1975). The actual concentration

of the effective saturation concentration can also be estimated by accounting for the added hydrostatic pressure at some depth (Colt, 2012).

$$C_{se} = \sum \chi_i \, \beta_i'(P_t - P_{wv}) \qquad \text{Eq. 13}$$

where β_i' is the conversion factor from pressure (mmHg) to concentration (mg/L) P_t is the total pressure (barometric pressure plus hydrostatic pressure) at some depth.

2.3 Total Dissolved Gas Prediction

Johnson and King (1975) stated that the TDG present at hydraulic structures is dependent on the type of structure, the magnitude of the discharge, barometric pressure, and water temperature. The gas-transfer equation they presented is taken from integrating Eq. 8 with respect to time upstream and downstream of a hydraulic structure.

$$C_d = C_{se} - (C_{se} - C_u)e^{-K't} \qquad \text{Eq. 14}$$

where C_u is a measured (or assumed) upstream concentration, K' is a constant of proportionality determined by a specific structures ability to dissolve gas. Time (t) is the smaller of two values; the vertical bubble rise time in the stilling basin, or the bubble travel time through the stilling basin. An important assumption made about the saturation concentration is that the water jet would plunge to the bottom of the stilling basin and that the diffusion of velocity would be linear, forming a triangular bubble swarm. The location of gas-transfer would then take place predominantly at 2/3 the tailwater depth. Most of the work that followed these authors made modifications to this general mass-transfer equation.

Since any hydraulic structure that entrains air may theoretically raise TDG levels, a number of empirical and semi-empirical equations have been developed for weirs, spillways, closed conduits, sills, etc. Gulliver et al. (1998) reviewed 12 such equations for different structures and determined which ones predicted dissolved oxygen (DO) with the smallest standard error (regardless of what structure the equation was intended for). These equations were temperature corrected according

to Gulliver et al. (1990). No equation proved to be useful in predicting DO downstream of closed-conduits and although the other equations appeared to produce acceptable results, the authors state that the best way to determine a particular structures oxygen transfer characteristics is through field observations.

Typically, bubble-mediated gas-transfer is the predominant means of TDG generation inside a stilling basin. This is typically illustrated in predictive equations as the $K_L a t_b$ bulk mass-transfer coefficient. Although within the stilling basin this may be true, it has been observed from field observations (Geldert et al., 1998; Urban et al., 2008) that bubbles may remain in the flow well beyond the end of the stilling basin. Bubbles that remain in the flow generally rise to the surface where most of the transfer takes place across the free surface of the river. This gives rise to the potential importance of surface-mediated gas-transfer, $K_L a t_s$. Geldert et al. (1998) gives the following equation that accounts for downstream concentration including surface transfer terms and is an expansion of Eq. 14,

$$C_d = C_{se} - (C_{se} - C_u)\left[e^{-(K_L a t_b + K_L a t_s)} + \left(\frac{K_L a t_s}{K_L a t_b + K_L a t_s}\right) \cdot \left(\frac{C_{se} - C_s}{C_{se} - C_u}\right)\left(1 - e^{-(K_L a t_b + K_L a t_s)}\right)\right] \quad \text{Eq. 15}$$

The contribution of bubbles generating TDG downstream of the stilling basins was found to be important for the estimation of the effective depth and saturation concentration. The bubble half-life ($X_{1/2}$) described by Geldert et al. (1998) is the distance to which one-half of the air has left the basin. At high discharges, it is expected that this distance is greater than the length of the stilling basin, the downstream river should then be considered in the estimation of the effective depth. The parameter which relates the stilling basin's effective depth to the river region's effective depth is β. The estimation of the effective depth in this way will be described in a later section when this model is utilized.

The surface-mediated gas-transfer term $K_L a t_s$ is a fitted parameter that may be important at some dams depending on the tailwater depth and degree of turbulence. Following Eq. 15, the equation for $K_L a t_b$ is as follows,

$$K_L a t_b = \alpha\phi \frac{(1-\phi)^{1/2}}{(1-\phi^{5/3})^{1/4}} {W_e}^{3/5} R^{\eta} {S_c}^{-1/2} {R_r}^{-1} \qquad \text{Eq. 16}$$

where W_e is the Weber number, R is the Reynolds number, R_r is the rise velocity Reynolds number, S_c is the Schmidt number, α and η are a fitted coefficient (expected range for η from the literature is 0.55 – 0.75). The air-void fraction ϕ is computed as,

$$\phi = \frac{q_a}{q_a + q_w} = \frac{v_j \lambda}{v_j \lambda + q_w} \qquad \text{Eq. 17}$$

where q_a is specific air flow rate (m^2/s), v_j is the velocity of the water jet at the tailwater surface (m/s), and λ is the air layer thickness, a fitted parameter (expected range from the literature is 0.15 – 0.30m).

Other one-dimensional prediction equations take a similar form (University of Washington, 2000; Li et al., 2009), and nearly all of them have some empirical aspect that requires knowledge of the individual structure in question and field data. This limits the potential for these equations to be applied more generally, furthermore, most of these equations have only been applied to spillway type hydraulic structures and although the physical processes governing gas-transfer should remain the same, applying these equations to closed-conduits has not been adequately explored.

A report by the University of Washington (2000) outlines the Columbia River Salmon Passage Model (CRiSP). This model is used to evaluate the risks salmon may be exposed to including predation and total dissolved gas. The TDG component of the model was based on a number of simple, empirical equations in which several calibration parameters were determined by best fit multiple linear regression for each dam. A mechanistic model developed by Roesner and Norton (1971) and utilized by some United States Army Corps of Engineers (USACE)

dams, known as the Gasspill 1 and 2 models were given as back up models to the other empirical solutions. The model results in a concentration of downstream TDG, this means that temperature data is required for all scenarios to determine the equilibrium saturation concentration and the measured forebay and tailrace concentrations. The following equation is the mechanistic model suggested by the report.

$$C_d = C_s \frac{P_{avg}}{101325} - \left(C_s \frac{P_{avg}}{101325} - C_u\right) e^{\left(-\frac{K_e}{Q_s} W L \Delta\right)} \qquad \text{Eq. 18}$$

where C_d, C_s, and C_u are the stilling basin, equilibrium, and forebay concentration (mg/L), respectively. P_{avg} is the average hydrostatic pressure in the stilling basin divided by standard pressure (101325 Pa), K_e is the bubble entrainment coefficient, Q_s is the spillway discharge, W and L are the stilling basin width and length respectively, and Δ is the differential pressure factor. The model requires specifying three dam-dependent empirical coefficients determined from regression and are used in the Gasspill 1 and 2 models to determine K_e.

Aside from determining empirical coefficients from nonlinear regression analysis, the primary challenge in developing these predictive equations is defining the variables for mass-transfer K_L, a, and t. Most often, these parameters are solved individually (Johnson and King, 1975), grouped together (Geldert et al., 1998), solved via numerical models (Urban et al., 2008; Politano et al., 2017) or defined by some dimensionless parameter (Li et al., 2009).

The most difficult parameter to estimate is the liquid-side mass-transfer coefficient K_L. This value has been estimated based on experiments (Kawase et al. 1992; Takemura and Yabe, 1998), and the ranges of these values depending on what equations are used vary from 1.0×10^{-10} to 1.0×10^{-4}. Most numerical models calculate K_L explicitly at each time step. In the model described by Johnson and King (1975), K' represents a "constant of proportionality" and is representative of the structures ability to dissolve gas.

The specific area available for gas-transfer a also has experimental relationships that can be found in the literature (Gulliver et al., 1990; Chanson, 1996). It may also be estimated by the following relationship,

$$a = \frac{\phi}{V_b} A_b \qquad \text{Eq. 19}$$

where V_b (m^3) is the volume of one bubble of a given diameter, and A_b (m^2) is the surface area of one bubble of a given diameter, and ϕ is the air-void fraction (ϕ/V_b is the number of bubbles per m^3 of solution). This equation requires the assumption of a bubble size. The typical range of bubble sizes is from 0.7 mm to 2.7 mm (Gulliver et al., 1990). More recent numerical models consider different bubble size distributions as well as changing bubble sizes with time. The bubble sizes in these models have been tested over wider ranges and have also included some very small diameters (Politano et al., 2005; Ma et al., 2016; Wang et al., 2018). For many of the predictive equations (Geldert et al., 1998; Urban et al., 2008), K_L and a are estimated together using an analysis modified from Thompson and Gulliver (1997) combined with an empirical factor meant to fit the equation to the turbulent flow conditions present in the stilling basins.

The specific area is an important parameter to estimate because it describes the air-water contact area that allows gas to dissolve through. The gas-transfer rate increases greatly when the air-water contact area increases as a result of having smaller bubbles (Qu et al., 2011a).

The air-void fraction is an important parameter to consider and is the ratio of entrained air to the unit volume of air and water. It can be estimated by,

$$\phi = \frac{Q_a}{Q_a + Q_w} \qquad \text{Eq. 20}$$

where Q_a is the air flow rate, and Q_w is the water flow rate. The volumetric flow rate Q may also be taken to be the specific discharge q (m^2/s). Taken as a percent, this parameter represents the amount of entrained air that is available for gas-transfer.

Bubble residence time t is the duration over which gas-transfer can take place. Throughout most of the literature on predictive equations, the parameter t is only calculated on its own in Johnson and King (1975), here, t is taken as the smaller of two values, the bubble rise time and the basin retention time. In all other relevant papers, the duration of gas-transfer is implicitly included within some dimensionless parameter, the computation for a bulk mass-transfer term $K_L a t_b$, or in the case of a numerical model, determined over a number of time-steps. This variable is made very difficult to estimate in one-dimensional non-numerical models because the flow patterns within the stilling basin make the path a bubble takes to the surface very uncertain in turbulent conditions, which are typical in many stilling basins.

2.4 Air Entrainment at Hydraulic Structures

It is important to understand that there are two points of inception for air entrainment to occur across a dam spillway. When water spills over the dam, at some location beyond the crest of the spillway the boundary layer expands to coincide with the free surface introducing significant turbulence downstream of that point. This is the first inception point where air may be entrained as bubbles in the flow. The second and possibly more obvious point of air entrainment occurs at the tailwater surface when the jet of water plunges into the stilling basin, drawing a significant amount of air down with it. Closed-conduits may also entrain air under certain hydraulic conditions. This section will discuss the types of entrainment processes and how they might impact gas transfer.

When solving for the bulk mass-transfer term $K_L a t_b$, Geldert et al. (1998) estimated the air-void fraction downstream of the spillway jet plunge point by Eq. 17. The air layer thickness was determined with a nonlinear regression analysis along with a number of other empirical variables and was taken to be 0.19 m for all three dams that were being investigated.

Interestingly, Johnson and King (1975) described conditions under which little apparent air entrainment was present as a result of a smooth water surface and small amounts of air near the tailwater surface, yet the operation of these structures in some instances created the worst supersaturated conditions. No explanation was given for this phenomenon except that it was, therefore, assumed that only a small amount of entrained air is required to account for the increase in dissolved gas concentration.

Ervine (1998) reviews the mechanisms of plunge point aeration at hydraulic structures and describes three mechanisms; 1) surface disturbances drag air near the water surface in the direction of the flow where it may be entrained at the plunge point, 2) if the water surface is smooth a thin layer of air may be dragged into the flow at the location of the plunge point, and 3) air entrainment through the free surface which is increased with turbulence and commonly seen at hydraulic jumps. The paper describes the air entrainment in closed-conduits to be a function of the length-to-diameter ratio, where a conduit may be described as a short, intermediate, or long conduit with unique air transport characteristics.

When measuring dissolved oxygen (DO) downstream of a high-head gated conduit during a laboratory experiment Ozkan et al. (2006) stated that the level of DO in the downstream water was independent of pipe slope. The conduit had an air vent downstream of the gate. Ozkan et al. (2014) also indicated that the high-head gated conduit was very efficient at aerating the water.

Mortensen et al. (2011) summarized the results of earlier experimental investigations on air entrainment of closed-conduits to observe scale effects as a result of size and temperature differences. The experiments investigated included those of Kalinske and Robertson (1943) who showed that regardless of pipe slope, downstream air demand was dependent only on the upstream Froude number. There were some significant differences between various authors as outlined by Escarameia (2007) who indicated it was likely the result of different conduit cross-

sections. The authors concluded that the air demand is not impacted by pipe size if a hydraulic jump is formed and fully contained within the pipe, but that an increase in temperature will decrease the amount of air entrained. These size-scale effects do become important, however, when the downstream end of the hydraulic jump is not fully confined within the closed-conduit.

Mortensen et al. (2012) investigated the impact of hydraulic jump location within closed conduits on air entrainment downstream of the gate and air vent. The authors summarized three cases that were defined by the length of the pipe (L), the length of the aerated region (L_a), and the length of the roller (L_r). For each case, an equation was proposed based on experimental results. The results are limited to Froude numbers from 4-12 and within circular pipes at a 4% slope. Again, it was found that for hydraulic jumps where the roller length was truncated by the conduit outlet, an increase in air demand should be accounted for.

Although the air entrainment within closed-conduits may not be as significant or obvious as in the case of spillways, the low-level outlets of dams have been known to generate significant levels of dissolved gas downstream of these facilities. Qu et al. (2011b) described situations in which spill tunnel discharge at Ertan Dam in China contributed significantly to downstream TDG supersaturation and that the generation of TDG is also dependent on the type of structure discharging water. Not only should the type of structure be considered when predicting the amount of air entrainment into the downstream water, but the complex hydraulic conditions of the stilling basin may also determine to what degree a structure may dissolve gas (Johnson and King, 1975).

Regardless of the model used, the literature would indicate that a degree of empiricism is present within all models, whether a numerical model approach or a one-dimensional, control-volume approach is taken. The literature also lacks a general description of how the operation of closed-conduits may impact TDG generation despite Ozkan et al. (2014) explaining the great efficiency gated closed-

conduits have at saturating previously undersaturated water in their experiments and Qu et al. (2011b) describing the significant contribution to TDG by low-level outlets in Chinese dams.

2.5 Previous Investigations at Hugh L. Keenleyside Dam

Since Hugh L. Keenleyside Dam is a treaty dam on the Columbia River, it has been monitored in the past for TDG generation and a number of consulting engineers and environmental scientists have attempted to explain and predict the TDG generating mechanisms from the different outlet structures. Typically, TDG is predicted at HLK dam via regression analysis with a number of different parameters to determine a predictive equation. These predictive tools have had limited success and in 2003 the Arrow Lakes Generation Station (ALGS) had come into use, changing the discharge operations and tailrace levels at HLK. These empirical models are no longer relevant and more work is needed to predict TDG over a wider range of hydraulic and operational conditions.

In 1992 and 1993 Klohn-Crippen Integ (1994) installed three total dissolved gas probes near Hugh L. Keenleyside Dam. One probe was located on the upstream face of the dam in the forebay, another 5.7 km downstream at Robson, and a final one located 29 km downstream. The report found that the northern low-level outlets generated significantly less TDG than their southern counterparts or spillways. The study recommends a revised operating order to maximize the use of the northern low-level operating gates but recognized the need for a cavitation monitoring program.

Aspen Applied Sciences Ltd. (1995) collected data gathered from 1992 – 1994 by Klohn-Crippen Integ and R.L. & L. Environmental Services Ltd. to develop a system-wide Lower Columbia River TDG model. A general discussion about the potential mechanisms of TDG generation between the north and south outlets concluded that it was likely surface turbulence and plunging flow caused by a roller in the southern basins that is the primary reason for higher TDG generation. The

northern outlets, with a much deeper tailwater, are more efficient at dissipating the energy of the incoming jet of water and therefore have little surface turbulence and air entrainment.

In a report by Klohn Crippen (2001), the potential cavitation risks were identified for the low-level outlet gates, and as part of that study, the air demand in the conduits under certain gate openings was estimated. This analysis estimated air demand using the following equation from the USACE.

$$Q_a = 0.03 Q_w (F_r - 1)^{1.06} \quad \text{Eq. 21}$$

where F_r is the Froude number.

Bruce and Plate (2013) sought to determine the impact on downstream TDG as a result of reducing low-level outlet use due to the addition of ALGS. Using what was able to be recovered from the database of Aspen Applied Sciences Ltd. and Klohn-Crippen Integ, a revised database was collated correcting for some errors.

An outlier analysis was done by examining the collected data for significant deviations from historical records and when found, were replaced by values calculated by predictive equations supplied by BC Hydro, which typically increased the goodness of fit with historical records.

Unlike the operational and hydraulic parameters that could be checked against historical records or predictive equations, TDG measurements could not be independently verified. Although the above-mentioned corrections were made to the dataset, the number of errors encountered does bring into question the overall quality of the information. Nonetheless, the database by Bruce and Plate (2013) is considered the most accurate and correct collection of previous data sampled at Hugh L. Keenleyside Dam.

Chapter 3: Hugh L. Keenleyside Dam Facility and TDG Measurement

3.1 Facility and Site Description

Hugh L. Keenleyside Dam spills water through two types of discharge structures; spillways and low-level outlets. There are four spillway operating gates (labeled SP1-4) in between two sets of four low-level outlet gates. These two sets of outlets are identified by their location relative to the spillways; northern low-level outlet gates (labeled NL1-4) and southern low-level outlet gates (labeled SL5-8). All gates combined have a discharge capacity of 10,500 m^3/s. The Arrow Lakes Generation Station (ALGS) maximum turbine discharge is 1,500 m^3/s. These flows are passed in accordance with the Columbia River Treaty between Canada and the United States. Measurements were taken downstream of the dam at a number of transects. The transects and limits of work related to TDG generation are as far as 6.7 km downstream.

The four spillway bays have vertical sluice gates to control the outflow of water. The ogee spillways all have a crest elevation of 424.9 m and the spill bays are 15.2 m wide. Each spillway terminates in a plunge pool energy dissipator with a series of tall end sills staggered at the end of the stilling basin. Three of the four stilling basins (SP2-4) have floors at the same elevation, 399.9 m, and SP1 has a floor elevation of 396.2 m. These differences in floor elevation are a result of the dam being built to conform to the solid bedrock formation beneath it. The differences in floor elevation also affect the difference in end sill height between SP2-4 and SP1. The end sills of SP2-4 have a top elevation of 413 m and the top elevations of those in the SP1 stilling basin are 409.4 m. The differences in these geometries are believed to have a significant impact on the TDG generation mechanisms and result in different magnitudes of TDG generation, this will be explored in Chapter 4. See Figure 3 for the layout of HLK dam, Figure 4 for the plan view of the HLK discharge structures, and Figure 5 and Figure 6 for the cross-sectional views of the spillways.

The low-level outlets that flank the spillways at HLK are considered the northern and southern low-level outlets. The geometries are different between the two sets of closed-conduits but each set of four has a consistent cross-section and stilling basin geometry. These are shown in Figure 7 and Figure 8. The northern low-level outlets (NL1-4) have an inlet crest elevation of 411.5 m and the gate sill elevation within the conduit is 408.7 m. The rectangular conduit is sloped at 19.61° and has a width of 6.092 m and a height of 7.315 m. The stilling basins associated with the northern low-level outlets also have similarly staggered end sills as the spillways but are relatively shorter. The stilling basin floor is also significantly deeper than any other basin floors with an elevation of 391.7 m, the end sills have a top elevation of 401.1 m. The southern low-level outlets have an identical cross-section to their northern counterparts but are sloped at a shallower angle of 14.76°. The inlet crest elevation is also 411.5 m but the gate sill elevation is 409.4 m. The stilling basin floor illustrates the greatest difference between the two closed-conduit structures with a bottom elevation of 399.9 m (the same as SP2-4), the depth of water above the stilling basin floor is 8.2 m shallower than in the northern stilling basins. The end sills are also taller and top out at a higher elevation of 413 m. These stilling basin and energy dissipator geometrical differences is hypothesized to be the prevailing factor in the difference in relative TDG generation between the northern and southern low-level outlets. A summary of the geometrical differences in low-level outlet structures is found in Table 1.

Another important physical feature of the low-level outlets that may contribute to TDG generation is that the gate slots within the conduits are open to atmosphere, allowing air to move in and out of the shafts when in operation. This is one way in which the cavitation of the conduits is minimized. This ability for air to move into and out of the conduit has been described by Klohn Crippen (2001) and is believed to be the primary source of air entrainment from which gas may be dissolved, as will be discussed in Chapter 5.

3.2 Collected TDG and Operational Data

Data were collected from the field observations that took place from July 26 – July 30, 2016, by the University of Alberta research team on an 18 km stretch of the Lower Columbia River downstream of Hugh L. Keenleyside Dam. Data collected by Klohn-Crippen Integ (1994) and Aspen Applied Sciences Ltd. (1995), screened for errors and presented by Bruce and Plate (2013) was also used to analyze the response of both spillways and low-level outlets. This section describes the fieldwork observations in July 2016 as well as supplementary data collected from previous investigations at Hugh L. Keenleyside Dam that will be used in subsequent chapters to illustrate trends in TDG generation by each of the structures.

3.2.1 Field Data

Six scenarios were tested which consisted of different combinations of gates to spill water through HLK. During this time ALGS also continued to discharge water through the turbines. ALGS discharge was held mostly constant for the duration of the fieldwork. Total discharge from the spillways and low-level outlets varied from 934.8 m^3/s to 1289.8 m^3/s. The scenario summary, including duration, gate configuration, and HLK and ALGS discharge is found in Table 2.

During these scenarios, measurements were taken in two different ways. Floating platforms were deployed at eight locations downstream of HLK and held probes submerged about 1.5 m below the surface which continuously collected TDG data for the duration of the field observations (Figure 9). Two probes were placed by Creekside Aquatic Sciences Ltd. closest to the outlet works at the end of a rock berm separating the outlet structures and the boat lock to the south. Six probes were installed by the University of Alberta research team and were placed near the banks of the river due to restrictions they may have imposed to navigation, the great depth of flow near the middle of the river, and the high-velocity currents in some locations that threatened the integrity of the platforms. The second way in which TDG was measured was by taking spot measurements from a boat which traveled across the width of the river at a number of transects. Approximately five measurements were

taken at each transect. Due to the time constraints of some scenarios, not every transect was able to be measured by boat and no spot measurements were taken for scenario 4. In total, six transects were determined for taking spot measurements, in addition, some spot measurements were taken in the forebay of HLK (Figure 10) and in the tailrace region for some scenarios. The transects and the corresponding spot measurements and continuous monitoring data that will be considered for the purposes of investigating TDG generation are located in the forebay, tailrace region (approximately 300 m downstream of the outlet structures), 0.6 km, 1.0 km, 2.0 km, 4.4 km, and 6.7 km downstream of HLK (Figure 11). Continuous monitoring stations installed by the University of Alberta research team were located on the left bank (LB) at 1.0 km, and on the right bank (RB) at 4.4 km and 6.7 km. Further downstream measurements made during the field work which are not considered in the current analysis can be found in Kamal et al. (2018).

Measurements were taken using the PT4 Smart Total Gas Pressure (TGP) probe (for continuous monitoring) and the Lumi4 DO-TGP probe (for spot measurements) purchased from Point Four Systems, Inc. These probes measure total dissolved gas pressure and barometric pressure with an accuracy of +/- 2 mmHg and total dissolved gas supersaturation with a derived accuracy of +/- 4%. Both types of probes also measure water temperature with an accuracy of +/- 0.2˚C (Pentair Aquatic Eco-Systems instrument manual).

The continuously recording probes that were installed by the University of Alberta research team collected data at two-minute intervals throughout the duration of the field observations and the two probes installed by Creekside Aquatic Sciences Ltd. collected data at five-minute intervals (M1 and M2). It was found that only data from M2 appeared to be useful and the poor measurements from M1 are likely due to the location that was selected for the installation and the uncertainty around how the M1 and M2 probes may have been calibrated. The flow patterns near the rock berm appear to be very irregular and these increases and decreases in the data were not consistent with the M2 station. It was also found that regular fluctuations of

barometric pressure measured at the 6.7 km station were unlike all the other TDG probe data. These significant fluctuations in barometric pressure are also inconsistent with barometric pressure data from local weather stations. Therefore, the present analysis will ignore the TDG readings collected at the 6.7 km monitoring station. Figure 12 displays the continuous TDG pressure data from the monitoring stations and Figure 13 displays the TDG (%) data from the three useful stations throughout the entire period of field observation.

The collection of spot measurements was done by maintaining a single position in the river either by anchoring or by the maneuvering of the boat operator. The probe was lowered approximately 1 – 1.5 m into the water for a period of about 10 – 20 minutes which allowed the TDG reading to stabilize. A handheld GPS device was used to record the location of each of these measurements. Forebay TDG levels were also collected approximately 1.6 km upstream of the dam. Three measurements were taken from the reservoir and ranged from 108% to 111% supersaturation. These measurements were taken 1 – 1.5 m below the surface, one other measurement was taken at a depth of 15 m and resulted in 107% TDG. These differences in measurements within the reservoir are too small to be significant and an average constant value of 109% was adopted for later analysis.

The transition from one scenario to another lasted about 30 minutes and typically was done in the afternoon of each day. This allowed a period of at least 16.5 hours before the first spot measurements were taken for each scenario giving plenty of time for TDG levels in the river to stabilize to the new gate configurations. The exception to this was during scenarios 2 and 4, where they were each in operation for only two hours. In the case of scenario 2, 1.5 hours was allowed to elapse before the first spot measurements and no spot measurements were taken during scenario 4. Figure 14 shows the transect spot measurements for all scenarios at 0.6 km, 1.0 km, and 2.0 km.

Scenario 1 consisted of three northern low-level outlet gates, two partially opened and one fully opened. Having scenarios with only one type of structure in operation is important for later analysis to determine how much TDG generation is likely to occur during the operation of any one type of structure, before considering how more than one type of structure used in combination may impact overall measured TDG downstream. This pattern was operating for a total of 26 hours and 22.5 hours had elapsed before the first measurement was taken. Data were collected from the boat at all but the first two transects nearest to HLK dam.

The following scenario was in operation for a significantly shorter period of time. Two spillway gates were open partially to the same height to discharge water and was the second smallest outflow from the dam during the entire field work campaign. There had been 1.5 hours of spillway operation before the first measurement was taken and the overall duration of this scenario was only 2 hours. Data were collected at the first three transects for scenario 2.

During scenario 3, three southern low-level outlets were partially opened and produced a slightly smaller discharge than scenario 2. Data were able to be collected at all transect locations as well as at a point approximately 300 m downstream of the dam at the edge of the tailrace, this point resulted in the largest measured TDG supersaturation during this field work campaign. The scenario ran for a total of 22 hours, 17 hours had elapsed before the first measurement.

Scenario 4 consisted of two, fully-open southern low-level outlets, but due to the similarity of the preceding scenario, namely that it operated the southern low-level outlets again and the short planned duration of the scenario, it was not measured at any transect. It was only operated for 2 hours before the gates were changed again.

Scenarios 5 and 6 were combination scenarios where both northern and southern low-level outlets were being used. The gate openings varied in most cases and the scenario durations were 24 hours each. In the case of scenario 5, 18 hours had

elapsed and for scenario 6, 16.5 hours had elapsed before the first measurements. Scenario 5 had a slightly higher discharge and operated two southern low-level outlets and two northern low-level outlets, scenario 6 operated with one less southern low-level outlet. Measurements were carried out at every transect for both scenarios.

Figure 14 shows that a gradient exists between the left and right banks, particularly at transects closest to the dam (0.6 km and 1.0 km). This is likely explained by examining the orientation of ALGS and HLK outlet works. It would appear that ALGS flow is held near the left bank and remains somewhat separated from HLK spill flow which tends to remain near the right bank, at least until some distance further downstream. The measurements, therefore, along the left bank agree with the widely held belief that TDG concentrations remain unchanged as water from the forebay passes through the generation station and contribute to a dilution of TDG supersaturation further downstream (Politano et al., 2009; Qu et al., 2011b). The high TDG right bank measurements are then considered to be indicative of HLK spill flow only. A summary of the maximum measured TDG values at each location for all scenarios is shown in Table 3.

3.2.2 Supplementary Data

In the early 1990's Klohn-Crippen Integ. conducted a field work campaign to gather TDG data at HLK. The purpose of this work was to analyze the impacts of gate operations on TDG generation downstream. Aspen Applied Sciences Ltd. (1995) then used the collected data and produced a statistical model based on various discharge related parameters to establish a new operating order for the spillways and low-level outlets to minimize TDG generation. Since the development of that model, the Arrow Lakes Generation Station was constructed and Bruce and Plate (2013) developed a revised model to also determine if certain low-level outlet use could be minimized in order to avoid further cavitation damage that had been recently noticed. They revised the dataset initially used by Aspen Applied Sciences

Ltd. (1995) by screening it for outliers and correcting for assumed errors in the information (based on gate operating equations provided by BC Hydro).

Although Bruce and Plate (2013) have provided the most comprehensive set of data from previous field work campaigns at Hugh L. Keenleyside Dam some of the variables and measurements listed in their dataset were adjusted to correct for some errors.

The listed tailwater depth is calculated by taking the tailwater elevation and subtracting it from the elevation half-way up the end sill. This is claimed to be in keeping with a method for adjusting the tailwater depth due to a "spillway deflector" in the stilling basin which goes across half the width of the stilling basin described by Hibbs and Gulliver (1997). It is believed that this may be somewhat inaccurate and it is currently uncertain if the spillway deflectors written about in Hibbs and Gulliver (1997) was indeed the end sill in the stilling basin or the deflector located on the face of the spillway. In either case, the correction to tailwater depth is small because the end sills or spillway deflectors are themselves, short. At Hugh L. Keenleyside Dam, however, the end sills are very tall and reduce the tailwater depth by several meters (sometimes as much as 6.5 m in the spillway stilling basins). It is believed this type of correction is too large and may lead to inaccurate conclusions about the importance of tailwater depth on the generation of TDG in the stilling basin and was certainly much larger than the corrections made by Hibbs and Gulliver (1997), who stated that the corrections were small. Many meters of hydrostatic pressure cannot be neglected from the present analysis and be adequately justified. Therefore, the tailwater depth is simply calculated from the tailwater surface and to a weighted average stilling basin floor elevation (SP1 is deeper than SP2-4). This will serve as a more meaningful estimation of tailwater depth to which further adjustments may be made if necessary.

The appended dataset by Bruce and Plate (2013) also lists a variable called *TGP_Diff* which is the difference between the observed downstream TDG and

barometric pressure. Since most data from Klohn-Crippen Integ and Aspen Applied Sciences Ltd. (1995) did not include barometric pressure in their tabulations (except for data from 1994), it was assumed for these measurements that the barometric pressure was 730 mmHg, which is near the average for that location. It was decided, based on the fact that the range of data spans all seasons of the year that a more accurate barometric pressure be determined for each data point. Historical hourly barometric pressure was found at *climate.weather.gc.ca* for a weather station at Castlegar, BC. This barometric pressure was used for the present analysis. There also seems to be some slight error in the calculation for head above the spillway gates, this has also been corrected.

The location of the data collected in the 1990's was mentioned to be at a distance approximately 5.7 km downstream of HLK dam, compared to the locations of the maximum TDG recorded in 2016 of 300 m to 0.6 km. It is not believed that this will impact the results of the work to follow very significantly. This is because there is likely to be very little dissipation of TDG within 5.7 km of the dam, particularly because of the large depth and therefore low level of turbulence of the river. The transect measurements indicate a couple percent difference but given instrument uncertainty, this is not considered significant. Also, ALGS was not online during the 1990's data collection, therefore no dilution would have been present as a result of generation flow.

Appendix A holds the adjusted dataset that will be used for analysis hereafter. The original dataset can be found in Bruce and Plate (2013) or Bruce (2016).

3.3 Calculation of Dissolved Gas Concentration

Evaluating the percent increase in total dissolved gas is a simple way for evaluating the risk for fish downstream of hydropower facilities, however, an estimate of a structures ability to generate dissolved gas as measured in terms of actual concentration (mg/L) may be a more appropriate approach for investigating the differences in each structures ability to entrain air and to then dissolve that air.

In order to calculate the concentration of dissolved gas in water, the water temperature must be known. During the 2016 field work campaign, water temperature was recorded by the TGP probes at the same time interval as the TDG information. For the 1990's dataset, temperature data were tabulated for the 1994 scenarios (Aspen Applied Sciences Ltd., 1995), but for all other scenarios temperature data was available only in chart form and the data was pulled from Klohn-Crippen Integ (1994).

The first objective is to determine the saturation concentrations of air in water for each scenario. This is done with Eq. 4. Since, according to Henry's law, the solubility of air in water must increase with pressure, the saturation concentration deep in the stilling basin will be higher than it is in the atmosphere and the dissolution of gas into the water will be governed by this increase in local solubility. Hibbs and Gulliver (1997) calls this the effective saturation concentration C_{se}. The effective saturation concentration is calculated at some depth, typically taken to be the average depth or 2/3 the tailwater depth. The increased saturation concentration of air at some depth in the stilling basin can be calculated by Eq. 13. In deep plunge pools, the effective saturation concentration can easily exceed 240% of the local atmospheric saturation concentration. Finally, Eq. 5 is used to calculate the concentration of total dissolved gas based on the gas pressure measurements taken by the TGP probe.

Now that the actual concentrations of dissolved gas have been determined, it is possible to estimate the actual total dissolved gas generation (ΔC, mg/L) between the forebay and tailrace based on the dataset measurements from the 1990's and 2016, this is tabulated in Table 4 for the 2016 scenarios. Consider the ΔC value for SC 1 (0.79 mg/L) and SC 3 (3.95 mg/L), for very similar conditions, the southern low-level outlets generated five times more TDG (an additional 12% TDG) than their northern counterparts.

The following calculations illustrate the process for computing the saturation and dissolved gas concentrations for scenario 5:

Observed Conditions:

Water temperature = 18.3 ˚C

P_{wv} = 2.1032 kPa or 15.8 mmHg (Colt, 2012)

C_u (forebay) = 109%

P_{atm} = 99.99 kPa or 750.0 mmHg

Characteristic parameters of gases listed in the table below can be found in Colt (2012);

Gas	C_o (mg/L)	χ	β (L real gas/(L atm))	β' (mg/(L mmHg))	A
Oxygen	9.409	0.20946	0.0321	0.0604	0.5318
Nitrogen	15.498	0.78084	0.0162	0.0267	0.6078
Argon	0.5754	0.00934	0.0353	0.0828	0.4260
Carbon Dioxide	0.6886	0.00039	0.9155	2.3812	0.3845

$$C_s = \sum C_{o,i}\left(\frac{P_{atm} - P_{wv}}{760 - P_{wv}}\right) = 25.82 mg/L$$

$$TDG = \frac{P_d}{P_{atm}} \times 100\%$$

Since C_u = 109%, P_d (forebay) = 817.5mmHg

$$C_u(forebay) = \sum \chi_i\,(P_d - P_{wv})\left(\frac{\beta_i}{A_i}\right) = 28.20 mg/L$$

$$d_{eff}(NL3{,}4) = \left(\frac{2}{3}\right) y_t = 19.98m$$

$$P_t = P_{atm} + \gamma d_{eff} = 295.99\ kPa\ or\ 2220.1 mmHg$$

$$C_{se,B}(NL3{,}4) = \sum \chi_i\,\beta_i'(P_t - P_{wv}) = 77.52 mg/L$$

where γ = 9.81 kN/m^3

$$d_{eff}(SL5,6) = \left(\frac{2}{3}\right) y_t = 14.51m$$

$$P_t = P_{atm} + \gamma d_{eff} = 342.23\ kPa\ or\ 2566.9mmHg$$

$$C_{se,B}(SL5,6) = \sum \chi_i\, \beta_i'(P_t - P_{wv}) = 63.38mg/L$$

These calculations are summarized for all scenarios in Table 4.

Chapter 4: Spillway TDG Generation

4.1 Creating a Calibration Data Subset

Spillways at HLK dam have always generated a significant amount of TDG, mostly due to the large tailwater depths associated with the plunge pool energy dissipators. The 1990's dataset has a total of 76 scenarios tested across 1992-'94. However, no apparent trend stands out between TDG and any singular operational parameter, this is mostly due to the different operational conditions between each scenario. There also appears to be no consistent trend between test years, and the overall quality of the data has been called into question (Bruce and Plate, 2013). Since there are doubts as to the integrity of the data, and in hopes of removing some of the significant scatter between data subsets (gates used and year of testing), a collection of data points was selected to test the applicability of TDG prediction equations and validate the models against the single 2016 scenario (SC 2).

The most number of spillway TDG observations were made in 1993 (n = 46), then in order to more closely match the 2016 scenario, all 1993 scenarios that had spillway bay one (SP1) in use were removed. This left 20 scenarios in the new subset of data. These 20 observations also occurred during the summer months of May to August, making this collection of scenarios the most closely related to the 2016 scenario. It has been observed in the reports mentioned in Chapter 2.5 that predictive equations were unable to estimate TDG from scenarios in which SP1 was in operation. This spillway stilling basin has a slightly different geometry than SP2-4, namely that the stilling basin floor is deeper. This has resulted in higher levels of TDG whenever spill operations include SP1. It appears that SP1 would need to be treated separately from SP2-4 in order for a predictive model to work. Attempts to integrate SP1 were made in the present work but no decent results could be achieved by including scenarios with SP1. This is in part caused by the fact that there are no scenarios in which SP1 was in use on its own, therefore defining unique parameters for this spillway was not possible. Thus the decision was made to leave SP1 out of the present analysis.

4.2 Spillway Operating Gates

Spillways are typically the main method of discharging excess water over dams and quite often with medium to high head dams such as HLK, the method of energy dissipation is in a plunge pool. The mechanisms of air entrainment in self-aerated flows are three-fold; 1) air is entrained into the flow of water as it travels down the face of the spillway, 2) air is entrained at the plunge point of the water jet with the tailwater surface, and 3) air is entrained at the surface of the plunge pool as it becomes more turbulent (Ervine, 1998). These obvious mechanisms for air entrainment and the impact of the plunging jet on bubble penetration depths are what make spillways the most likely source for high levels of TDG generation.

The field work efforts in 2016 provided only one scenario in which spillways were operated. It was expected to see the highest levels of TDG occur as a result of scenario 2 in which the spillway discharge total was 981 m^3/s. No tailrace measurements were taken (300 m downstream of outlet works) but measurements at 0.6 km indicate 122% supersaturation making it one of the higher TDG generating scenarios. It is important to note that the scenario duration was only two hours long and 1.5 hours elapsed before the first measurement was taken. This may not have been enough time for the river to reach a steady-state TDG level. Aspen Applied Sciences Ltd. (1995) indicated that at least 12 hours should elapse to ensure a steady-state TDG situation. This is because of a zone of slow-moving water south of the boat lock that acts to dilute the spill flow for a period of time before it also becomes equilibrated with the gate configuration. It is not believed that the measurement was made in error because spot measurements made during that scenario along the transects show a reasonable pattern of TDG supersaturation between transects and across the width of the river for a particular transect. This being that the supersaturation levels increased from left bank to right bank and that they were higher at the transects nearest to the dam. It is difficult to say how high the TDG may have increased, if any further, but the trend of increased TDG at the 4.4 km continuous monitoring station looks as if it did not quite reach a steady state. This isn't to say that a scenario should be operated for at least 12 hours before

measurements are taken but perhaps they should be in operation longer than 1.5 hours. This is debatable however and remains one of the uncertainties regarding the measurements made during scenario 2.

4.3 Analysis of Dissolved Gas Measurements

The spillways at HLK dam typically generate the most TDG downstream. On average the 1993 subset of data shows that SP2-4 generate 7.65 mg/L (~135%) of dissolved gas. That number changes to 9.14 mg/L (~136%) if scenarios with SP1 in operation are included. These values may appear strange in that there is a 1.49 mg/L increase in TDG concentration but only a 1% increase in percent supersaturation. This is explained by the later dataset including several measurements taken during the winter months where the water temperature is significantly lower than in the summer. A lower water temperature will increase the saturation concentration of air and therefore allow more gas to be readily dissolved, coupled with a greater plunging depth for SP1, hence the larger average concentration. However, since the saturation concentration has also increased, the relative increase in TDG as a percent of saturation concentration remains nearly the same. During 2016 only one scenario was measured in which spillways were the mode of dam discharge, only 3.39 mg/L of dissolved gas was observed (122%). The reason for this smaller value is unknown, although it could be for other reasons suggested by Aspen Applied Sciences Ltd. (1995) and mentioned in the previous section.

Another potential reason for the lower level of TDG measured in 2016 is that the tailwater elevation was 2.1 m higher than the average tailwater elevation of the 1993 scenarios. This resulted in a much lower differential head across the structure (3.68 m below the 1993 average). Since the energy that needs to be dissipated during scenario 2 is comparably less than at previous times it may be assumed that the ensuing turbulence in the stilling basins would also be less, leading to less shearing of bubbles to smaller sizes. SP2, 3, and 4 had their gates open to a height of 4.65 m, also much higher than the average gate opening in 1993 (2.39 m), this

was accompanied by lower than average velocity at the tailwater surface. Smaller velocities would also precede shallower bubble plunging depths and thus lower TDG. These are some potential factors impacting spillway-generated TDG that may explain the large difference in measured TDG between 2016 and 1993.

4.4 Models for Predicting Downstream Total Dissolved Gas

Spillways are the most studied structure with regards to total dissolved gas, for obvious reasons. As a result, a number of analytical or numerical models have been put forward to predict TDG under a given operational condition.

Expressing TDG concentrations as a percent of barometric pressure as would be measured directly in the field and estimating an effective saturation concentration as per Eq. 12; the model by Johnson and King (1975), Eq. 14, was used to estimate TDG generation at HLK during the scenarios of 1993.

C_{se} is computed at two-thirds the tailwater depth assuming that the entrained air bubbles plunge to the bottom of the stilling basin and rise towards the surface in a linear fashion. The time which gas is being dissolved into the water is defined as the smaller of two values; the basin retention time and the bubble rise time. The basin retention time (the length of the stilling basin divided by the average flow velocity in the basin) is almost always the smaller value. K' is dependent on the structure and may be determined from a figure displaying a family of curves, these curves, however, do not lend themselves well at all to graphically determining K' at HLK dam. This value was then computed by regression to most closely match a number of measured downstream TDG values.

For scenario 2, the effective depth is calculated as,

$$d_{eff} = \frac{2}{3} y_t = \frac{2}{3}(21.68) = 14.45m$$

following Eq. 12;

$$C_{se} = C_s\left(1 + \frac{d_{eff}\gamma}{P_{atm}}\right) = 100\left(1 + \frac{14.45(9.81)}{97.19}\right) = 246\%$$

The process for estimating the final velocity within the stilling basin that would move a bubble from the plunge point to a location where it would be forced upward to an elevation where it would contribute little to dissolved gas generation has several steps associated with it. A number of figures and curves are used along with dimensional properties of the stilling basin and spillway jet to determine the velocity and can be found in Johnson and King (1975), here the final velocity which is used for this scenario, v_{avg}, is 11.09 m/s. The length of the stilling basin, where the jet plunges into the tailrace to the end sill (L) is approximately 33.3 m, therefore, the bubble retention time is computed as,

$$t = \frac{L}{v_{avg}} = \frac{33.3}{11.09} = 3.0 seconds$$

The final parameter to determine is K', this value would typically vary with different operational scenarios, however, since the family of curves used to derive this term do not appear to apply to HLK dam, it was taken as a single parameter, attempting to fit the structures ability to generate gas to a single value. This undoubtedly becomes a limitation of using this model. It appears that perhaps the dam geometry that was used at most tested dams by Johnson and King (1975) were of a different type and therefore produced curves that do not wholly apply in the present case. Nonetheless, an attempt is made here. The value determined from regression for K' is 0.094. With the above information known, and an upstream forebay TDG of 109%, Eq. 14 is solved;

$$C_d = C_{se} - (C_{se} - C_u)e^{-K't} = 246 - (246 - 109)e^{-(0.094)(3.0)} = \mathbf{143}\%$$

The results of this analysis are given in Figure 15 and show the measured and predicted values of the 1993 dataset as well as the 2016 scenario. The RMSE for this model is 2.9% but the 2016 scenario was overestimated by 21%. This model is unlikely to illustrate very well any particular mechanism for generating TDG at

HLK because of the scarcity of parameters that it considers, this large overestimation, however, will occur in every predictive model to follow.

One of the likely explanations for the inadequate application of this model to the spillways at HLK dam is the shape of the stilling basins. Assuming that the velocity in the basins would be allowed to dissipate linearly as flow moved through the basin is very unlikely. The presence of the tall end sills at the end of the basins are likely to cause very different and more chaotic flow patterns than the idealized scenario put forward by Johnson and King (1975) who also recognized that the difference in dam type and geometry would impact the results of predictive models.

To further explore the potential mechanisms of TDG generation at HLK, Eq. 15 was utilized to estimate the impact of the downstream river region and surface-mediated gas-transfer on downstream TDG. Since there are many fitted parameters, solving these values through nonlinear regression becomes highly sensitive to initial conditions, therefore many iterations were conducted to produce acceptable values within their given ranges.

In the end, most parameters were held at a constant value at one end of their theoretical ranges, then α was solved for to produce the lowest RMSE. If these values are relaxed it is possible to achieve a somewhat lower RMSE, however, the justification for these adjustments have not been explored for Hugh L. Keenleyside Dam's unique stilling basin geometry especially since many of these parameters are physically meaningful and often based on other experimental or field observations.

A brief discussion about the parameters identified through nonlinear regression is warranted. These final values can be found in Table 5. The first parameter to consider is β, this value relates the stilling basin region and the downstream river region for determining an effective saturation concentration. It is expected that during high flow events, bubbles will remain in the flow beyond the stilling basin

and therefore the bubble centroid used for estimating the mean point for TDG generation should include the downstream river region. It was found that no iteration of regression produced desirable results for β. Most iterations landed this value well outside the expected values described in Geldert et al. (1998). The paper suggests that when a significant amount of air entrainment exists beyond the stilling basin region (10 – 50% of the initial concentration) then the river region should be considered. This would give ranges of β of 1 - 3.3. These values, however, did not yield promising results, as a consequence, this parameter was ignored in the present calculation and the effective saturation concentration was assumed to be located at a depth computed within the stilling basin region only. This may be an inadequate characterization of the bubble swarm within the basins at HLK and it is, therefore, a point of uncertainty. Since the geometry of the stilling basins and resulting flow patterns are complex, it is possible that to characterize the effective saturation concentration at a single location in the tailrace is a poor approach. Furthermore, the type of end sills at HLK dam should allow for bubbles to be transported downstream because they are staggered. Certainly, some of the flow will be directed upwards, but there is likely half of the flow to be sent downstream which passess between the tallest parts of the end sills. Therefore, it is expected that bubbles would be present downstream of the stilling basin, especialy if any plunging flow patterns over the tops of the end sills are present. In further discussions, an attempt will be made to treat the stilling basin and downstream river regions more separately than the present model would allow.

The value for η was set to 0.55 in the final calibration which is the lower range of expected values found in the literature (the higher range being 0.75). This parameter is the exponent to which the Reynolds number is raised and is, therefore, describing the degree to which turbulence impacts bubble gas-transfer. During the iterations for determining these parameters η varied between 0.54 and 0.59, with 0.55 yielding the best result. The parameter λ, as described in Chapter 2.3 represents an air layer thickness along the spillway face that is used to estimate the air flow rate entering the stilling basin. This value ranged widely and because of the physical

dimension associated with this variable the value which produced the best fit of the data was 0.15 m, this is the lower limit given by Geldert et al. (1998). For the three dams that were tested in the literature the value for λ used was 0.19 m, trying this value in the present model results in a worse RMSE and a larger overestimate for scenario 2.

$K_L at_s$ was set to zero in the final calibration of these parameters because no other reasonable value could be determined. This does not necessarily lead to the conclusion that surface mediated gas-transfer is an insignificant component in spillway TDG generation, especially since a large degree of surface turbulence may be observed, but that it is most likely this model does not adequately rectify the interaction between the stilling basin and downstream river regions ability to predict overall TDG generation. Methods for computing $K_L at_s$ directly will be discussed in other models to come.

Since in the end most parameters were set to zero or are equivalent to a value found in the literature, α was the only truly fitted parameter. This value was the most widely ranging number as different values of the other parameters were tested. This parameter simply relates the theoretical and empirical foundation of Eq. 16 to the field measurements. A value of 2.46 was found to achieve the lowest RMSE overall.

Using the data collected during scenario 2 (Table 2, Table 4, Table 5, and Table 6), the following calculations were made;

$$v_j = \sqrt{2g(FB_{elev} - TW_{elev})} = \sqrt{2(9.81)(433.5 - 421.58)} = 15.29\ m/s$$

$$d_j = \frac{q_w}{v_j} = \frac{32.27}{15.29} = 2.11\ m$$

Since β is zero, only the stilling basin centroid is considered and the effective depth may be solved by Eq. 10 and Eq. 11.

$$y_p = (2.11)\left[\frac{\frac{15.29}{0.25} + \sqrt{\left(\frac{15.29}{0.25}\right)^2 - \frac{41.73tan14}{sin^2 30}}}{\frac{6.46tan14}{sin^{3/2}30}}\right]^2 = 1513\ m$$

$$\frac{1}{\left(\frac{d_{eff}}{21.68}\right)} = \frac{1}{0.32\left(\frac{1513}{21.68}\right)} + \frac{1}{\left(\frac{2}{3}\right)}, d_{eff} = 14.05\ m$$

The value of y_p is very large in this instance and is often found to be several hundred meters in the literature, regardless, the impact it has on the effective depth is always small at HLK dam. Since these values are always large the effective depth approaches 2/3 of the tailwater depth in most instances.

Now the effective saturation concentration may be solved by using Eq. 12.

$$C_{se} = 100\left(1 + \frac{14.05(9.81)}{97.19}\right) = 242\ \%$$

Next, an estimate for the bubble gas-transfer coefficient is determined.

$$R_r = \frac{v_b y_t}{\nu} = \frac{0.25(21.68)}{1.08 \times 10^{-6}} = 5.01 \times 10^6$$

where ν is the kinematic viscosity of water.

$$R = \frac{q_w}{\nu} = \frac{32.27}{1.08 \times 10^{-6}} = 2.99 \times 10^7$$

$$S_c = \frac{\nu}{D} = \frac{1.08 \times 10^{-6}}{2.00 \times 10^{-9}} = 541$$

where D is the diffusivity of air in water.

$$W_e = \frac{\rho_w {q_w}^2}{\sigma d_j} = \frac{1000(32.27)^2}{0.0712(2.11)} = 6.93 \times 10^6$$

where ρ_w is the density of water, and σ is the surface tension of water.

$$\phi = \frac{v_j \lambda}{v_j \lambda + q_w} = \frac{15.29(0.15)}{15.29(0.15) + 32.27} = 0.066$$

$$K_L a t_b = 2.46(0.066)\frac{(1 - 0.066)^{1/2}}{(1 - 0.066^{5/3})^{1/4}}(6.93 \times 10^6)^{3/5}(2.99 \times 10^7)^{0.55} \cdot$$

$$541^{-1/2}(5.01 \times 10^6)^{-1} = 0.223$$

Finally,

$$C_d = 242 - (242 - 109)\left[e^{-(0.223+0)} + \left(\frac{0}{0.223+0}\right)\cdot\left(\frac{242-100}{242-109}\right)\left(1 - e^{-(0.223+0)}\right)\right] = \mathbf{136\ \%}$$

The RMSE is 3.8% for the 1993 subset of scenarios and the results can be seen in Figure 16. These are not great results despite the fact that this model considers some physically meaningful parameters. Like the previous model the 2016 scenario was overestimated, this time by 14%. A possible improvement of this model, to make it more applicable to HLK, would be to treat the stilling basin and downstream river region separately. Since the flow patterns around the staggered end sills at HLK are likely to make the path of the bubble swarm uncertain and the estimation of a centroid very difficult, a single effective saturation concentration using the methods in this model at one location may not be the best approach.

This model, along with the parameters found through regression were tested to predict the values shown in Geldert et al. (1998). One of the dams in the literature, Ice Harbor, also had zero surface mass-transfer, therefore this dam will be used to test the model parameters found in this study. At a specific flow rate of 20 m^2/s, the resulting TDG downstream is approximately 134-135%. Using the operational parameters in the literature (FB_{ELEV} = 133.8m, TW_{ELEV} = 104.8m, y_t = 12.2m, C_u = 103.5%, and assuming P_{atm} = 101.325kPa), and the fitted parameters from Table 5 the resulting predicted TDG is 139%, a 4-5% overestimation and nearly within instrument uncertainty.

As described earlier, the University of Washington (2000) predictive model (Eq. 18) illustrates TDG generating mechanisms primarily driven by forebay TDG and basin geometry. The schematic diagram that defines the variables to be used in the model indicates the length of the stilling basin to be measured from the toe of the spillway. Since the stilling basin at HLK is a plunge pool with a tall end sill, the distance from the toe to the end sill is very short and in earlier models (Johnson and King, 1975) the length of the basin is taken as the distance from the plunge point at

the tailwater surface to the point at which the flow is driven upwards by the end sill. Therefore, this model was tested using both distances, estimated from the engineering drawings, as well as an intermediate distance taken as the horizontal distance from the top of the end sill to the spillway. The short and medium distances are different between SP1 and SP2-4. The long distance is the same between the two gate sets.

For estimating the equilibrium concentration, the model uses an empirical formula that is dependent on temperature, however, it was found that these values were very low compared to what was expected. Instead, Eq. 4 was used in the end to estimate equilibrium concentration. This also produced much better end results.

The entrainment coefficient K_e was estimated in three ways. It was first derived as the model was originally intended, which was to use the Gasspill 2 model to estimate a temperature corrected entrainment coefficient (K_{20}) and then K_e could be determined. This involved nonlinear regression to determine values for coefficients m, n, and l. The next attempt was to circumvent Gasspill 2 by determining a single K_{20} value to estimate K_e for each scenario. Finally, K_e itself became a fitted parameter to see if the measured TDG values could be described by a single entrainment coefficient. The Gasspill 2 model is defined as,

$$K_{20} = m + (nE) + (lC_u) \qquad \text{Eq. 22}$$

And,

$$E = \frac{Q_s}{LWy_t}(H_0 - y_t) - \left(\frac{Q_s}{y_t}\right)^3 \frac{1}{2gL} \qquad \text{Eq. 23}$$

where E is the energy loss rate, L is length of the basin (m), H_0 is the hydraulic head expressed as the vertical distance from the forebay elevation to the stilling basin floor (m), C_u is the forebay percent saturation, and m, n, and l are dam-dependent empirical coefficients. Finally, K_e is computed by,

$$K_e = K_{20}(1.028)^{(T-20)} \qquad \text{Eq. 24}$$

where K_e has units of m s^{-1} $Pa^{-1/3}$ and T is temperature (˚C).

It was found that the results did not change significantly for most iterations between different values of *L*. The model tests that resulted in the lowest RMSE were those of the 1993 subset of data and that used the Gasspill 2 model for determining K_{20} and K_e. The RMSE of these iterations is 2.8% (See Figure 17). The results of the dam-dependent coefficients *m*, *n*, and *l* are given in Table 7. There appears to be no physical basis for these coefficients, however.

The following calculations illustrate the predictive TDG model described in the University of Washington (2000) report.

$$P_{avg} = P_{atm} + \frac{\alpha_0 \rho_w g}{2}(y_t - d_j) + \frac{\rho_w g}{4}(y_t + d_j) \qquad \text{Eq. 25}$$

where P_{avg} is the average hydrostatic pressure in the stilling basin (Pa), P_{atm} is the barometric pressure (Pa), ρ_w is the density of water (1000 kg/m^3), g is the acceleration due to gravity, α_0 is the specific gravity of roller at base of spill, and depends on degree of aeration (assume unity), and d_j is the thickness of spillway jet at bottom of spillway (m).

$$d_j = \frac{Q_s}{W\sqrt{2gH_0}} = \frac{490.52}{15.2\sqrt{2(9.81)(6.26)}} = 1.26\ m \qquad \text{Eq. 26}$$

$$P_{avg} = 97190 + \frac{1000(9.81)}{2}(21.68 - 1.26) + \frac{1000(9.81)}{4}(21.68 + 1.26)$$

$$= 253618\ Pa\ or\ 253.6\ kPa$$

$$\Delta = \left(P_{avg} + \frac{\rho_w g}{4}(y_t + d_j)\right)^{1/3} - \left(P_{avg} - \frac{\rho_w g}{4}(y_t + d_j)\right)^{1/3} \qquad \text{Eq. 27}$$

$$\Delta = \left(253618 + \frac{1000(9.81)}{4}(21.68 + 1.26)\right)^{\frac{1}{3}}$$

$$- \left(253618 - \frac{1000(9.81)}{4}(21.68 + 1.26)\right)^{\frac{1}{3}} = 9.45\ Pa^{1/3}$$

$$E = \frac{490.52}{33.3(15.2)(21.68)}(33.6 - 21.68) - \left(\frac{490.52}{21.68}\right)^3 \frac{1}{2(9.81)(33.3)} = -17.20$$

$$K_{20} = 0.090 + [-0.001(-17.20)] + [-0.001(109)] = 0.025$$

$$K_e = 0.025(1.028)^{(16.9-20)} = 0.023\ \frac{m}{s\ Pa^{1/3}}$$

$$C_d = 28.3\left(\frac{253618}{101325}\right) - \left(28.3\left(\frac{253618}{101325}\right) - 30.86\right)e^{\left(-\frac{0.023}{490.52}15.2(33.3)(9.45)\right)}$$

$$= \mathbf{38.75\ mg/L\ or\ 137\%}$$

When the model values of the 1993 data subset with no SP1 is used to predict the 2016 scenario, the result is 137% TDG. The model did not perform any better than the model by Geldert et al. (1998) and overpredicted the 2016 scenario by 15%. This model utilizes less mass-transfer theory than the preceding model, namely its exclusion of anything approximating the bubble or surface mediated gas-transfer coefficients. However, it does focus on the geometry of the basin by including both the width and length of the basins over which bubble gas-transfer is most likely to dominate. It also focuses on the energy loss rate which is analogous to the amount of turbulence needing to be dissipated by the stilling basins.

As discussed in Chapter 2.5, consultants collected a number of TDG measurements at Hugh L. Keenleyside Dam in the early 1990's. These measurements were screened for errors and collated into a single database by Bruce and Plate (2013) and developed new models for predicting TDG at HLK in Bruce (2016). They utilize some physical parameters such as head above the spillway gates, tailwater depth, and Froude number, however, it simply attempts to correlate these parameters to the measured gate operations and therefore has a number of limitations. These limitations include uncertainty when using the model outside of the ranges of conditions that were tested to develop it and the lack of a physical or first-principal approach for its development does not allow for any physical interpretation of the results. The computation of variables in this model are slightly different than in other models presented in this section, therefore unique variable symbols were given for this model.

$$\text{if } H_g = FB_{elev} - \left(424.9 + 0.5\left(d_g\right)\right) \geq 6.30 \qquad \text{Eq. 28}$$

$$TDG(mmHg) = 10.84y_e' + 896.3 \quad \text{Eq. 29}$$

If $H_g < 6.30$

$$TDG(mmHg) = -37.395F_{r,TW} + 14.956H_s + 936.28 \quad \text{Eq. 30}$$

where d_g is the gate opening (m), H_g is the head above the gate at the center of the opening (m), y_e' is the tailwater depth at the end sill (approximate end sill height is 13 m), $F_{r,TW}$ is the Froude number at the tailrace surface immediately downstream of the spillway structure, and H_s is the forebay elevation minus the gate sill elevation (424.9 m). The following calculations show an example of using this model for scenario 2.

$$H_g = 433.50 - \big(424.9 + 0.5(4.65)\big) = 6.275m$$

$$y_e' = TW_{ELEV} - 399.9 - 13 = 421.58 - 399.9 - 13 = 8.68m$$

$$H_s = FB_{ELEV} - 424.9 = 433.50 - 424.9 = 8.60m$$

$$F_{r,TW} = \frac{v_{TR}}{\sqrt{gd_{TW}}} \quad \text{Eq. 31}$$

where V_{TR} is the water velocity at the tailrace surface below spillway (m/s). The velocity of the gate was estimated by taking the gate discharge and dividing it by the flow area.

$$v_{TR} = \sqrt{{v_g}^2 + 2g(424.9 - TW_{ELEV})} = \sqrt{(6.94)^2 + 2(9.81)(424.9 - 421.58)}$$

$$= 10.64m/s$$

and d_{TW} is the depth of the jet at the tailwater surface (m),

$$d_{TW} = d_g sin(30^\circ) = (4.65)sin(30^\circ) = 2.33m$$

$$F_{r,TW} = \frac{10.64}{\sqrt{9.81(2.33)}} = 2.23$$

$$TDG(mmHg) = -37.395(2.23) + 14.956(8.60) + 936.28 = \mathbf{981.5mmHg}$$

Barometric pressure was about 729 mmHg, therefore the percent supersaturation is 135%.

The RMSE for the 1993 subset of data is 4.2%, although one of the scenarios appears to be a potential outlier and if removed would greatly improve this error (Figure 18). When tested to predict the measurement of scenario 2 from July 2016, the model overestimates the measured value by 13%.

A final model to consider is one that more explicitly and separately computes the potential TDG generated in the stilling basin and the downstream river region. The approach by Urban et al. (2008) was a numerical model that applied a one-dimensional transport equation to a series of control volumes downstream of a dam spillway. There were three regions that were solved for, the jet expansion region, the return roller region, and the downstream river region where the jet broke the surface of the water. The benefits of this model are the inclusion of bubble size in the computation, the estimation of surface transfer $K_L a_s$ (instead of it being purely a fitted parameter), and the separation of the generation process into separate regions to account for changes in effective depth before and after the end sills. This model is modified and heavily simplified to be less numerical in nature so as to be more easily adapted to HLK and given the limited scope of the present work. It is hoped that the currently modified version of the model will be used to the benefit that it separates the stilling basin and river regions.

$$C_d = K_L a_b t_b (C_{se} - C_u) + K_L a_s t_s (C_s - C_u) + C_u \qquad \text{Eq. 32}$$

where, $K_L a_b$ is the bubble mass-transfer coefficient, t_b is the time over which bubble mass-transfer takes place (seconds), C_{se} is the effective saturation concentration (mg/L) within the region, $K_L a_s$ is the surface mass-transfer coefficient, t_s is the time over which surface mass-transfer takes place, C_u is the upstream TDG concentration (mg/L), this is either the forebay concentration, or the resulting TDG from the stilling basin region when computing the TDG for the river region.

Eq. 32 is applied to the stilling basin region first and is then computed for the river region, using the results from the stilling basin region as upstream inputs. The most

complicated part of the model is estimating the mass-transfer coefficients $K_L a_b$ and $K_L a_s$, as they include a number of fitted parameters unique to gates SP2-4.

$$K_L a_b = \beta_1 \frac{\phi(1-\phi)^{1/2} D^{1/2} \left(k^{1/2}\right)^{\eta}}{d_b (1-\phi^{5/3})^{1/4} (L_r)^{1-\eta} (\nu)^{\eta-1/2}} \quad \text{Eq. 33}$$

where β_1 is a fitted parameter, ϕ is the air-void ratio of the incoming air from the plunging jet or the resulting air-void ratio from the stilling basin region, D is the diffusivity of air in water (m^2/s), k is the turbulent kinetic energy per unit mass in the flow (here taken to be a fitted parameter), d_b is the bubble diameter (m) limited to the typical values 0.7 mm to 2.7 mm and is also a fitted parameter, L_r is the representative scale of turbulent eddies (m), and ν is the kinematic viscosity of water (m^2/s). Some of the above variables will be different between the stilling basin region and river region, to differentiate them the subscripts B and R will be used.

The representative eddy length L_r is computed as,

$$L_r = 0.62h \quad \text{Eq. 34}$$

where h is the depth over which mass-transfer takes place within the region (m), subscript b and s represent bubble mass-transfer and surface mass-transfer respectively. This depth is computed slightly differently between the basin region and the river region. For instance, $h_{b,B}$ is the depth over which bubble mass-transfer takes place in the basin region, it is simply taken as the tailwater depth y_t. In the river region, $h_{b,R}$ is computed as the tailwater elevation minus the river bed elevation for SP2-4 this is approximately 411 m. The time over which bubble mass-transfer takes place, t_b is estimated to be the h_b divided by the average velocity in the region.

The average velocity v_{avg} in the stilling basin region is computed as the average of the jet velocity v_j, and the velocity at the end sill, v_e.

$$v_e = \frac{q_w}{y_e} \quad \text{Eq. 35}$$

The average velocity in the river region will be the average of v_e and the velocity in the river v_R, taken to be,

$$v_R = \frac{q_w}{y_{t,R}} \qquad \text{Eq. 36}$$

The tailwater depth in the river region, $y_{t,R}$ is approximately the tailwater depth minus 411 m.

The stilling basin region air-void fraction is ϕ_B, once the basin region TDG ($C_{d,B}$) is computed, a new air-void ratio must be estimated for use within the river region ϕ_R. This new air-void ratio is calculated by

$$\phi_R = \phi_B - \frac{(C_{d,B} - C_u)}{1247 mg/L} \qquad \text{Eq. 37}$$

where 1247mg/L is the density of air at 15°C.

The surface mass-transfer coefficient $K_L a_s$ is calculated by,

$$K_L a_s = \beta_2 \left(\frac{1}{h}\right)\left(\frac{\nu}{D}\right)^{-1/2}\left(\frac{k^{3/2}\nu}{h}\right)^{1/4}\left[1 + \beta_3 (W_e F_t)^{\beta_4}\right] \qquad \text{Eq. 38}$$

where β_2, β_3, and β_4 are fitted parameters, W_e is the Weber number, and F_t is the turbulent Froude number.

$$F_t = \frac{k^{1/2}}{\sqrt{gh}} \qquad \text{Eq. 39}$$

An example of using this model is given below.

<u>SP3,4: Basin Region</u>

$$V_j = \sqrt{2g\Delta H} = 15.29\ m/s$$
$$d_j = \frac{Q_w}{V_j W} = 2.11\ m$$

where g = 9.81m/s^2 and W = 15.2 m

$$V_e = \frac{q_w}{y_e} = 3.76\ m/s$$

$$V_{avg,B} = \frac{V_j + V_e}{2} = 9.53\ m/s$$

$$K_L a_b = \beta_1 \frac{\phi(1-\phi)^{1/2} D^{1/2} \left(k^{1/2}\right)^{\eta}}{d_b (1-\phi^{5/3})^{1/4} (L_r)^{1-\eta} (\nu)^{\eta-1/2}}$$

where,
$\beta_1 = 4.94\text{x}10^{-5}$, $k = 1.42$, $\eta = 1.43$, $d_{b,B} = 0.00078$ m, $D = 2.0\text{x}10^{-9}$ m^2/s, $\nu = 1.08\text{x}10^{-6}$ m^2/s, $h_{b,B} = y_t = 21.68$ m, $L_r = 0.62 h_{b,B} = 13.44$ m, $t_{b,B} = h_{b,B}/V_{avg,B} = 2.28$ s

and, $K_L a_{b,B} = 0.10890$ s^{-1}

Eq. 17 was used to estimate the air entrainment downstream of the dam using $\lambda = 0.15$ m (Geldert et al., 1998). However, this value in the subsequent model did not produce accurate results and therefore a single air-void ratio was assumed for all cases, $\phi = 0.03$, which is a value used for spillways in the literature (Politano et al., 2011).

$$K_L a_s = \beta_2 \left(\frac{1}{h}\right)\left(\frac{\nu}{D}\right)^{-1/2}\left(\frac{k^{3/2}\nu}{h}\right)^{1/4}\left[1+\beta_3 (W_e F_t)^{\beta_4}\right] \qquad \text{Eq. 40}$$

where,
$\beta_2 = 14.16$, $\beta_3 = 1.19$, $\beta_4 = 0.25$, $h_{s,B} = y_t - d_j = 19.57$ m, $t_{s,B} = h_{s,B}/V_{avg,B} = 2.05$ s, $\sigma = 0.0712$ N/m

$$W_e = \frac{\rho_w k h_{s,B}}{\sigma} = 390303$$

$$F_t = \frac{k^{1/2}}{\sqrt{g h_{s,B}}} = 0.086$$

where $\rho = 1000$ kg/m^3

and, $K_L a_{s,B} = 0.00936$ s^{-1}

$$C_{d,B} = K_L a_b t_b (C_{se} - C_u) + K_L a_s t_s (C_s - C_u) + C_u = 37.05\ mg/L$$

SP3,4: River Region

$$\phi_R = \phi_B - \frac{(C_{d,B} - C_u)}{\frac{1247mg}{L}} = 0.0229$$

$$V_R = \frac{q_w}{y_{t,R}} = 3.05\ m/s$$

$$V_{avg,R} = \frac{V_e + V_R}{2} = 3.41\ m/s$$

$K_L a_{b,R} = 0.06860$ s^{-1}

where,
$d_{b,R}$ = 0.0007 m, $h_{s,R} = y_t - 411$ = 10.58 m, $t_{s,R} = h_{s,R}/V_{avg,R}$ = 3.11 s, $L_r = 0.62h_{b,R}$ = 6.56 m, $C_{se,R}$ = 44.52 mg/L, where P_t is calculated at a depth 2/3 of $h_{s,R}$.

$$W_e = \frac{\rho_w k h_{s,R}}{\sigma} = 211009$$

$$F_t = \frac{k^{1/2}}{\sqrt{g h_{s,R}}} = 0.117$$

$K_L a_{s,R}$ = 0.01878 s^{-1}

$$C_{d,R} = K_L a_b t_b \left(C_{se} - C_{d,B}\right) + K_L a_s t_s \left(C_s - C_{d,B}\right) + C_{d,B} = 37.98\ mg/L$$

Since C_s = 25.79 mg/L

$$TDG = \frac{C_d}{C_s} \times 100\% = \mathbf{147}\%$$

The maximum measured value was 122%. A 25% overestimation.

The model put forward by Urban et al. (2008) appears to predict TDG the best for the spillways (SP2-4) at HLK dam. The RMSE for this model is 1.5% which is acceptable when considering the instrument uncertainty. Compared to the model by Geldert et al. (1998), this approach to solving TDG between two separate regions (basin and river) appears to improve the predictions of the 1993 data subset, presumably because turbulence characteristics and large differences in hydrostatic pressure may be accounted for without resorting to averaging these variables.

Two bubble sizes were determined and this resulted in a stilling basin bubble size of 0.78 mm and a river region bubble size of 0.70 mm. The remaining coefficients determined from nonlinear regression are listed in Table 8. A significant limitation to this model is the estimate for turbulent kinetic energy *k*. This parameter was taken as a fitted value, limiting it to be constant for the entire structure. Naturally, this value will vary with distance from the spillway and with different operational conditions. Also, taking the bubble sizes to be a fitted parameter limits them from changing under different operational conditions. These values may be determined

within a numerical model but are perhaps not suited to be fitted in the way suggested here. Future, non-numerical models should consider other ways of handling changing bubble sizes and differences in turbulence between the stilling basin and river regions.

The results also indicated that the vast majority of the gas-transfer occurs in the stilling basin, which is not surprising as the depth of bubble plunging and the average flow velocity is greatest in this region. The surface mass-transfer is smaller than the bubble mass-transfer in both regions but it is more significant in the river region, this is caused by the upwelling of the flow of water over the stilling basin end sill. Without a conceptual CFD model or physical model to visualize potential flow patterns around the end sills and within the stilling basin, it may be difficult to determine appropriate points of analysis for simple models such as this one. Assumptions that would benefit further investigation are the depth at which the effective saturation concentration should be computed, the actual average flow velocity in the basin, and the potential impact velocity flow patterns may have on the residence time over a range of hydraulic operating conditions.

Although this model appears to predict the 1993 subset of data most accurately, it still greatly overpredicted the 2016 scenario by 25%. This is a much greater overprediction of scenario 2 in 2016 than that of the previously mentioned models. The trend of overestimation brings into question the quality of the measurement. One significant difference between the operating conditions of 1993 and 2016 is the addition of ALGS. Powerhouse flows would undoubtedly mix and dilute the high TDG concentrated waters from the spillways, but the scenario 2 measurement was conducted at a location believed to be unaffected by ALGS discharge. This does not seem to be the reason for the discrepancy in the model prediction and field observation.

One other reason is a zone of relatively slow moving water south of the boat lock at HLK. This zone resembles a very large eddy that perhaps delays the uptake in

TDG as a result of dam discharge. All scenarios were given at least 16.5 hours to stabilize before measurements were taken along the transects except for scenario 2, which had only 1.5 hours before the first measurement was taken. Perhaps 1.5 hours was not long enough to allow the river TDG readings to stabilize to a new gate configuration. The continuous monitoring station at M2 appears like it may have stabilized (being located within the tailrace) within the two-hour scenario, but further downstream on the right bank at 4.4 km, the high TDG measurements during scenario 2 only peaked and then fell, presumably once the two-hours had elapsed, indicating that if the scenario lasted longer, a further increase in TDG may have been recorded. Aspen Applied Sciences Ltd. (1995) discussed this when putting together a tabulated list of scenarios. They only included measurements from their continuous monitoring stations that had a single gate configuration for at least 12 hours.

In an effort to validate this particular model for TDG generation, measurements from 1994 were tested. These measurements were originally screened out of the database for reasons that included uncertainty around the accuracy of the discharge parameters, the method of instrument calibration, and general poor agreement with trends found with the larger 1993 dataset. However, a few of these measurements may be applied here to assess the goodness of fit with the present predictive model. These results are illustrated in Figure 19 and show a surprisingly good fit with the predicted values. These scenarios appear not to vary in TDG generation since they occurred within the same few days in late October 1994. This lack of operational variation is a weakness of this small data subset and they should be considered carefully, but it may provide a small degree of validation to the present model. The range of important parameters for these structures can be found in Table 9.

Since this model was based primarily on the method of Urban et al. (2008), an attempt was made to predict the results of that research paper using the parameters suggested here. The dam which was measured was Ice Harbor Dam and five scenarios were tested. The dam's operational conditions can be found in Urban et

al. (2008). For the five scenarios, only the two conditions with the smallest flow rates were predicted to within 4% of the measured value. The specific flowrates which defined the five scenarios were 4.55, 5.52, 7.41, 9.30, and 11.12 m^2/s, and the difference in predicted and measured TDG was 3, -1, -7, -13, and -16%, respectively. These poor predictions are not surprising as some of the parameters solved through regression in the current study would likely be usefull to HLK dam only, such as the turbulent kinetic energy, and bubble diameters. As discussed above, future, non-numerical models should avoid the assumption of a single turbulent kinetic energy value and bubble diameters that are unable to vary across different operational conditions.

It would appear that a more complete and accurate picture of the TDG generation downstream of HLK dam spillways remains partially unresolved. Therefore, it is believed that more detailed physical or numerical modeling will be required to better understand this problem.

4.5 Spillway Total Dissolved Gas Generation Trends

Another way to analyze the field measurements between 1993 and 2016 is to plot the change in TDG downstream against typical parameters that are known to increase TDG. This may shed some light on whether or not the 2016 spillway measurement may be considered a potential outlier.

Since it is well known that hydrostatic pressure plays a significant (if not the most significant) role in generating TDG, and the effective saturation concentration critical in TDG prediction is a function of the tailwater depth, ΔC is plotted against y_t in Figure 20. As one should expect, with an increase in tailwater depth, the measured TDG generation increases and shows very good agreement with the 1993 data subset. The measurement for scenario 2 however, appears to be an outlier compared to the other data points, showing a much smaller ΔC even though it has the deepest tailwater of all scenarios. Typically, an increase in unit discharge is also accompanied by an increase in TDG. This is because greater discharges tend to

increase the plunging depth of bubbles in the stilling basin (See Figure 21). It is difficult to perfectly separate the impacts of discharge from tailwater depth, however. This is because each scenario was tested days apart in most cases and therefore increases in discharge for the same tailwater depth were not tested, such as incrementally increasing the gate opening of a particular spillway bay over the course of a single day or two, where the tailwater may have fluctuated very little. Figure 22 indicates that an increase in unit discharge is tightly correlated with an increase in tailwater depth, this makes it difficult to determine to what degree tailwater depth and unit discharge independently have on TDG generated. In any case, it is expected that either an increase in tailwater depth or unit discharge or both would lead to an increase in TDG as a result of an increase in hydrostatic pressure acting on the submerged bubbles.

Since the majority of the TDG generation occurs in the stilling basin, it is expected that an increase in $K_L a t_{b,B}$ would also show an increase in measured ΔC. Indeed, this is what Figure 23 illustrates. Likewise, Figure 24 illustrates that an increase in $K_L a t_{s,B}$ shows a decrease in ΔC. Both trends are tightly correlated to the measured field data of 1993 but both do not indicate a good fit with scenario 2.

If the 2016 measurement is set aside for the moment, a few important points can be concluded from the preceding discussion about TDG generation at HLK dam as a consequence of spillway operation. The first is that predictive models from the literature, which are not entirely numerical in nature, may not estimate TDG very well. One reason for this is stated to be the impact of the complicated stilling basin geometry which deviates from the stilling basins of those dams in the literature. This would result in the importance of accurately estimating the level of turbulence, bubble retention time, and bubble size within the basin. These complex parameters may be best reflected in a computational fluid dynamics model.

Another conclusion is that the downstream river region plays an important role in accurately predicting TDG at HLK dam. The model by Geldert et al. (1998)

attempted to make this clear by incorporating the river region into the prediction, however, it would appear that the estimation of a single effective saturation concentration cannot capture accurately enough the spatial variability in saturation concentration at depth at HLK, probably due to the rapidly changing geometry between the stilling basin and river regions since the end sills are so close to the toe of the dam. Since there are large differences (geometrically and hydraulically) between the stilling basin and river regions only a short distance from HLK dam, treating them separately is a better way to predict downstream TDG, as evidenced in Section 4.4. It is also important to note that the elevations used for the river region in calculating variables such as the average river velocity and effective depth were estimated from the engineering drawings (Figure 5 and Figure 6). These may not be accurate elevations to assume since the river bathymetry has likely changed over time, especially if plunging flow patterns are observed downstream of the end sills causing scour. These elevations may also vary laterally across the different stilling basins and may not be applied for a significant distance downstream in the river, these represent further uncertainties.

Chapter 5: Low-Level Outlet TDG Generation

5.1 Low-Level Operating Gates

From the field work campaign of 2016 at Hugh L. Keenleyside Dam, a few important questions need to be investigated. Namely, what is the air entrainment mechanism in the low-level outlets and why do the southern low-level outlets generate significantly more total dissolved gas than their northern counterparts?

Compared to scenario 2, scenario 3 had three southern low-level outlets in operation, a slightly smaller total discharge of 934.8 m^3/s resulted in a maximum TDG of 122% measured at the same 0.6 km transect. It measured higher (124%) slightly upstream of that location. This is an interesting occurrence since the mechanism for air entrainment around the low-level outlets is not obvious. If air is indeed entrained, as these measurements clearly suggest, it might be easy to understand why such a large degree of TDG generation occurs, since these air bubbles (if entrained upstream of the conduit outlet) would enter the stilling basin near the bottom and therefore be exposed to the greatest amount of hydrostatic pressure instantly. Another phenomenon occurs after comparing the results of scenarios 1 and 3. Scenario 1 (which consisted of NL2-4) generated a maximum TDG level of 112% (measured at M2, spot measurements indicate 111%), this level of TDG generation was accomplished with a higher flow rate than that of scenario 3 and results in downstream TDG barely higher than background forebay supersaturation. The northern and southern low-level outlets are similar structures in principle but there are geometrical differences in their stilling basins that may account for the difference in ability to generate TDG (assuming that the air entrainment mechanism is the same between them).

Bruce (2015) discuss three possible scenarios for air entrainment at these closed-conduit structures; 1) vortices form in the reservoir drawing in air from the atmosphere into the conduit, 2) air is entrained around the gate slot within the conduit because these gate slots are open to atmosphere and there are no other forced air vent structures, and 3) entrainment against the face of the dam as a result

of turbulent return rollers at the tailwater surface. It was estimated that mechanisms 1 and 3 were unlikely to occur over the range of normal operating conditions at HLK which suggested that air was likely entrained into the flow via the gate slot. Total dissolved gas measurements were conducted in the early 1990's (Klohn-Crippen Integ, 1994) and airflow measurements were taken near the gate hoist house of the low-level outlets to validate concerns over pulsating air movement when certain gate openings were used. As per the local operating order of the time, the gates were to be either fully open or opened in the range of 0 – 4.9 m to avoid vibration of the gates. The report of Klohn-Crippen Integ (1994) shows that operations outside of these ranges resulted in slug-flows of air that clearly validated the operating restrictions that were imposed. The air-flow measurements showed that for normal operations the potential for entrained air is the same between the northern and southern low-level outlets (pressure fluctuations in the hoist house were about +/- 0.10 lb/in^2, or 0.69 kPa). If the amount of air entrained at the gates is the same between the two sets of outlets for a given operating condition, then it stands to reason that the difference in TDG generated downstream would be a consequence of the difference in geometry of the stilling basins.

The stilling basin design at HLK is complicated and not a typical forced hydraulic jump-type basin. The varying elevations of stilling basin floors and end sills is a result of the dam being built to conform to the bedrock foundation and therefore the resulting basin geometry between the northern low-level outlets and southern low-level outlets is significantly different. Table 1 summarizes the geometries of these outlets and Figure 7 and Figure 8 display the engineering drawings of the structures.

What these differences amount to is that the southern low-level outlets discharge into a tailwater 8.2 m shallower than the northern outlets at most. This parameter alone would make one suggest that the southern low-level outlets would dissolve smaller amounts of air as a result of a reduced tailwater depth, of course, the measurements contradict this analysis and therefore other factors must be

important. Another likely important parameter is the height of the end sills since the end sills in the southern basins top out at an elevation 11.9 m higher than the northern sills, there is far less distance above them to the water surface. With a shallower and more closed-off stilling basin, the southern low-level outlets may produce much more turbulent flow conditions, what this means for TDG generation is that there may be larger shear forces causing entrained air bubbles to break up into smaller sizes, increasing the surface area available for gas-transfer to occur. It is also possible that if stronger return roller conditions exist, bubble retention times may be increased which would allow for more gas to be dissolved under hydrostatic pressure. This increase in turbulence of course likely extends to the surface and therefore promotes degassing.

With regard to retention time, Urban et al. (2008) explained that the shorter residence time as a result of greater velocities in the stilling basins was overcome by the increase in turbulence causing bubbles to shear to smaller sizes and increase TDG on net.

If overall turbulence is much smaller in the northern stilling basins it is possible that any entrained air bubbles are able to quickly rise to the surface and contribute less to TDG downstream despite being subjected initially to greater hydrostatic pressures. All of these factors contribute in complicated ways and therefore it is believed that a more detailed physical or numerical model will be required to better understand this problem.

5.2 Estimating Low-Level Outlet Air Entrainment

If the primary mechanism for air entrainment is through the gate slots, as would be indicated by the discussion by Bruce (2015) as well as the investigation by Klohn Crippen (2001) into the potential for cavitation in the low-level outlets, then the air flow rate may be estimated in the same way as Klohn Crippen (2001). An equation developed by the USACE relating the Froude number and water flow rate in the low-level outlet to the air flow rate from the gate slot is given by Eq. 21. This

equation was used by Klohn Crippen (2001) to estimate the air demand in the low-level outlets for gate openings of 5.79 m and 7.32 m. The air flow rate was typically between 6 – 8% of the water flow rate and ranged from 37.5 m^3/s to 44.6 m^3/s. Whether this is a realistic estimate of air demand or not will be discussed in a later section.

To estimate the Froude number just downstream of the gate, a similar approach was taken as Klohn Crippen (2001), where the energy grade line at the gate is assumed to be the forebay elevation minus the inlet head losses (here the head losses will be assumed to be zero for simplicity). The velocity head (h_v) is calculated by subtracting the gate lintel elevation (top of gate slot - 416.47 m for the southern outlets and 416.87 m for the northern outlets - and is the assumed maximum water surface elevation in the conduit) from the energy grade line elevation. The apparent jet depth is then estimated by the following equation,

$$d_j = \sqrt{\frac{{Q_w}^2}{2gh_vW^2}} = \frac{Q_w}{v_jW} \qquad \text{Eq. 41}$$

where d_j is the contracted depth of the jet just downstream of the gate (m), h_v is the velocity head (m), W is the width of the conduit (6.092m), and g is the acceleration due to gravity (m/s^2). The estimated air flow rate and air-void fractions for the 1990's dataset and for the 2016 scenarios can be found in Table 10 to Table 12.

The air-void fractions for the northern low-level outlets range from 2 – 10%, and for the southern low-level outlets from 4 – 5%. The limited range of the southern low-level outlet scenarios is understandable when it is considered that there are far fewer data points in the southern low-level outlet database and the range of tested discharges was also smaller.

5.3 Dimensional Analysis of Low-Level Outlets

Certainly, the complex two-phase flow downstream of the low-level outlets and spillways makes developing a predictive equation challenging and so many

attempts at developing such an equation for HLK dam have resulted in mostly empirically based models. These models are developed using some form of regression analysis where the variables required are determined by trial and error correlation. These variables are related to TDG generation in the form of polynomial equations (Klohn-Crippen Integ, 1994; Aspen Applied Sciences Ltd., 1995).

These correlating variables can, however, be used to gain insight into potentially important hydraulic and operational conditions on the generated TDG. To this end, it may be useful to undertake a dimensional analysis of pertinent variables at HLK to come up with a list of dimensionless parameters that can be tested against TDG generation. Instead of taking a trial and error approach to coming up with correlating parameters, the variables chosen for analysis are based on an understanding of the current literature and physical properties of HLK in particular. Variables included in the analysis are the tailwater depth (y_t), incoming jet velocity (v_j), density of water (ρ_w), differential head (ΔH), height of the end sill (h_e), depth of water above the end sill (y_e), head above the gate (H_g), average velocity in the stilling basin (v_{avg}), air demand (Q_a), surface tension of water (σ), dynamic viscosity of water (μ), and the acceleration due to gravity (g).

$$\Delta C = f\left(y_t, v_j, \rho_w, \Delta H, h_e, y_e, H_g, v_{avg}, Q_a, \sigma, \mu, g\right) \qquad \text{Eq. 42}$$

where y_t, v_j, and ρ_w are the repeating variables. The Buckingham-Pi theorem was used to result in the following 9 Pi-parameters:

$$\Pi_1 = \frac{\Delta H}{y_t}, \quad \Pi_2 = \frac{h_e}{y_t}, \quad \Pi_3 = \frac{y_e}{y_t},$$
$$\Pi_4 = \frac{H_g}{y_t}, \quad \Pi_5 = \frac{v_{avg}}{v_j}, \quad \Pi_6 = \frac{Q_a}{{y_t}^2 v_j}, \qquad \text{Eq. 43}$$
$$\Pi_7 = \frac{\sigma}{y_t {v_j}^2 \rho_w}, \quad \Pi_8 = \frac{\mu}{y_t v_j \rho_w}, \quad \Pi_9 = \frac{g y_t}{{v_j}^2}$$

Figure 25 to Figure 33 displays how the change in TDG concentration correlates with each parameter. R-squared values are for 1990's data only.

Clearly, some trends exist between TDG generation, most parameters that correlate well, correlate differently for the southern low-level outlets and the northern low-level outlets.

The most strongly correlated parameter is Π_6. It also appears to predict ΔC equally well between north and south low-level outlets. Oddly enough, it would appear that a small increase in tailwater depth will have a significant decreasing effect on TDG. This is contrary to Figure 34 which shows that, at least for the southern low-level outlets, a small increase in tailwater depth will have a significant increase in TDG. Clearly, this multivariable problem cannot be boiled down to trends of single variables since the system overall is so complex and dynamic. The tailwater depth is not an adequate predictor of TDG for the northern low-level outlets. Figure 35 indicates a strong correlation with increasing specific discharge with increasing TDG generation for the southern low-level outlets, as was the case for the spillways. There is a weak trend in the other direction with regards to the northern low-level outlets however which is perhaps too weak to draw any conclusions from. There are also a number of data points with the same specific discharge which appears to diminish the goodness of fit.

One of the immediate drawbacks of older predictive models developed by regression analysis and correlating parameters is that they do not perform adequately when testing scenarios outside the operational parameters the model was developed with. Plotting the 2016 TDG measurements for scenarios 1, 3, 5, and 6 indicate that Π_6 is a good predictor of all scenarios in the database, regardless of operational changes made since the commissioning of ALGS.

The goodness of fit with this parameter against ΔC illustrates the importance of the interplay between tailwater depth and air demand in the low-level outlets. Other variables that are implicitly included in this parameter are the forebay elevation, water flow rate (Q_w), and jet thickness (d_j) downstream of the gate.

5.4 Models for Predicting Downstream Total Dissolved Gas

Predictive models for downstream total dissolved gas have been proposed for a number of dams, early models primarily influenced by the work of Roesner and Norton (1971) and Johnson and King (1975). These equations as well as the following equations developed by other authors discussed in Chapter 2 are models based on the gas-transfer process with a number of fitted parameters unique to each dam and/or structure. Virtually all of these models have been tested downstream of dam spillways and none have been applied to closed-conduit structures. The only exception was discussed by Gulliver et al. (1998) in which it was concluded that none of the transfer efficiency formulas presented predicted downstream dissolved oxygen with acceptable accuracy. Some of the models discussed in Chapter 4 were applied to HLK low-level outlet structures in hopes of gaining insight into the dissolved gas generation mechanisms and to explain the difference between the north and south structures.

Bruce (2016) presented equations for north and south low-level outlet TDG generation. This model utilizes some physical parameters such as tailwater depth and Froude number, however, it simply attempts to correlate these parameters to the measured gate operations and therefore has a number of limitations as discussed earlier. It also lacks the ability to compare generation mechanisms from northern outlets to southern outlets. Figure 36 shows the prediction results for the 1990's dataset and scenarios 1, 3, 4, 5, and 6. The model is as follows;

NL2-4: $$dP_{TW} = 1.1511 dP_{FB} + 11.051 F_{r,G} - 10.129 \quad \text{Eq. 44}$$

SL5-7: $$dP_{TW} = 1.1511 dP_{FB} + 11.051 F_{r,G} + 54.825 y_t - 986.67 \quad \text{Eq. 45}$$

where dP_{TW} is the difference in TDG (mmHg) between the tailwater and the barometric pressure, dP_{FB} is the difference in TDG (mmHg) between the forebay and the barometric pressure, and $F_{r,G}$ is the Froude number at the gate.

For scenario 5, the contribution to TDG by the northern low-level outlet gates NL3,4 would be as follows;

$$dP_{FB} = C_u - P_{atm} = 1.09(750) - 750 = 67.5mmHg$$

$$F_{r,G} = \frac{v_g}{\sqrt{g d_g}} = \frac{10.78}{\sqrt{9.81(4.23)}} = 1.67$$

The velocity of the gate was estimated by taking the gate discharge and dividing it by the flow area.

$$dP_{TW} = 1.1511(67.5) + 11.051(1.67) - 10.129 = 86.0mmHg$$

$$C_d = \frac{86.0 + 750}{750} \times 100 = \mathbf{111}\%$$

The contribution to TDG by the southern low-level outlet gates SL5,6 would be as follows;

$$F_{r,G} = \frac{v_g}{\sqrt{g d_g}} = \frac{11.11}{\sqrt{9.81(4.10)}} = 1.75$$

The tailwater depth, y_t is 21.77m,

$$dP_{TW} = 1.1511(67.5) + 11.051(1.75) + 54.825(21.77) - 986.67$$
$$= 303.9mmHg$$

$$C_d = \frac{303.9 + 750}{750} \times 100 = \mathbf{141}\%$$

Finally an average downstream TDG weighted by discharge where the discharge per gate for NL3,4 and SL5,6 is 277.85 m^3/s and 277.4 m^3/s, respectively is;

$$C_d(mixed) = \frac{(111)(277.85)(2) + (141)(277.40)(2)}{\big((277.85)(2) + (277.40)(2)\big)} = \mathbf{126}\%$$

The RMSE for the northern low-level outlets is 1.11% and 1.09% for the southern low-level outlets. These are very good results for the 1990's database, of course, this is strongly a regression-based model and its limitations become apparent when predicting scenario 3 in 2016. The model overpredicts TDG by 15%. This is because scenario 3 is outside of the range of operational parameters of the 1990's dataset. The specific discharge is 4.65 m^2/s higher than the largest specific discharge in the past and the forebay elevation is 5.86 m higher than what was in the past. A good model should be able to predict TDG outside the range of the 1990's dataset because it should be rooted in first-principles. Scenario 1, on the

other hand, is within the range of the old dataset most of the time (except for NL4), and therefore is predicted to within instrument uncertainty.

TDG is estimated for each gate in scenarios 4, 5, and 6, and the percent supersaturation values are weighted by discharge to determine the final average TDG generated. Scenario 4 is predicted to have TDG = 143%, scenario 5 TDG = 126%, and scenario 6 TDG = 117%. It would appear that any scenario that consists of southern low-level outlets is likely to be overestimated. There are only eight data points from which the model for southern low-level outlets is derived from and therefore has a large degree of uncertainty associated with it. Overall, this most current model developed for HLK specifically does not adequately predict current TDG generation.

Li et al. (2009) developed a model for predicting TDG downstream of a very high dam in China that spilled its water as a jet into a plunge pool. This plunge pool is formed by a second downstream dam. The model developed utilized a dimensionless parameter from USACE (2005) that is the ratio of the height of the second dam to the head of water above the second dam, raised to the power of 3/2.

This model is a two-stage model in which the first stage is the increase in TDG as a result of the large tailwater depth in the plunge pool. The second stage is the TDG release stage as the pressure quickly and greatly decreases as the water passes over top of the second dam. Two fitted parameters are required, one for the correction of the plunge pool pressure, and one for the TDG release factor near the second dam. It was thought that this 'two dam' model could be applied to the low-level outlet basins because the end sills, in effect, act as second dams in which the water is forced upward into a zone of lower hydrostatic pressure. No good results were obtained by using this model, however, and no correlation between the USACE dimensionless parameter and percent TDG was found.

Since the working hypothesis is that the primary difference in TDG generation downstream of the low-level outlets is a result of the different flow conditions within and perhaps directly downstream of the stilling basins, the model suggested by Geldert et al. (1998) was adopted to the use of these structures. The air entrainment was estimated with Eq. 17 reducing the number of fitted parameters. The final values for the fitted parameters are listed in Table 13. A very good RMSE was achieved for the 1990's dataset considering north and south low-level outlets separately, 0.32% for southern low-level outlets and 1.28% for northern low-level outlets. The average RMSE for all scenarios is 1.13%. Using Table 4, Table 6, and Table 13 the prediction for scenario 5 is as follows;

Northern low-level outlets NL3,4:

$$h_v = FB_{elev} - gate\ lintel\ elevation = 433.38 - 416.47 = 16.91m$$

$$v_j = \sqrt{2g(h_v)} = \sqrt{2(9.81)(16.91)} = 18.21\ m/s$$

$$d_j = \frac{q_w}{v_j} = \frac{45.61}{18.21} = 2.50\ m$$

$$d_{eff} = h_{c1}\left[exp\left(1 - \frac{\beta X_{1/2}}{L}\right)\right] + h_{c2}\left[1 - exp\left(1 - \frac{\beta X_{1/2}}{L}\right)\right] for\ \frac{\beta X_{1/2}}{L} > 1$$

$$\text{And, } d_{eff} = h_{c1}\ for\ \frac{\beta X_{1/2}}{L} \leq 1$$

where, h_{c1} is the centroid about the water surface (effective depth) in the stilling basin, h_{c2} is the centroid about the water surface in the river region, $X_{1/2}$ is the bubble half-life, and L is the length of the expanding jet region, simply assumed to be the basin length (37.1m for the northern outlets and 37.5 for the southern outlets).

$$X_{1/2} = -\frac{q_w}{v_r} ln(0.5) = -\frac{45.61}{0.25} ln(0.5) = 126.46m$$

$$\frac{\beta X_{1/2}}{L} = \frac{1.00(126.46)}{37.1} = 3.41$$

$$h_{c1} = \frac{2}{3} y_t = \frac{2}{3}(29.97) = 19.98m$$

$$h_{c2} = \frac{2}{3}(TW_{elev} - river\ bottom) = \frac{2}{3}(421.67 - 392) = 19.78m$$

$$d_{eff} = 19.98[exp(1-3.41)] + 19.78[1-exp(1-3.41)] = 19.80m$$

Now the effective saturation concentration may be solved using Eq. 12.

$$C_{se} = 100\left(1 + \frac{19.80(9.81)}{99.99}\right) = 294\ \%$$

Next, an estimate for the bubble gas-transfer coefficient is determined.

$$R_r = \frac{v_b y_t}{\nu} = \frac{0.25(29.97)}{1.08 \times 10^{-6}} = 6.94 \times 10^6$$

$$R = \frac{q_w}{\nu} = \frac{45.61}{1.08 \times 10^{-6}} = 4.22 \times 10^7$$

$$S_c = \frac{\nu}{D} = \frac{1.08 \times 10^{-6}}{2.00 \times 10^{-9}} = 541$$

$$W_e = \frac{\rho_w {q_w}^2}{\sigma d_j} = \frac{1000(45.61)^2}{0.0712(2.50)} = 6.91 \times 10^6$$

The air-void fraction will be estimated with Eq. 20 and Eq. 21.

$$F_r = \frac{v_j}{\sqrt{g d_j}} = \frac{18.21}{\sqrt{9.81(2.50)}} = 3.68$$

$$Q_a = 0.03(277.85)(3.68-1)^{1.06} = 23.70 m^3/s$$

$$\phi = \frac{23.70}{23.70 + 277.85} = 0.0785$$

From Eq. 16,

$$K_L a t_b = 0.15(0.0785)\frac{(1-0.0785)^{\frac{1}{2}}}{\left(1-0.0785^{\frac{5}{3}}\right)^{\frac{1}{4}}}(6.91 \times 10^6)^{\frac{3}{5}}(4.22 \times 10^7)^{0.55} 541^{-\frac{1}{2}} (6.94 \times 10^6)^{-1} = 0.014$$

From Eq. 15,

$$C_d = 294 - (294-109)\left[e^{-(0.014+0)} + \left(\frac{0}{0.014+0}\right)\cdot\left(\frac{294-100}{294-109}\right)\left(1 - e^{-(0.014+0)}\right)\right] = 112\ \%$$

<u>Southern low-level outlets SL5,6:</u>

$$h_v = FB_{elev} - gate\ lintel\ elevation = 433.38 - 416.97 = 16.41m$$

$$v_j = \sqrt{2(9.81)(16.41)} = 17.94\ m/s$$

$$d_j = \frac{45.54}{17.94} = 2.54\ m$$

$$X_{1/2} = -\frac{45.54}{0.25} ln(0.5) = 126.26m$$

$$\frac{\beta X_{1/2}}{L} = \frac{1.47(126.26)}{37.5} = 4.95$$

$$h_{c1} = \frac{2}{3}(21.77) = 14.51m$$

$$h_{c2} = \frac{2}{3}(421.67 - 411) = 7.11m$$

$$d_{eff} = 14.51[exp(1 - 4.95)] + 7.11[1 - exp(1 - 4.95)] = 7.25m$$

Now the effective saturation concentration may be solved by using Eq. 12.

$$C_{se} = 100\left(1 + \frac{7.25(9.81)}{99.99}\right) = 171\ \%$$

Next, an estimate for the bubble gas-transfer coefficient is determined.

$$R_r = \frac{v_b y_t}{\nu} = \frac{0.25(21.77)}{1.08 \times 10^{-6}} = 5.03 \times 10^6$$

$$R = \frac{q_w}{\nu} = \frac{45.54}{1.08 \times 10^{-6}} = 4.21 \times 10^7$$

$$S_c = \frac{\nu}{D} = \frac{1.08 \times 10^{-6}}{2.00 \times 10^{-9}} = 541$$

$$W_e = \frac{\rho_w {q_w}^2}{\sigma d_j} = \frac{1000(45.54)^2}{0.0712(2.54)} = 7.10 \times 10^6$$

The air-void fraction will be estimated with Eq. 20 and Eq. 21.

$$F_r = \frac{17.94}{\sqrt{9.81(2.54)}} = 3.60$$

$$Q_a = 0.03(277.40)(3.60 - 1)^{1.06} = 22.88 m^3/s$$

$$\phi = \frac{22.88}{22.88 + 277.40} = 0.0762$$

From Eq. 16,

$$K_L a t_b = 0.14(0.0762)\frac{(1 - 0.0762)^{\frac{1}{2}}}{\left(1 - 0.0762^{\frac{5}{3}}\right)^{\frac{1}{4}}}(5.03 \times 10^6)^{\frac{3}{5}}(4.21$$

$$\times 10^7)^{0.75} 541^{-\frac{1}{2}} (7.10 \times 10^6)^{-1} = 0.550$$

From Eq. 15,

$$C_d = 171 - (171 - 109)\left[e^{-(0.550+0.200)} + \left(\frac{0.200}{0.555+0.200}\right)\cdot\left(\frac{171-100}{171-109}\right)\left(1 - e^{-(0.550+0.200)}\right)\right] = \mathbf{132\ \%}$$

Taking a weighted average using the discharge of each set of gates yields a final TDG of 122%**.** This number is a 6% overestimate for the entire scenario.

For the 2016 scenarios Figure 37 shows good predictions of measured values, however, the results of the southern low-level outlets poorly agree and overestimate the measured values by several percent (10% for scenario 3). Large overestimations of the southern low-level outlets are characteristic of using this model and only by taking a weighted average of south and north outlet TDG generation do scenarios 5 and 6 produce acceptable results. One potential reason for this is the fact that the tailwater levels between the 1990's dataset are on average, 2.48 m shallower than in 2016 as a result of ALGS commissioning. What this means is that due to a shallower tailwater depth in the stilling basins, turbulence may have been higher in the past than in 2016. The fitted parameters impacting the level of turbulence, namely η may be too high to accurately depict 2016 scenarios. This would lead to an overestimation of bubble mass-transfer coefficients and subsequently TDG. The southern low-level outlets are likely going to be much more sensitive to changes in tailwater level because of how shallow those levels already are relative to the northern stilling basins. A small change in tailwater depth may have a significant impact on the true value of η.

Considering each fitted parameter may offer some insight into the differences between north and south outlet structures, each parameter will be discussed in turn. The parameter β represents a correction factor between the effective depths of the basin region and the river region. This value is large when a significant amount of bubbles remains in the flow beyond the stilling basin. It was discussed earlier that this value is expected to be between 1.00 and 3.30. Holding these limits and solving for this parameter simultaneously with the others produced a value of 1.00 for the

northern outlets and 1.47 for the south. This would indicate that more bubbles are likely to remain in the flow beyond the end sills of the southern stilling basins and contribute to TDG generation in the river.

The parameter η is the power to which the Reynold's number is raised and represents the degree of turbulence in the basin. The values as earlier discussed were held between 0.55 and 0.75. These limits were reached by both north and south outlets but on either end of the limit. The northern low-level outlets have a value of 0.55 and the southern outlets a value of 0.75, indicating the southern low-level outlets are more turbulent, this is in fact what has been observed, both in the the 1990's and in 2016. This is the biggest reason why the average bubble mass-transfer coefficient in the southern outlets is higher than the average value in the northern outlets, 0.278 and 0.011 respectively.

There is also a difference in surface mass-transfer coefficients between north and south. The value of $K_L at_s$ for the northern low-level outlets is 0.00 and for the southern low-level outlets, it is 0.20. This would indicate that surface mass-transfer is more important in the southern basins, and negligible in the northern basins. As has been observed during the field work, much more surface turbulence was found during operations of the southern low-level outlets. With greater surface turbulence comes the greater potential for degasification. Although this would theoretically reduce TDG in the southern basins, there still appears to be a net increase in downstream TDG.

Finally, these comparisons are meaningful because of two reasons. First, the air entrainment is estimated in the same way between both north and south outlets. This assumes that there is an equal chance for entraining air through the gate shaft for a given operational condition. Secondly, the final fitted parameter α is very nearly the same between both north and south low-level outlets, 0.15 and 0.14 respectively. These values have no physical meaning and no upper and lower limit is placed on them in the literature. Estimating air entrainment in the same manner

and coming up with similar α values allows for a more accurate account of the potential hydraulic reasons behind the differences in TDG generation.

The disadvantages of this model are the same as discussed for the spillways and include the fact that it takes a single effective depth to compute the dissolved gas for the entire scenario and does not consider the river region and basin region separately. Flow patterns are likely to be different between the stilling basin and the downstream river, residence times and levels of turbulence are likely going to be very different. Another disadvantage is the inability to estimate surface mass-transfer on a physical basis and instead uses it as a fitted parameter.

Since there is a poor prediction of the southern low-level outlets and there is uncertainty about its application to closed-conduits in general, it may not be a significant improvement over using Bruce (2016) for prediction purposes. This model does give some insight into important considerations for future models of these structures, namely the impact of the downstream river region on TDG generation and the different degrees of turbulence that can manifest in either stilling basin.

5.5 A Proposed Model for TDG Prediction

The prediction of total dissolved gas downstream of Hugh L. Keenleyside Dam has been challenging using previously developed models primarily created for spillway operations. There have been some good results mathematically, but it would appear that an explanation for the differences in TDG generation between the northern and southern low-level outlets could be addressed further. A better understanding of the flow conditions within the basins and the immediate downstream river would be useful to further hypothesize on the exact mechanism distinguishing the two sets of structures. Building upon what has been concluded from the preceding prediction models, namely that a downstream component to TDG generation is important, an idealized form of the model put forward by Urban et al. (2008), modified for the low-level outlets will be presented, similar to the spillway model discussed above.

One of the major differences between the north and south low-level outlets indicated by the previous model was the degree to which the downstream river region impacted the final concentration of TDG. It appears at first glance that the downstream river region is not a significant factor for the northern low-level outlets but it is in the southern low-level outlets. This was illustrated by the difference in surface mass-transfer coefficients $K_L a t_s$ and the factor correcting for the difference between the basin and river regions effective depth, β. With these things in mind it may be assumed that although bubbles will likely remain in the flow beyond the northern stilling basin end sill, they will not likely contribute much to TDG, therefore, in the computation of a river region effective depth, 2/3 of the total river depth may be too deep to estimate an effective saturation concentration and point of gas dissolution. It may be more likely that if any bubbles reach the end sills in the northern stilling basins that they quickly rise to the surface. In this new model, the effective depth in the river region of the northern low-level outlets will be considered from the top of the end sill. For the southern low-level outlets, where the downstream river region appears important for both surface mass-transfer and effective depth computation, the total depth of the river will be considered.

Consider Figure 38 and Figure 39, these figures represent the basis for a new model for TDG generation that will be based upon the model for TDG prediction by Urban et al. (2008). For the present analysis, a modification and simplification of this model will be used to estimate TDG downstream of the low-level outlets in hopes of also explaining the difference between north and south low-level outlet TDG generation.

As per Figure 38 and Figure 39, the model will be separated into two regions, the stilling basin region, and the downstream river region, separated by the end sills. The benefits of this model are the inclusion of bubble size in the computation, the estimation of surface mass-transfer $K_L a_s$ (instead of it being purely a fitted parameter), and the separation of the generation process into two regions to account

for differing hydraulic conditions on either side of the stilling basin end sills. This follows from Eq. 32 to Eq. 39.

Eq. 32, as in the spillway model, is applied to the stilling basin region first and is then computed for the river region, using the results from the stilling basin region as upstream inputs. Mass-transfer coefficients $K_L a_b$ and $K_L a_s$ will be complicated to estimate because they include a number of fitted parameters unique to each set of low-level outlets, this is because the flow conditions between the two sets of structures are different.

In Eq. 34 this depth is computed slightly differently between the basin region and the river region, and differently between the northern and southern sets of outlets. For instance, $h_{b,B}$ is the depth over which bubble mass-transfer takes place in the basin region and is estimated the same way in the basin region of both structures, it is simply taken as the tailwater depth y_t. In the river region, $h_{b,R}$ is computed as the tailwater elevation minus the river bed elevation for the southern low-level outlet structures (411 m). This is because, from the previously discussed model, the river depth plays a significant part in TDG generation downstream of the southern basins. For the northern low-level outlets, $h_{b,R}$ is computed by taking the tailwater elevation minus the top of the end sill (401.1 m) this is because it is assumed that the bubble mass-transfer would not take place any deeper than approximately the elevation of the top of the end sill since there is little impact on the downstream river region on TDG generation relative to what takes place downstream of the southern basins. The time over which bubble mass-transfer takes place, t_b is estimated to be h_b divided by the average velocity in the region.

The average velocity v_{avg} in the stilling basin region is computed as previously stated and where the width W_B is approximately 11 m. The average velocity in the river region will be the average of end sill velocity $v_{e,}$ and the velocity in the river v_R, as before. The tailwater depth in the river region, $y_{t,R}$ is approximately the tailwater depth minus 392 m for the northern region and 411 m for the southern

river region. All other parameters in the model are estimated in the same way as described for the spillways in Chapter 4.

The results of using this model for predicting TDG downstream of the low-level outlets is promising. The results are shown in Figure 40, the range of important parameters are listed in Table 14 and the fitted parameters are in Table 15. The overall RMSE for this model is 1.14% (0.76% for north outlets and 1.87% for south outlets), which is a very good result and the predictions for the 2016 scenarios are within instrument uncertainty.

The model results in Table 14 and Table 15 support some concepts hypothesized about the flow conditions downstream of the low-level outlets. Consider the northern low-level outlets, the bubble mass-transfer coefficients are larger in the river than in the basin, this is largely because the bubble sizes in the river are smaller than in the basin region. Bubbles that are smaller are more likely to remain in the flow, and since there are larger residence times in the relatively slower moving water in the river region the net increase in TDG is larger in the river than in the stilling basin. This is in addition to the larger air-water contact area increasing the rate of gas-transfer. The surface mass-transfer coefficient is larger in the river region as a result of a shallower depth considered in the mass-transfer process, because the difference between the incoming stilling basin TDG and the saturation concentration is small, the surface mass-transfer does not play a significant role in degassing the basin-generated TDG. A test of sensitivity can be applied by setting the fitted parameter β_4 to zero. This parameter represents the degree to which surface curvature of the region plays a part in degassing TDG. Doing this has a negligible impact on the final results for the northern low-level outlets and supports the observation that the water surface downstream of the northern low-level outlets is relatively calm.

The southern low-level outlets perform quite differently than the northern low-level outlets. The stilling basin bubble mass-transfer coefficient is significantly higher

than in the river region, this is because of the very small bubble sizes in the basin and a relatively large value for η, which is a measure of the turbulence in a rising bubble plume (Urban et al., 2008). Since the bubble mass-transfer coefficient is so large, there is a significant net increase in TDG within the stilling basin, and although the surface mass-transfer coefficient is large as well, the difference between the upstream TDG and the saturation concentration in most scenarios is small. Within the river region, however, things are quite different. The surface mass-transfer coefficient is very large compared to the bubble mass-transfer and this drives a significant degassing process. The significance of mass-transfer becomes obvious in the southern river region because of the large increase in TDG within the basin region. This creates a large difference between the incoming TDG and the saturation concentration in the atmosphere, surface curvature and turbulence allow mass-transfer to take place at an accelerated rate. This would also be obvious by a visual inspection of the water surface in this region, see Figure 41. This net loss of TDG in the river region is not enough, however, to offset the TDG increase from the stilling basin, resulting in an overall net increase in TDG.

Considering the fitted parameters η and k (associated with the general turbulence of the bubble plume and stilling basin and river regions) are both larger for the southern low-level outlets, it makes sense that the bubble mass-transfer coefficients for both regions are significantly larger for the southern low-level outlets than the northern outlets. This results in smaller bubbles associated with the southern stilling basins. One strange result is the presence of larger bubbles in the river region of the southern low-level outlets. The bubble size is on the large side of the constraint and is larger than both the bubble sizes associated with the stilling basin and with the northern low-level outlets. One possible explanation is that larger bubbles are able to be contained within the flow of the river as a result of a relatively strong plunging flow pattern. Another potential reason is that due to strong surface turbulence larger bubbles are present in the river region but do not significantly contribute to TDG generation because they are not plunged to great depths and do not have large residence times. Forcing this bubble size to the small end of the constraint and

equating it with the same size as the bubbles within the river region of the northern low-level outlets or with the size in the southern outlet stilling basins makes no large difference in the final results of the model, indicating again, that the surface transfer in the river region of the southern low-level outlets is the primary component driving mass-transfer.

Overall, this model and the results it has generated predict TDG at HLK dam with the best accuracy (as measured by the RMSE) of any model modified for this purpose. It also allows for an explanation of the causes of TDG generation from the low-level outlets and describes the differences between the northern and southern low-level outlets in a way that agrees with field observations. The limits of this model obviously include the empirical nature of these types of problems. There is no way around simplifying the mechanisms of TDG generation around hydropower dams and although because of this empiricism, the model with the same determined fitted parameters may not be applicable to other structures because of the different flow patterns, it provides for an explanation of how closed conduits may generate significant levels of TDG without the same plunging jet that is typical of spillways. Example calculations for scenario 5 using the above model are given below.

NL3,4: Basin Region

$$h_v = FB_{elev} - 416.47 = 16.91\ m$$

$$v_j = \sqrt{2gh_v} = 18.21\ m/s$$

$$d_j = \frac{Q_w}{v_j W} = 2.50\ m$$

where g = 9.81m/s^2 and W = 6.092m

$$F_r = \frac{v}{\sqrt{gd_j}} = 3.68$$

$$Q_a = 0.03Q_w(F_r - 1)^{1.06} = 23.66\ m^3/s$$

$$\phi_B = \frac{Q_a}{Q_a + Q_w} = 0.0785$$

$$v_e = \frac{Q_w}{y_e W_B} = 1.23\ m/s$$

where W_B = 11.0m

$$v_{avg,B} = \frac{v_j + v_e}{2} = 9.72\ m/s$$

$$K_L a_b = \beta_1 \frac{\phi(1-\phi)^{1/2} D^{1/2} \left(k^{1/2}\right)^{\eta}}{d_b (1-\phi^{5/3})^{1/4} (L_r)^{1-\eta} (\nu)^{\eta-1/2}} = 0.00028 \mathrm{s}^{-1}$$

where,

$\beta_1 = 3.0\text{x}10^{-5}$, $k = 1.27$, $\eta = 1.12$, $d_{b,B} = 0.0027$ m, $D = 2.0\text{x}10^{-9}$ m^2/s, $\nu = 1.08\text{x}10^{-6}$ m^2/s, $h_{b,B} = y_t = 29.97$ m, $L_r = 0.62 h_{b,B} = 18.58$ m, $t_{b,B} = h_{b,B}/v_{avg,B} = 3.08$ s

$$K_L a_s = \beta_2 \left(\frac{1}{h}\right)\left(\frac{\nu}{D}\right)^{-1/2} \left(\frac{k^{3/2}\nu}{h}\right)^{1/4} \left[1 + \beta_3 (W_e F_t)^{\beta_4}\right] = 0.00150 \mathrm{s}^{-1}$$

where,

$\beta_2 = 10.61$, $\beta_3 = 0.92$, $\beta_4 = 0.16$, $h_{s,B} = y_t - d_j = 27.47$ m, $t_{s,B} = h_{s,B}/v_{avg,B} = 2.83$ s, $\sigma = 0.0712$ N/m

$$W_e = \frac{\rho_w k h_{s,B}}{\sigma} = 489249$$

$$F_t = \frac{k^{1/2}}{\sqrt{g h_{s,B}}} = 0.069$$

where $\rho_w = 1000$ kg/m^3

$$C_{d,B} = K_L a_b t_b (C_{se} - C_u) + K_L a_s t_s (C_s - C_u) + C_u = 28.23\ mg/L$$

NL3,4: River Region

$$\phi_R = \phi_B - \frac{(C_{d,B} - C_u)}{\frac{1247 mg}{L}} = 0.0784$$

$$v_R = \frac{Q_w}{y_{t,R} W_B} = 0.851\ m/s$$

$$v_{avg,R} = \frac{v_e + v_R}{2} = 1.04\ m/s$$

$$K_L a_b = \beta_1 \frac{\phi(1-\phi)^{1/2} D^{1/2} \left(k^{1/2}\right)^{\eta}}{d_b (1-\phi^{5/3})^{1/4} (L_r)^{1-\eta} (\nu)^{\eta-1/2}} = 0.00105 \mathrm{s}^{-1}$$

where,

$d_{b,R}$ = 0.0007 m, $h_{s,R} = y_t - 401.1 = 20.57$ m, $t_{s,R} = h_{s,R}/v_{avg,R} = 19.8$ s, $L_r = 0.62 h_{b,R}$ = 12.75 m, $C_{se,R}$ = 61.31 mg/L; where P_t is calculated at a depth 2/3 of $h_{s,R}$

$$W_e = \frac{\rho_w k h_{s,R}}{\sigma} = 366411$$

$$F_t = \frac{k^{1/2}}{\sqrt{g h_{s,R}}} = 0.079$$

$$K_L a_s = \beta_2 \left(\frac{1}{h}\right)\left(\frac{\nu}{D}\right)^{-1/2} \left(\frac{k^{3/2}\nu}{h}\right)^{1/4} \left[1 + \beta_3 (W_e F_t)^{\beta_4}\right] = 0.00212 \mathrm{s}^{-1}$$

$$C_{d,R} = K_L a_b t_b \left(C_{se} - C_{d,B}\right) + K_L a_s t_s \left(C_s - C_{d,B}\right) + C_{d,B} = 28.81\ mg/L$$

SL5,6: Basin Region

$$h_v = FB_{elev} - 416.97 = 16.41\ m$$

$$v_j = \sqrt{2 g h_v} = 17.94\ m/s$$

$$d_j = \frac{Q_w}{v_j w} = 2.54\ m$$

$$F_r = \frac{v_j}{\sqrt{g d_j}} = 3.60$$

$$Q_a = 0.03 Q_w (F_r - 1)^{1.06} = 22.88\ m^3/s$$

$$\phi_B = \frac{Q_a}{Q_a + Q_w} = 0.0762$$

$$v_e = \frac{Q_w}{y_e W_B} = 2.91\ m/s$$

$$v_{avg,B} = \frac{v_j + v_e}{2} = 10.43\ m/s$$

$$K_L a_b = \beta_1 \frac{\phi(1-\phi)^{1/2} D^{1/2} \left(k^{1/2}\right)^{\eta}}{d_b (1-\phi^{5/3})^{1/4} (L_r)^{1-\eta} (\nu)^{\eta-1/2}} = 0.15760 \mathrm{s}^{-1}$$

where,

$\beta_1 = 2.3\text{x}10^{-5}$, $k = 1.49$, $\eta = 1.33$, $d_{b,B} = 0.0008$ m, $D = 2.0\text{x}10^{-9}$ m^2/s, $\nu = 1.08\text{x}10^{-6}$ m^2/s, $h_{b,B} = y_t = 21.77$ m, $L_r = 0.62h_{b,B} = 13.50$ m, $t_{b,B} = h_{b,B}/V_{avg,B} = 2.09$ s

$$W_e = \frac{\rho_w k h_{s,B}}{\sigma} = 402214$$

$$F_t = \frac{k^{1/2}}{\sqrt{g h_{s,B}}} = 0.089$$

$$K_L a_s = \beta_2 \left(\frac{1}{h}\right)\left(\frac{\nu}{D}\right)^{-1/2}\left(\frac{k^{3/2}\nu}{h}\right)^{1/4}\left[1 + \beta_3 (W_e F_t)^{\beta_4}\right] = 0.07551\text{s}^{-1}$$

where,

$\beta_2 = 19.46$, $\beta_3 = 1.61$, $\beta_4 = 0.39$, $h_{s,B} = y_t - d_j = 19.23$ m, $t_{s,B} = h_{s,B}/v_{avg,B} = 1.84$ s, $\sigma = 0.0712$ N/m

$$C_{d,B} = K_L a_b t_b (C_{se} - C_u) + K_L a_s t_s (C_s - C_u) + C_u = 39.44\ mg/L$$

SL5,6: River Region

$$\phi_R = \phi_B - \frac{(C_{d,B} - C_u)}{\frac{1247 mg}{L}} = 0.0672$$

$$v_R = \frac{Q_w}{y_{t,R} W_B} = 2.36\ m/s$$

$$v_{avg,R} = \frac{v_e + v_R}{2} = 2.64\ m/s$$

$$K_L a_b = \beta_1 \frac{\phi(1-\phi)^{1/2} D^{1/2}\left(k^{1/2}\right)^{\eta}}{d_b (1-\phi^{5/3})^{1/4} (L_r)^{1-\eta} (\nu)^{\eta - 1/2}} = 0.003023\text{s}^{-1}$$

where,

$d_{b,B} = 0.0027$ m, $h_{s,R} = y_t - 411 = 10.67$ m, $L_r = 0.62h_{b,R} = 6.62$ m, $t_{s,R} = h_{s,R}/V_{avg,R} = 4.04$ s, $C_{se,R} = 44.23$ mg/L; where P_t is calculated at a depth 2/3 of $h_{s,R}$

$$W_e = \frac{\rho_w k h_{s,R}}{\sigma} = 223147$$

$$F_t = \frac{k^{1/2}}{\sqrt{g h_{s,R}}} = 0.119$$

$$K_L a_s = \beta_2 \left(\frac{1}{h}\right)\left(\frac{\nu}{D}\right)^{-1/2}\left(\frac{k^{3/2}\nu}{h}\right)^{1/4}\left[1+\beta_3(W_e F_t)^{\beta_4}\right] = 0.14076\mathrm{s}^{-1}$$

$$C_{d,R} = K_L a_b t_b\left(C_{se} - C_{d,B}\right) + K_L a_s t_s\left(C_s - C_{d,B}\right) + C_{d,B} = 32.27\ mg/L$$

Final Downstream TDG:

Assuming complete mixing of southern and northern low-level outlet discharge in the tailrace.

$$C_d(mixed) = \frac{(28.81)(277.85)(2) + (32.27)(277.40)(2)}{\left((277.85)(2) + (277.40)(2)\right)} = \mathbf{30.54\ mg/L}$$

$$TDG = \frac{C_d}{C_s} \times 100\% = \mathbf{118}\%$$

The maximum measured value was 116%. A 2% overestimation is within instrument uncertainty (+/- 4%).

Another point of discussion is the contribution to TDG by the river region. It has been discussed above that there is likely the potential for TDG generation to occur downstream of the stilling basins. As a result, an effort was made to separate these regions to produce better results for TDG prediction. Separating the regions at the end sill is a natural place to do this since it is the location where the flow is driven upwards, in some cases it may be that this brings bubbles from the deeper part of the stilling basins to the surface where little bubble-mediated gas-transfer will take place. Depending on the specific flow conditions around the end sills it may also mean that the surface turbulence just downstream of the end sills is significant, such as is the case for the southern low-level outlets. This surface turbulence, coupled with the upward movement of water that is greatly supersaturated may preclude a significant degassing process immediately downstream of the stilling basin. If significant amounts of TDG are generated as a result of substantial turbulence and small bubble sizes within the stilling basin, then a turbulent surface and the upward movement of this high TDG water may also greatly reduce the previously generated TDG. Surface-mediated gas-transfer would also be significant due to the large concentration difference between the supersaturated water and the atmosphere.

This is what the present model would suggest is occurring around the southern low-level outlets.

It is difficult to validate the magnitude of the stilling basin TDG generation and the subsequent river region degassing. However, the process of TDG generation and subsequent reduction is not unlikely to occur, given the visual observations in the field. Ideally, insitu TDG measurements would be taken within both regions to better understand this mechanism.

5.6 Sources of Uncertainty for Low-Level Outlet TDG Prediction

Although the preceding model for predicting TDG downstream of the low-level outlets at HLK dam has been shown to produce very acceptable results, it relies on a certain number of assumptions regarding air entrainment and gas dissolution that should be considered further. This discussion will highlight certain sources of uncertainties that may have to be addressed in further research on this topic.

5.6.1 Uncertainty Regarding Air Entrainment

First, the assumption of the air entrainment mechanism should be investigated further to determine the degree of confidence one has in applying Eq. 21. It has been discussed that the most likely source of air entrainment is through the gate shafts of the closed-conduits because they are open to the atmosphere during operation, in part to reduce potential cavitation damage. Since ALGS was going to be constructed at HLK dam, Klohn-Crippen Integ (1994) and Klohn Crippen (2001) investigated the impact on air velocity and pressure fluctuations during low-level outlet operation at some different differential heads. There were concerns raised from workers in the hoist rooms of the gate shafts regarding strong changes in air velocity and pressure during some gate operations. They conducted measurements during gate opening, and gate closing. From measurements taken, a range of gate openings was identified (approximately 75-94% open) that was associated with strong fluctuations of air velocity and pressure. In some cases, this would cause geysers to occur within the gate shafts and the gallery windows would bend. Further

use of the low-level outlets would avoid these openings, leaving the range of potential operations to be about 0-75% open, or fully open.

Eq. 21 was applied to the limits of the "problem zone" of gate openings to estimate air demand for cavitation potential. It was noted that little air movement was experienced outside of this range of gate openings. This may imply that the use of Eq. 21 may actually overestimate air demand in the low-level outlets during typical use. Almost all scenarios used in the development of the predictive models avoided this range of gate openings.

Other estimates for air entrainment exist beyond the equation used here, many are listed in Zounemat-Kermani and Scholz (2013), including the model used in this work. The ones that apply to air demand in closed-conduits assume the formation of a hydraulic jump filling the conduit, where the air demand of the jump is the driving force behind air entrainment downstream. In a situation like at HLK dam in 2016, there is a fairly significant amount of tailwater above the gate lintel that may prevent a hydraulic jump from forming within the conduit and leaving a free surface within the outlet to draw air from. It may be likely that the conduit remains flowing full most of the time and air entrainment is very limited, this would also reduce the applicability of Froude number and hydraulic jump-based air-demand equations of the type used in the preceding models.

It still stands to reason that some form of air entrainment must be present in the stilling basins of the outlets in order for TDG to increase to levels observed during operations of gates SL5-7. There is also no significant difference in air demand between north and south gate shafts as measured by Klohn-Crippen Integ (1994). Although it would appear that air entrainment potential at the tailwater surface is greatest in the southern stilling basins it is unclear if it would be possible to move the entrained air from the surface of the basin to a depth where gas dissolution might take place.

Considering the equations for air demand in a closed-conduit by Kalinske and Robertson (1943), Sharma (1976), and Escarameia (2007), which are included in the paper by Zounemat-Kermani and Scholz (2013), Figure 42 and Figure 43 were developed. They show the measured dissolved gas concentration of the 1990's data set plotted against the air-void fraction, which was estimated with the air demand computed by the equations of the previously mentioned authors as well as the USACE (1980). There is a large range of potential air-void fractions for a given scenario. The range in data may indicate the fact that at least some of these models were derived from scale models of circular conduits vs rectangular conduits.

The northern low-level outlet generated TDG correlates very well with each model, however, the southern low-level outlets do not. Why exactly, is difficult to determine, although the limited number of southern low-level outlet scenarios may certainly be a factor. It may also be the general lack of applicability of these models to the southern low-level outlets. Further research should consider accurate measurements of air flow for operational conditions occurring now that ALGS has been commissioned so as to update the earlier air flow measurements conducted in the 1990's. Physical models would also provide important insight into the hydraulic conditions within the closed-conduits themselves that could lead to the conclusion that these models for air demand do or do not apply to the low-level outlets at HLK dam.

5.6.2 Uncertainty Regarding Gas Dissolution Rate

The second point of uncertainty which follows that of the estimation of air entrainment is the gas dissolution rate. Specifically, the amount of gas that is dissolved for a given operational scenario relative to the amount of air that is entrained.

From Table 4, scenario 3 from 2016 generated ΔC = 3.95 mg/L, and the estimated air-void ratio for those gate positions and hydraulic conditions is ϕ = 0.0708. If the density of air is roughly 1247 mg/L (at 15˚C), and it is assumed that the same mass

of dissolved gas was in the gaseous phase, the minimum air-void fraction that would need to be achieved and completely dissolve to account for the 3.95 mg/L increase in TDG would be,

$$\phi_d = \frac{3.95 mg/L}{1247 mg/L} = 0.00322$$

where ϕ_d is the air-void fraction of dissolved gas. Therefore, the fraction of dissolved gas to entrained air is,

$$Efficiency = \frac{\phi_d}{\phi} = \frac{0.00317}{0.0708} = 0.0448 \; or \; 4.48\%$$

This indicates during scenario 3, 4.48% of entrained air inside the conduit was dissolved by some mechanism. This increase of dissolved gas is what was measured for that scenario (*TDG* = 124%). Table 10 and Table 11 list the ranges of efficiencies for the north and south low-level outlets. The average efficiency to dissolve gas in the north low-level outlet stilling basins is 0.58%, and 5.22% in the southern stilling basins.

The above analysis is computed using Eq. 21 for air entrainment estimates. Obviously, this value of efficiency would vary greatly depending on the model by which air entrainment is calculated.

If one considers the measurements of Klohn-Crippen Integ (1994), the average air velocity in the gate shafts varies from about 1 – 5 ft/s over the range of gate openings tested in the 1990's data set and in 2016. The typical values are usually on the lower end, say 2 ft/s or 0.61 m/s. The measurements were taken with a hot-wire anemometer and only recorded positive values. These measurements were taken at the top of the gate slot, the exact location of the top of the gate slot is uncertain given the available engineering drawings. The only area associated with air movement in the hoist rooms described in the report by Klohn Crippen (2001) is 3 m^2 for a louvered air vent within the viewing gallery for each outlet. This would yield an air flow rate of around 1.83 m^3/s.

This estimate of air entrainment is significantly smaller than the estimates calculated using Eq. 21. Such a discrepancy certainly needs to be addressed. Considering this smaller value for air entrainment a new air-void fraction for scenario 3 would follow,

$$\phi = \frac{Q_a}{Q_a + Q_w} = \frac{1.83}{1.83 + 311.50} = 0.0058$$

The efficiency for this scenario would now become 55.5%.

To estimate varying levels of gas dissolution, a simplified approach will be taken to explore the many different variables that may impact the degree to which the entrained air in any given scenario may be dissolved.

Taking the numerical form of Eq. 8 and only considering bubble mass-transfer, the change in dissolved gas concentration may be described by;

$$\frac{\Delta C}{\Delta t} = K_L a_b (C_{se} - C_s)$$

To simplify the estimation of the mass-transfer term $K_L a_b$, the liquid mass-transfer coefficient and the specific area will be solved separately using equations found in the literature. From Politano et al. (2017),

$$K_L = \frac{2D{P_b}^{0.5}}{d_b}\left[1 - \frac{2}{3\left(1 + 0.09{R_b}^{2/3}\right)^{0.75}}\right] \qquad \text{Eq. 46}$$

where P_b is the bubble Peclet number.

If it is assumed that the bubble diameter is 1mm;

$$P_b = \frac{v_b d_b}{D} = \frac{0.25(0.001)}{2.00 \times 10^{-9}} = 125000$$

$$R_b = \frac{v_b d_b}{\nu} = \frac{0.25(0.001)}{1.08 \times 10^{-6}} = 231$$

$$K_L = \frac{2DP_b}{d_b}\left[1 - \frac{2}{3\left(1 + 0.09{R_b}^{2/3}\right)^{0.75}}\right] = 1.103 \times 10^{-3} m/s$$

For the specific area, an equation by Gulliver et al. (1990),

$$a = 6.49\frac{\phi}{d_b} \qquad \text{Eq. 47}$$

To test whether or not an efficiency of 55.5% dissolution is reasonable, the air-void fraction of 0.0058 will be used.

$$a = 6.49\frac{\phi}{d_b} = 6.49\frac{0.0058}{0.001} = 37.6m^{-1}$$

The bubble mass-transfer rate $K_L a_b$ is now,

$$K_L a_b = 1.103 \times 10^{-3}(37.6) = 0.0415s^{-1}$$

From Table 4, the effective saturation concentration for scenario 3 is 63.93 mg/L and the saturation concentration is 25.82 mg/L, and assuming that the effective saturation concentration remains constant over the residence time of the bubble, our expression for the gas dissolution rate becomes,

$$\frac{\Delta C}{\Delta t} = 0.0415(63.93 - 25.82) = 1.58\frac{mg/L}{s}$$

At the above rate of dissolution, it would require only 2.5s of residence time to dissolve the measured 3.95 mg/L of TDG during scenario 3. If the air-void ratio is increased to the estimated 0.0708, then the time required to achieve the measured TDG is only 0.2s. Figure 44 indicates the dramatic increase in gas dissolution rate for a diminishing bubble size (holding the air-void fraction constant at 0.0058). This is especially true for bubble sizes less than 1mm. Similarly, Figure 45 indicates a sharp decrease in the amount of time required to dissolve the 3.95 mg/L of air for an increase in air-void fraction, that is, an increase in surface area available for mass-transfer.

Given the great sensitivity to gas dissolution for varying bubble sizes and air-void fractions, especially within the range of smaller air-void fractions and bubble sizes, it does not seem unreasonable for the southern low-level outlets to dissolve gas at such a high rate, even at the very low levels of air entrainment measured in the Klohn-Crippen Integ (1994) report. Combined with potentially varying bubble residence times between north and south low-level outlet stilling basins, the problem of TDG prediction becomes very complicated very quickly. Numerical

models in the literature are capable of inputting distributions of bubble sizes as well as computing the spatially varied air-void fractions and effective saturation concentrations, yet all models rely on some degree of fitted parameters to match the empirical equations to observed levels of TDG in the field.

The residence time of a bubble is a difficult parameter to estimate since bubbles are unlikely to move in a simple upward trajectory and may, in fact, remain in the flow for significant amounts of time if trapped in return rollers. Since the pressure acting on the entrained air is not constant as it moves throughout the stilling basin, the gas dissolution rate is also not a constant value over time and space. The 124% TDG measured during scenario 3 certainly took more than a couple of seconds to manifest 300 m downstream. Although, looking at the M2 TDG probe measurements in Figure 12 illustrates just how quickly an increase in TDG can occur very near the structures themselves. The very simplified estimates of gas dissolution presented in this section capture the degree to which dissolved gas generation is sensitive to air-void fractions.

Using constant values of air-void fractions for all scenarios for the purpose of predicting TDG did not yield reasonable results for the models discussed above. Using models of air entrainment based on the Froude number that resulted in smaller air demand values, also did not predict TDG well. In most cases, the smaller air-void fractions made it difficult to converge onto a solution that would produce the fitted parameters required for prediction. Since the nonlinear regression is so sensitive to initial conditions and it has been shown that the rate of gas dissolution is also sensitive to small air-void fractions, it stands to reason that more efficient or complex methods of solving these predictive equations are required, such as true numerical models.

Given the uncertainties described in the above sections, it is believed that although absolute values for air entrainment may be inaccurate, the relative difference in the

north and south low-level outlet's ability to dissolve the entrained air may still be adequately discussed given the results of the model in section 5.5.

Chapter 6: Conclusions and Recommendations

The primary purpose of this study has been to quantify the mechanisms of total dissolved gas generation at Hugh L. Keenleyside Dam near Castlegar, British Columbia along the Columbia River. A secondary challenge was to investigate and explain the apparent difference in the dissolved gas generation between two sets of low-level outlet structures. The first stage of implementation of this effort was the collection of field measurements during the summer of 2016, next, a collection of historical data was sifted through to create a comprehensive database of dam operations and the resulting dissolved gas generation downstream. The analysis was then conducted on the various field observations to confirm the previous reports of TDG measurement of this dam indicating the degree to which TDG generation differed between north and south low-level outlet structures. The validity of a number of TDG prediction models was tested for their applicability to HLK dam's unique stilling basin geometry and modifications were made where necessary to improve the ability of these models. Finally, the results of these models were assessed to address the low-level outlets ability to dissolve gas under certain conditions and a discussion regarding the potential air entrainment mechanism was put forward to test the reasonableness of the estimates.

6.1 Conclusions

During the summer of 2016, six operational scenarios at HLK dam were tested for TDG generation. These field observations required the placement of TDG probes at several stations along the Columbia River to record continuously. Spot measurements were also taken during most scenarios to quantify the spatial variability of TDG at a particular location. The maximum measured TDG, measured along the right bank of the river was used as the value to test predictive models against. Only one scenario was conducted that involved spillway discharge, this scenario was of a much shorter duration than the others and this was described as a potential reason for the poor predictability of the tested models to estimate the measured TDG. It was found that scenario 3 generated the most TDG (124%), this operation included SL5,6,7 discharging a total of 934.50 m^3/s. In contrast to

scenario 1, in which three northern low-level outlets, NL2,3,4, discharged 1024.82 m^3/s and generated only 112% TDG. Clearly, there is greater potential for the southern low-level outlets to generate TDG.

The database used was a collection of scenarios from the earlier reports and provided calibration sets for the various models tested. For spillway predictive models, good results were depicted by the adaptation of the model by Urban et al. (2008). The 1993 data subset was predicted with a root-mean-square-error of 1.5%, however, the 2016 scenario was greatly overestimated as was typical in all model predictions. Using a small subset of data from 1994, showed that this model also provided a good prediction for those scenarios as well, although they appear to be of a very similar operation and therefore not much variability in TDG generation is likely to be seen. More work on HLK dam's spillways may be required to develop a more accurate model portraying the important hydraulic parameters within its unique stilling basin geometry.

Following the partial success of the modified model applied to the spillways, the low-level outlet scenarios were best predicted by a model which took into account the stilling basin region and river region separately. Since the end sills are tall, staggered, and near the outlets themselves, complicated flow patterns are likely to arise that are distinct in the stilling basin and immediately downstream in the river. Following the literature, it becomes important to recognize that bubbles are likely to remain within the flow and contribute to TDG beyond the stilling basins, therefore accounting for this potential is critical in accurately depicting the TDG generation process. This appears to be particularly true for HLK dam and it would appear that this approach is the only way to get a good sense for why the southern low-level outlets generate more TDG than the northern low-level outlets.

It was concluded that smaller bubbles would likely be found in the southern stilling basins as a result of the larger degree of turbulence and that the larger degree of turbulence is likely due to the geometry of the basin. These smaller bubbles would

generate a significantly larger amount of TDG than the northern basins. Surface mass-transfer was more significant in the river region of the southern basins as well and would make sense because of the observed surface turbulence during these scenarios as evidenced in the field. The surface mass-transfer does not keep the southern outlets from generating more TDG than the north, however. The downstream river region for the northern outlets plays a much less significant role as a result of a much less turbulent surface, bubbles are therefore much more likely to quickly rise to the surface and not contribute much to TDG generation.

There are a number of limitations to the models described above. Most of these limitations and uncertainties come from the lack of measured hydrodynamic data near the stilling basins. This is difficult to remedy because of the dangerous conditions that exist within the basins and tailrace of dams. Specifically, information regarding the turbulent kinetic energy and bubble sizes would be required to better calibrate the models. In future models it may be more beneficial to introduce proxy variables for turbulence that can be better justified than the fitting of an actual value for k. As a result, the models proposed for the spillways and low-level outlets, are most useful for scenarios existing at HLK dam and are likely not applicable to other dam sites, because the turbulence characteristics would lead to different values for k and likely different bubble sizes. The values of the parameters determined for structures at HLK dam are of similar magnitudes to those same parameters found in the literature and provides some justification for their use but further validation should be pursued through more focused field work or experimental efforts.

6.2 Recommendations

Since the validation for the spillway prediction models is not very strong, and the single 2016 scenario is in doubt, more measurements during spillway operations are recommended for future model development. Beyond simply gathering more field data, a physical model identifying the flow patterns within the stilling basins and end sills would be very useful. There may be significant flow patterns such as

return rollers and plunging flow immediately downstream of the end sills that would impact both the residence times of the bubbles entrained as well as the hydrostatic pressure that would act on them to dissolve gas. These processes can only be accounted for by presenting the models with fitted parameters that attempt to match some empirically derived equation with the prototype situation. Complementing the physical models should be computational fluid dynamics models to validate the flow patterns and could therefore confidently be used when the natural next step would be to introduce the air phase into the flow and begin TDG prediction.

Much about what could be done to further the research at HLK spillways could be said for the low-level outlets. Flow patterns of the submerged jets are likely to be different from those of a plunging spillway jet, and therefore should also be considered in a physical and computational fluid dynamics model. On top of the flow pattern analysis of these structures, the exact quantification of air entrainment should also be studied in the field with more rigour. It has become obvious that the proper identification of the exact mechanism by which air is entrained into the stilling basins is of critical importance, and that whether the assumption that the same amount of air is actually entrained between both north and south outlets is true. If it is true, as discussed in the present work, it is likely a function of the basins geometry and downstream river regions that explain the difference in TDG generation. The next step would be to confirm the air flow measurements taken in the 1990's. Since the commissioning of ALGS slight differences in the flow patterns may be observed as a result of an increased tailwater elevation (at least as was the case in 2016). These differences may have a strong impact on the hydraulics within the low-level outlets and perhaps only small changes in air entrainment have occurred, but as previously discussed, this may be all that is required to increase TDG to a significant degree.

Overall, TDG prediction remains to be a challenging endeavour at HLK dam. It is suggested here that current models from the literature may be simplified and

modified to produce acceptable prediction results that may aid in the understanding of the mechanisms that drive TDG generation, particularly in the low-level outlets. For the reason that each dam and energy dissipator creates unique flow patterns, it remains difficult to provide a comprehensive prediction model without a significant amount of field investigation prior to model development. It may be that more informed energy dissipation design will be required to truly mitigate TDG generation at future hydropower dam locations. As dams are studied on a case-by-case basis, however, such as at HLK dam, the environmental risk to fish may be mitigated by advanced warning of potentially high TDG generating spill events. Models such as those presented in the present work can help do that.

Tables

Table 1: Northern and southern low-level outlet and stilling basin geometry

	Inlet Crest (m)	Conduit Slope (˚)	Gate Sill (m)	Basin Floor (m)	Top of End Sill (m)	End Sill Height (m)
NL1-4	411.5	19.61	408.7	391.7	401.1	9.4
SL5-8	411.5	14.76	409.4	399.9	413.0	13.1

Table 2: HLK scenario summary

SC	Start Time	End Time	Gate Number, (m^3/s)	HLK Spill (m^3/s)	ALGS (m^3/s)
1	July 26, 12:00	July 27, 14:00	NL2 (185.7) NL3 (187.8) NL4 (650.7)	1024.2	1085
2	July 27, 14:00	July 27, 16:00	SP4 (490.5) SP3 (490.5)	981.0	1085
3	July 27, 16:00	July 28, 14:00	SL5 (311.6) SL6 (311.6) SL7 (311.6)	934.8	1085
4	July 28, 14:00	July 28, 16:00	SL5 (644.9) SL6 (644.9)	1289.8	1100
5	July 28, 16:00	July 29, 16:00	SL5 (277.4) SL6 (277.4) NL3 (277.8) NL4 (277.8)	1110.4	1100
6	July 29, 16:00	July 30, 16:00	SL5 (191.7) NL3 (186.1) NL4 (645.5)	1022.7	1081

Table 3: Measured TDG per scenario (SC)

Transect	SC 1		SC 2		SC 3		SC 4*		SC 5		SC 6	
	LB	Max	LB	Max	LB	Max	LB	Max	LB	Max	LB	Max
M2	-	112	-	119	-	117	-	117	-	114	-	111
TR**	-	-	-	-	-	124	-	-	-	116	-	113
0.6 km	-	-	111	122	110	122	-	-	109	116	110	113
1.0 km	-	-	112	120	111	120	-	-	109	115	110	112
2.0 km	108	111	114	121	112	121	-	-	111	115	110	112
4.4 km	109	111	-	-	115	116	-	-	112	113	111	112
6.7 km	110	111	-	-	115	117	-	-	113	113	112	112

*Note that no measurements were taken for SC 4, this was a short duration scenario in which not enough time was available to gather complete measurements. The operating patterns were also similar to SC 3 and therefore not considered to be critical.

**Tailrace (TR) measurement from boat about 300 m downstream of HLK outlet works.

Table 4: 2016 scenario dissolved gas concentrations

	Gate #	TDG_{FB} (%)	TDG_{TW} (%)	P_{atm} (mmHg)	P_{wv} (mmHg)	C_s (mg/L)	C_{se} (mg/L)	C_{se} (%)	$C_{d,FB}$ (mg/L)	$C_{d,TW}$ (mg/L)	ΔC (mg/L)
SC 1	NL 2,3,4	109	112	730	14.2	25.98	79.23	305	28.37	29.16	0.79
SC 2	SP 3,4	109	122	729	14.4	25.79	64.17	249	28.17	31.56	3.39
SC 3	SL 5,6,7	109	124	730	14.4	25.82	63.93	248	28.20	32.15	3.95
SC 4	SL 5,6	109	-	728	14.4	25.75	64.65	251	28.12	-	-
SC 5	NL 3,4	109	116	750	15.8	25.82	77.52	300	28.20	30.04	1.85
	SL 5,6						63.38	245			
SC 6	NL 3	109	113	738	15.8	25.40	76.95	303	27.74	28.77	1.04
	NL 4						76.95	303			
	SL 5						62.80	247			

Table 5: Geldert et al. (1998) spillway parameter results

Parameter	Result
α	2.46
β	0.00
η	0.55
λ	0.15
$K_L at_s$	0.00

Table 6: Water levels and gate openings at HLK dam

Scenario	Forebay Elevation (m), FB_{Elev}	Tailwater Elevation (m), TW_{Elev}	Tailwater depth (m), y_t	Gate Opening (m), d_g
SC 1	433.62	421.61	29.91	2.74 (NL2) 2.83 (NL3) 7.32 (NL4)
SC 2	433.50	421.58	21.68	4.65 (SP3,4)
SC 3	433.48	421.42	21.52	4.54 (SL5,6,7)
SC 4	433.45	421.87	21.97	7.32 (SL5,6)
SC 5	433.38	421.67	29.97 (NL3,4)	4.23 (NL3,4)
			21.77 (SL5,6)	4.10 (SL5,6)
SC 6	433.29	421.58	29.88 (NL3,4)	2.83 (NL3) 7.32 (NL4)
			21.68 (SL5)	2.83 (SL5)

Table 7: University of Washington (2000) spillway coefficient results

Parameter	Result
m	0.090
n	-0.001
l	-0.001

Table 8: Urban et al. (2008) fitted spillway parameters

Structure	Parameter	Value
SP2-4	$d_{b,B}$ (mm)	0.78
	$d_{b,R}$ (mm)	0.70
	β_1	4.94×10^{-5}
	β_2	14.16
	β_3	1.18
	β_4	0.25
	η	1.43
	k	1.42

Table 9: Urban et al. (2008) range of important spillway parameters

Structure	Parameter	Min	Max	Average
SP2-4	K_Lab_B	0.10114	0.10808	0.10422
	K_Lab_R	0.06230	0.07091	0.06677
	K_Las_B	0.00975	0.01057	0.01013
	K_Las_R	0.01957	0.02936	0.02464
	ΔC_B (mg/L)	5.45	8.54	6.76
	ΔC_R (mg/L)	-0.23	1.10	0.72
	ΔC_{net} (mg/L)	5.97	9.64	7.48

Table 10: Northern low-level outlet air entrainment and efficiency from 1990's dataset

1990's Data	Min	Max	Average
Velocity, v_j (m/s)	11.66	18.50	15.70
Froude Number, F_r	1.84	4.57	3.26
Air Demand, Q_a (m^3/s)	7.41	21.79	16.27
Air-void Fraction, ϕ	0.024	0.103	0.066
Air-void Fraction of Dissolved Gas, ϕ_d	0.00	0.00104	0.00460
Efficiency (%)	0.00	1.09	0.58

Table 11: Southern low-level outlet air entrainment and efficiency from 1990's dataset

1990's Data	Min	Max	Average
Velocity, V (m/s)	10.92	14.46	13.14
Froude Number	2.18	2.63	2.45
Air Demand, Q_a (m^3/s)	6.02	13.74	10.62
Air-void Fraction, ϕ	0.035	0.048	0.043
Air-void Fraction of Dissolved Gas, ϕ_d	0.00127	0.00278	0.00220
Efficiency (%)	3.12	6.34	5.22

Table 12: Air-entrainment and efficiency from 2016 low-level outlet scenarios

2016 Data		Velocity, v_j (m/s)	Froude Number, F_r	Air Demand, Q_a (m^3/s)	Air-void Fraction, ϕ	Air-void Fraction of Dissolved Gas, ϕ_d	Efficiency (%)
SC 1	NL 2	18.34	4.54	21.32	0.0650	0.00064	0.98
	NL 3	18.34	4.51	21.40			
	NL 5	18.34	2.43	28.46			
SC 3	SL 5,6,7	18.00	3.41	23.73	0.0708	0.00317	4.48
SC 4	SL 5,6	18.25	2.42	28.05	0.0417	-	-
SC 5	NL 3,4	18.21	3.68	23.66	0.0773	0.00148	1.91
	SL 5,6	17.94	3.60	22.88			
SC 6	NL 3	18.17	4.47	20.89	0.0632	0.00083	1.32
	NL 4	18.17	2.40	27.70			
	SL 5	17.89	4.31	20.44			

Note: Where multiple gate openings were used in one scenario, the total air demand of all gates and the total water discharge from all gates was used to determine the air-void fraction. The efficiency therefore, represents the efficiency of the scenario as a whole and not of any one particular gate.

Table 13: Geldert et al. (1998) low-level outlet parameter results

Parameter	NL1-4	SL5-8
α	0.15	0.14
β	1.00	1.47
η	0.55	0.75
$K_L at_s$	0.00	0.20

Table 14: Urban et al. (2008) range of important low-level outlet parameters

Structure	Parameter	Min	Max	Average
NL1-4	$K_L ab_B$	0.00009	0.00037	0.00024
	$K_L ab_R$	0.00033	0.00134	0.00087
	$K_L as_B$	0.00162	0.00181	0.00169
	$K_L as_R$	0.00214	0.00264	0.00246
	ΔC_B (mg/L)	0.01	0.05	0.04
	ΔC_R (mg/L)	0.10	0.91	0.59
	ΔC_{net} (mg/L)	0.11	0.95	0.63
SL1-4	$K_L ab_B$	0.06811	0.09393	0.08379
	$K_L ab_R$	0.01120	0.01667	0.01477
	$K_L as_B$	0.09005	0.09716	0.09310
	$K_L as_R$	0.19087	0.21982	0.20009
	ΔC_B (mg/L)	5.19	8.03	6.43
	ΔC_R (mg/L)	-6.77	-2.73	-4.21
	ΔC_{net} (mg/L)	0.84	2.55	2.22

Table 15: Urban et al. (2008) fitted low-level outlet parameters

Structure	Parameter	Value
NL1-4	$d_{b,B}$ (mm)	2.70
	$d_{b,R}$ (mm)	0.70
	β_1	3.0×10^{-5}
	β_2	10.61
	β_3	0.92
	β_4	0.16
	η	1.12
	k	1.27
SL5-8	$d_{b,B}$ (mm)	0.80
	$d_{b,R}$ (mm)	2.70
	β_1	2.3×10^{-5}
	β_2	19.46
	β_3	1.61
	β_4	0.39
	η	1.44
	k	1.49

Figures

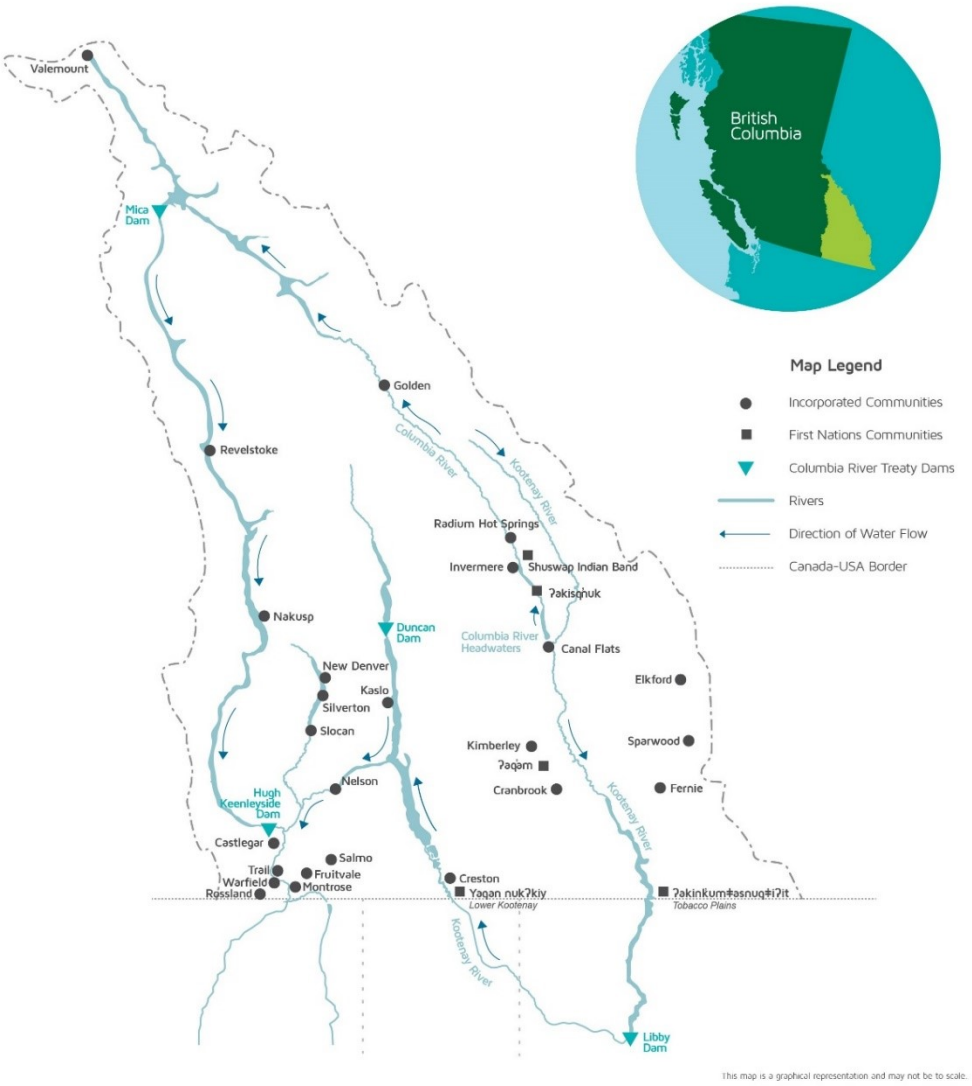

Figure 1: Upper Columbia River basin (taken from https://ourtrust.org/about/basin-map/)

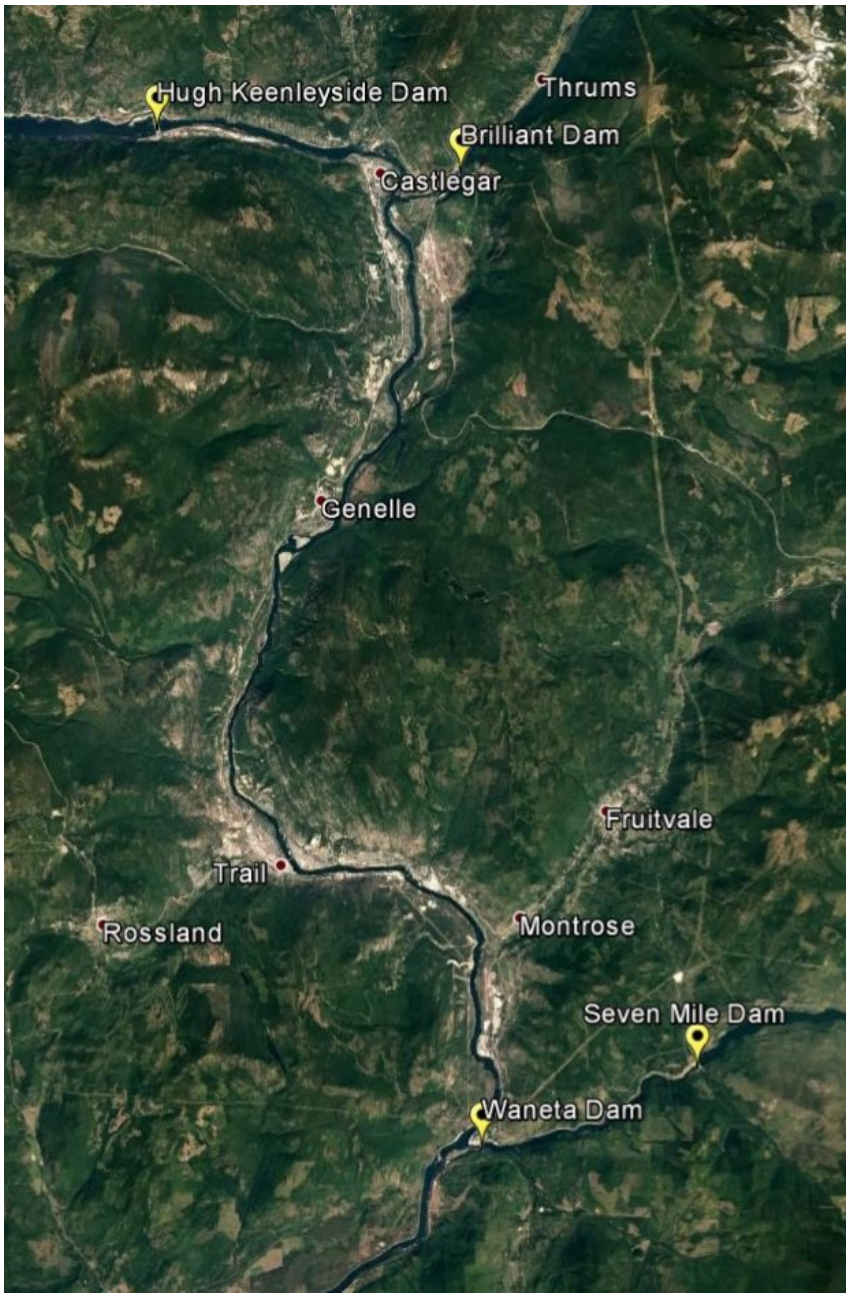

Figure 2: Lower Columbia River

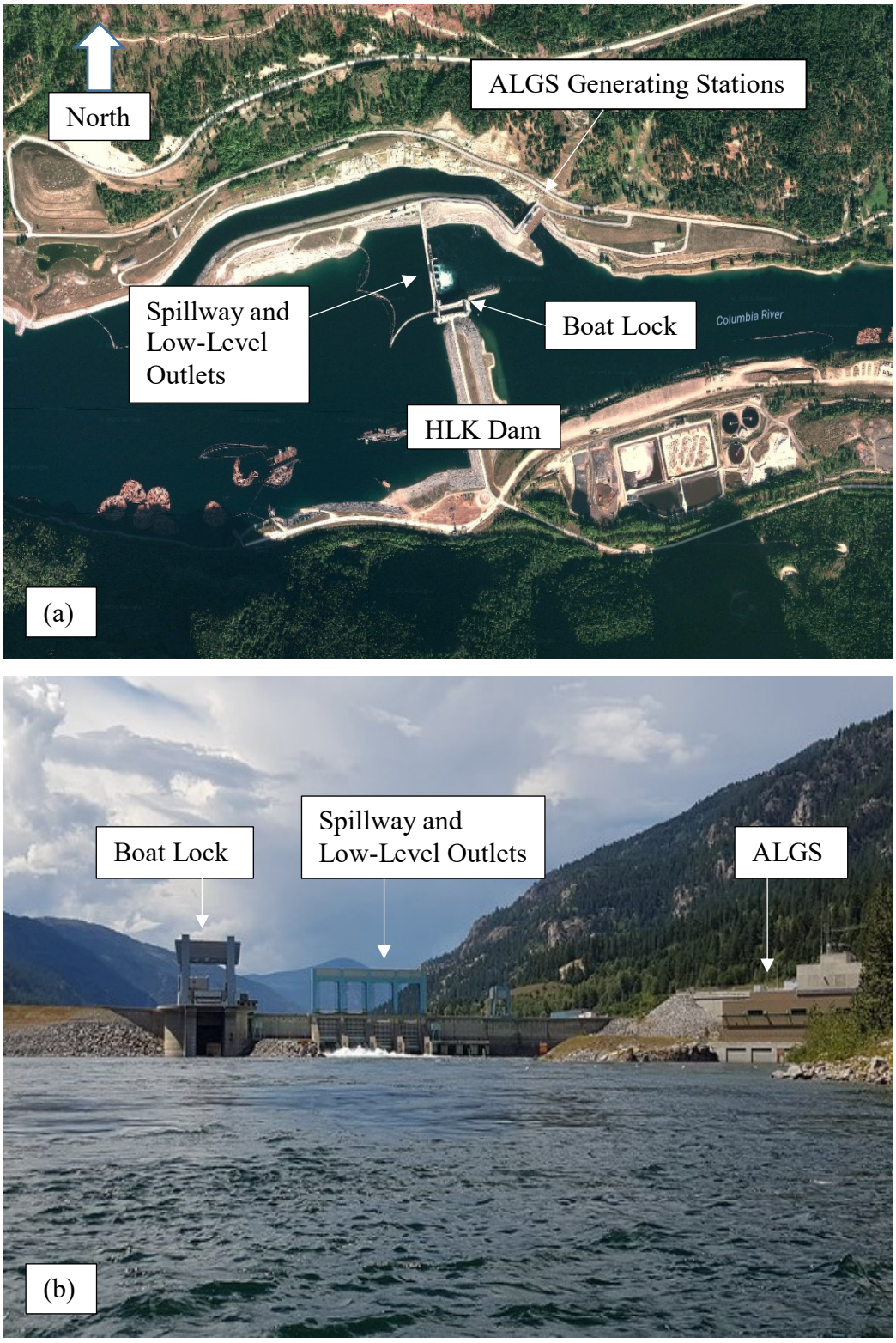

Figure 3: Site layout (a) and various components (b) at Hugh L. Keenleyside Dam (HLK)

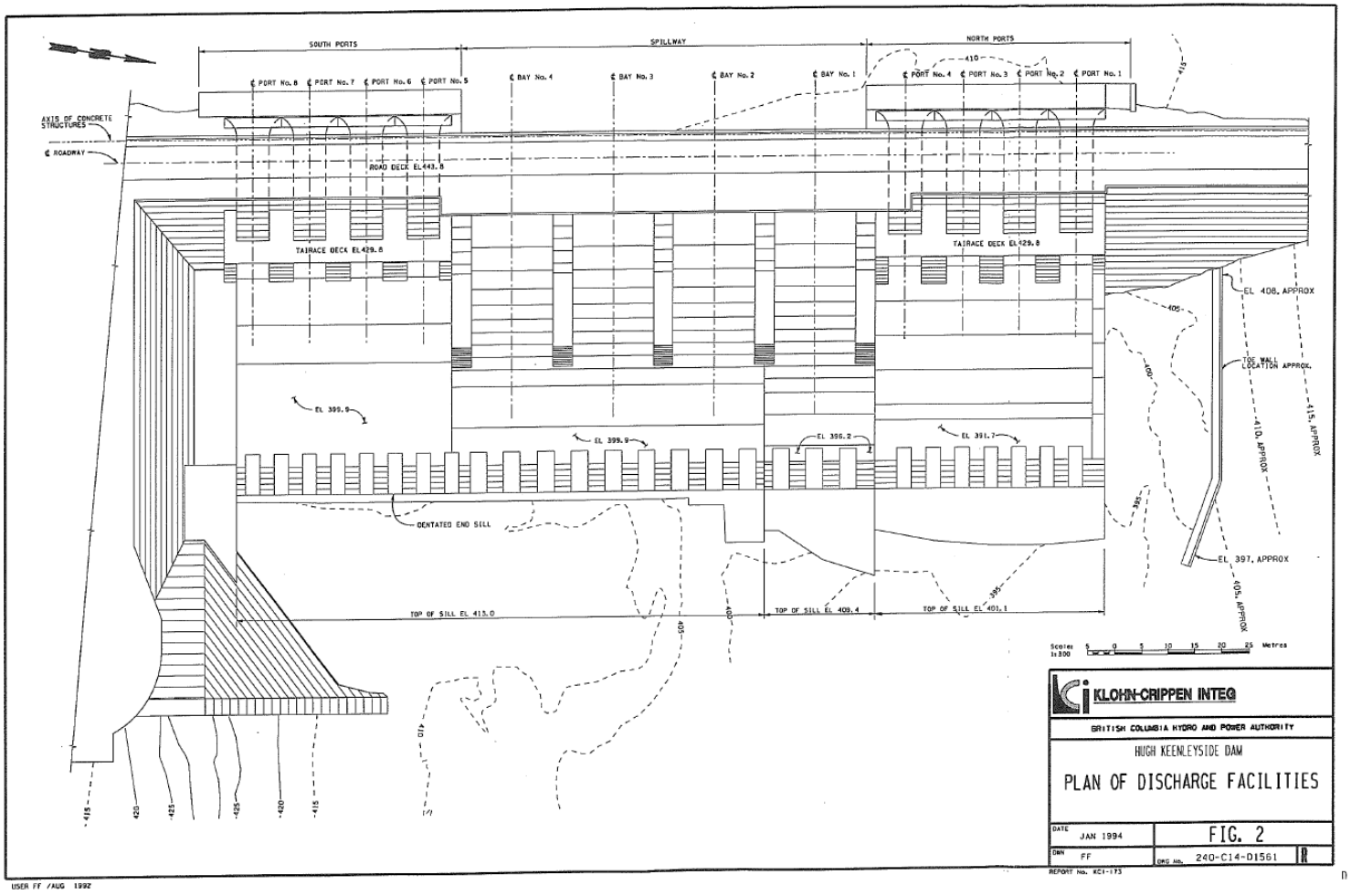

Figure 4: Plan view of HLK discharge facilities; Klohn-Crippen Integ (1994)

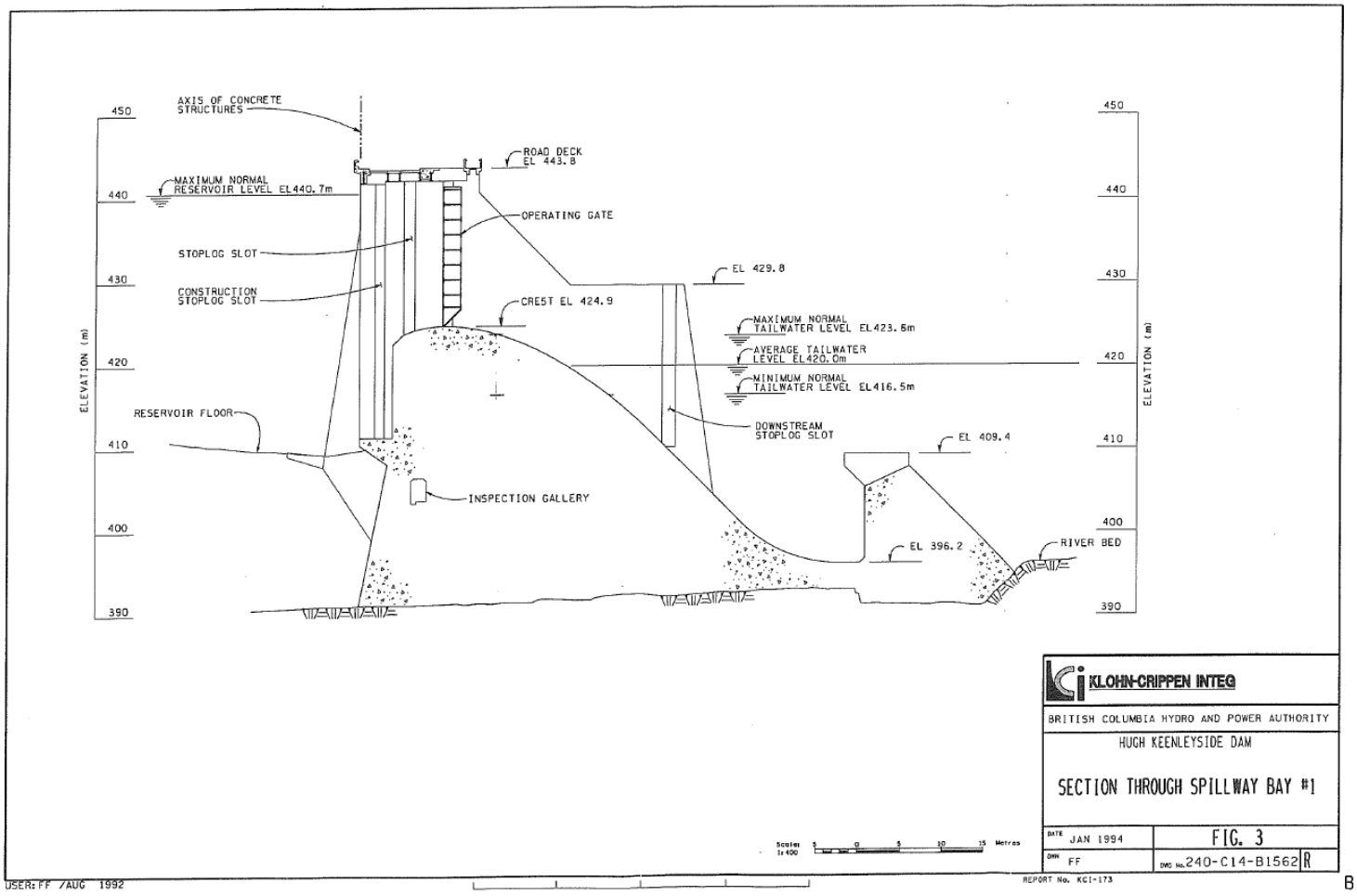

Figure 5: Cross-section of spillway 1; Klohn-Crippen Integ (1994)

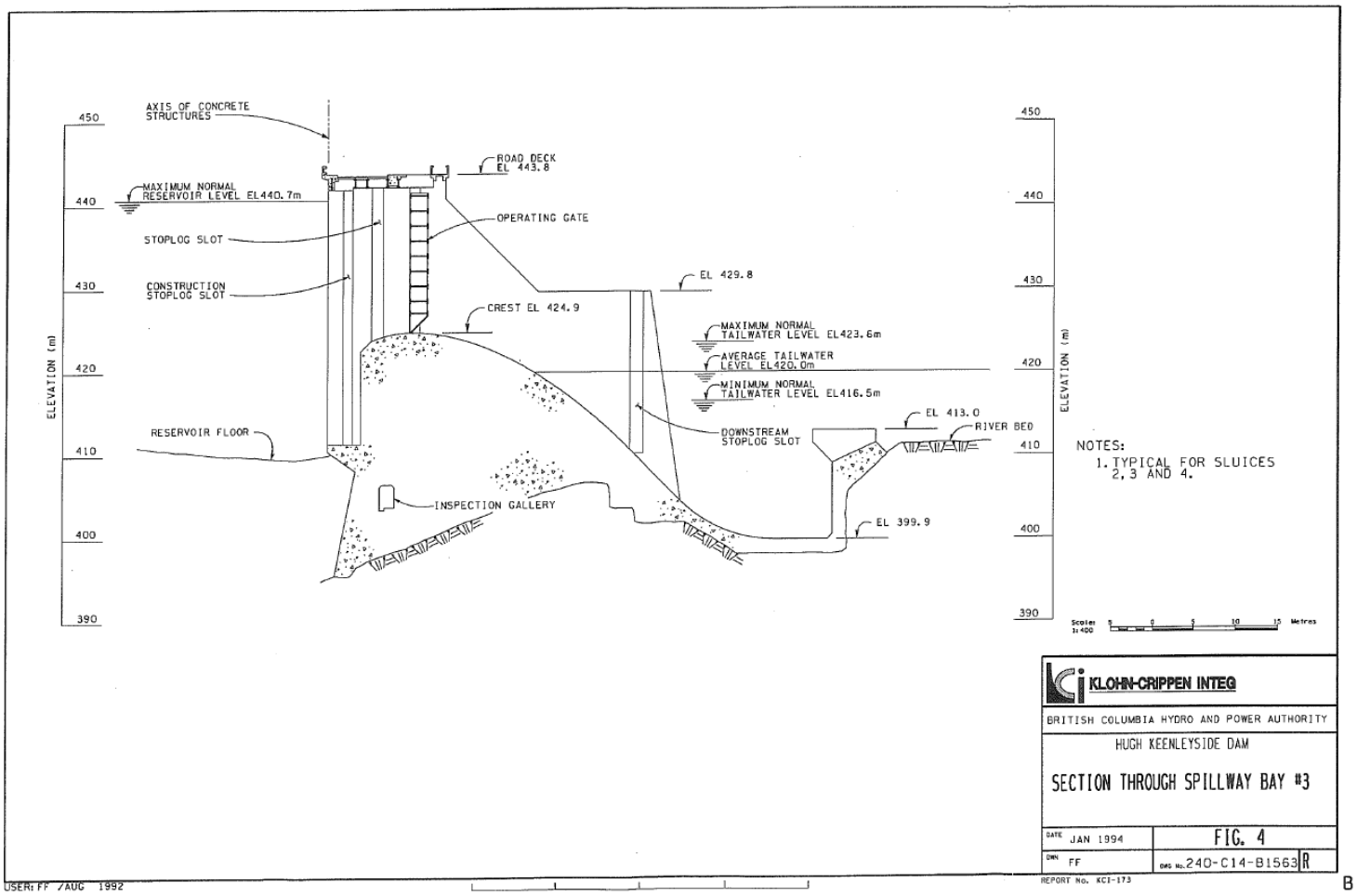

Figure 6: Cross-section of spillway 3 (typical of spillways SP2-4); Klohn-Crippen Integ (1994)

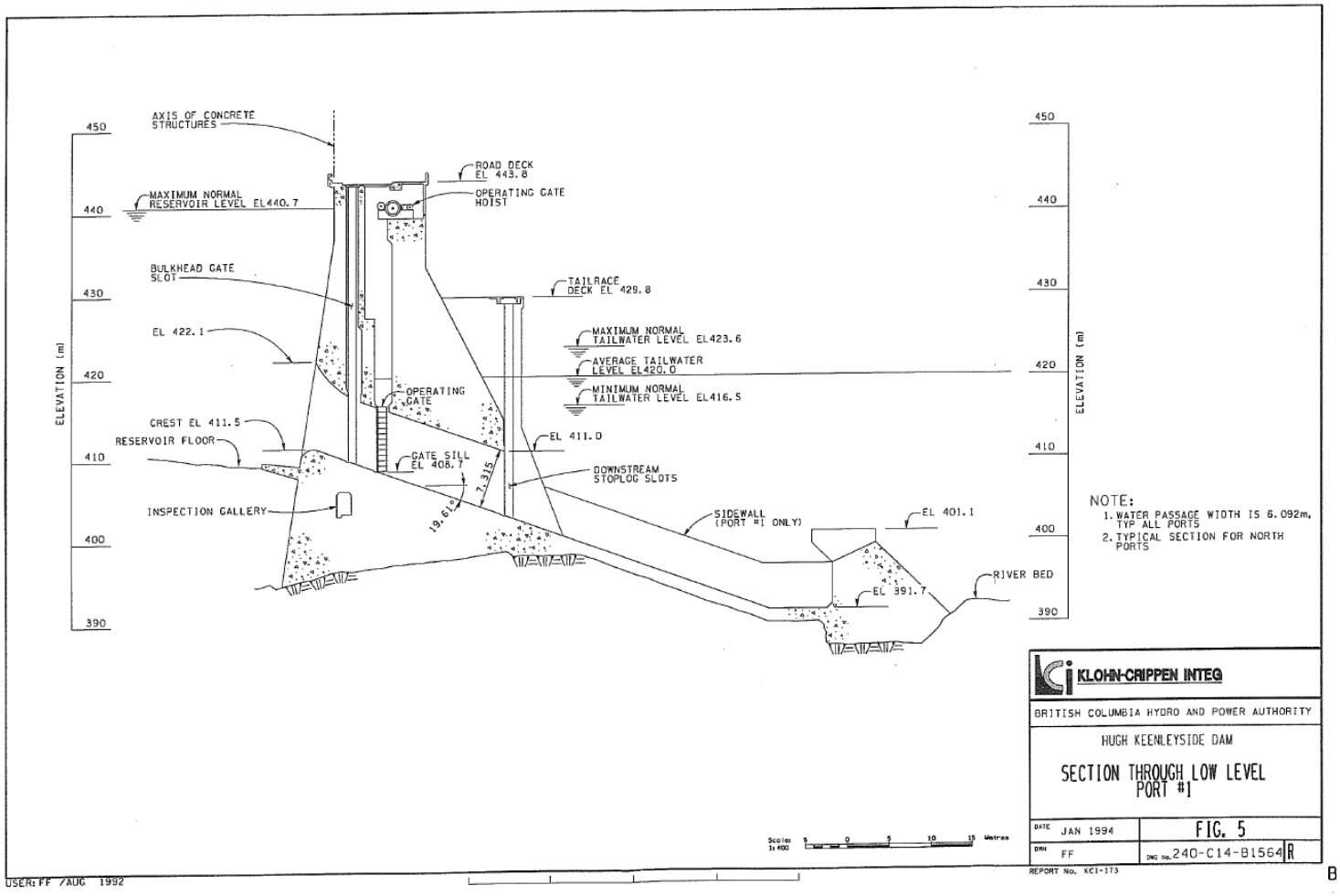

Figure 7: Cross-section of northern low-level outlet NL1 (typical of north ports); Klohn-Crippen Integ (1994)

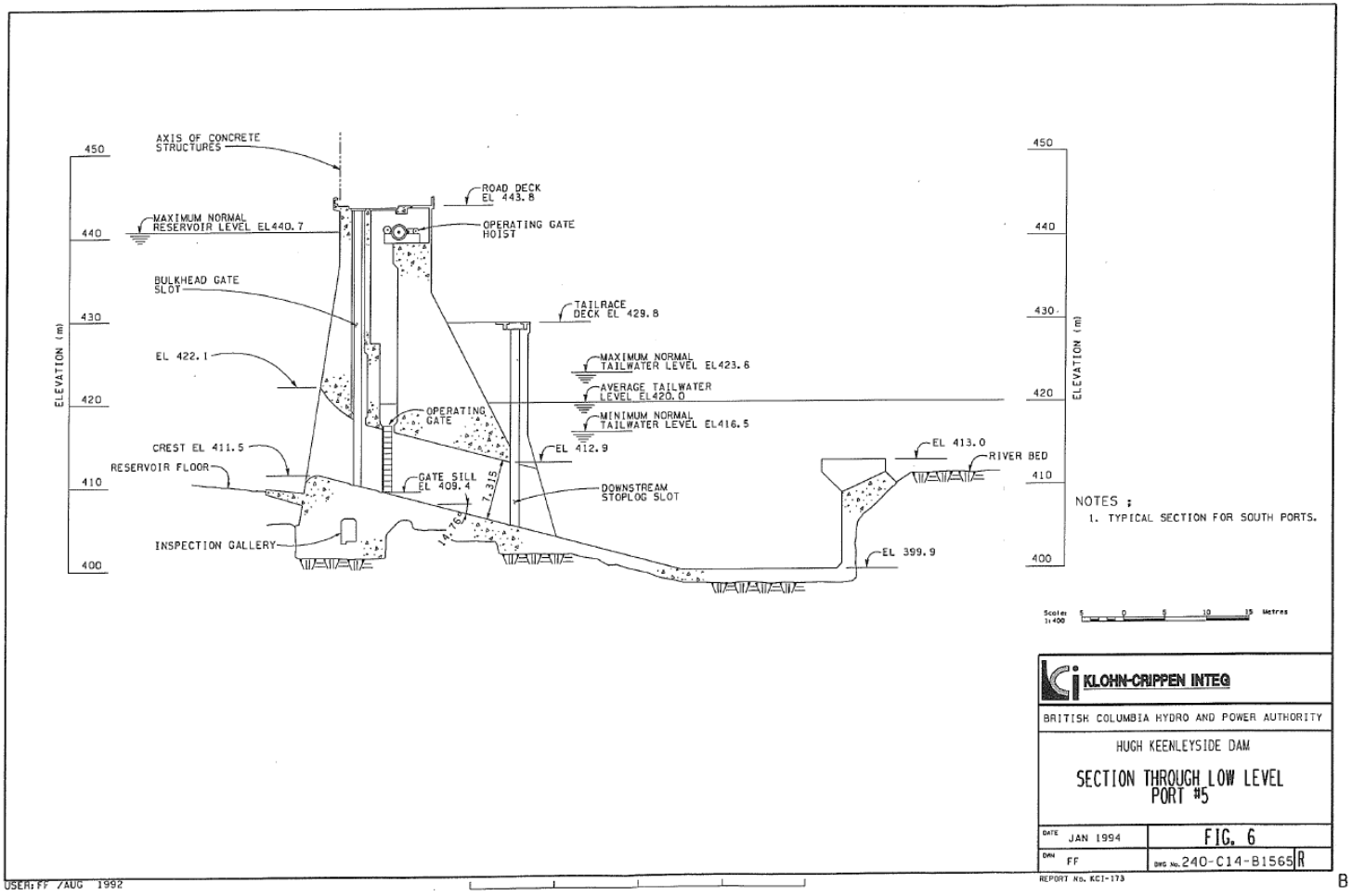

Figure 8: Cross-section of southern low-level outlet SL5 (typical of south ports); Klohn-Crippen Integ (1994)

Figure 9: Fixed monitoring platform at 1.0 km downstream of HLK

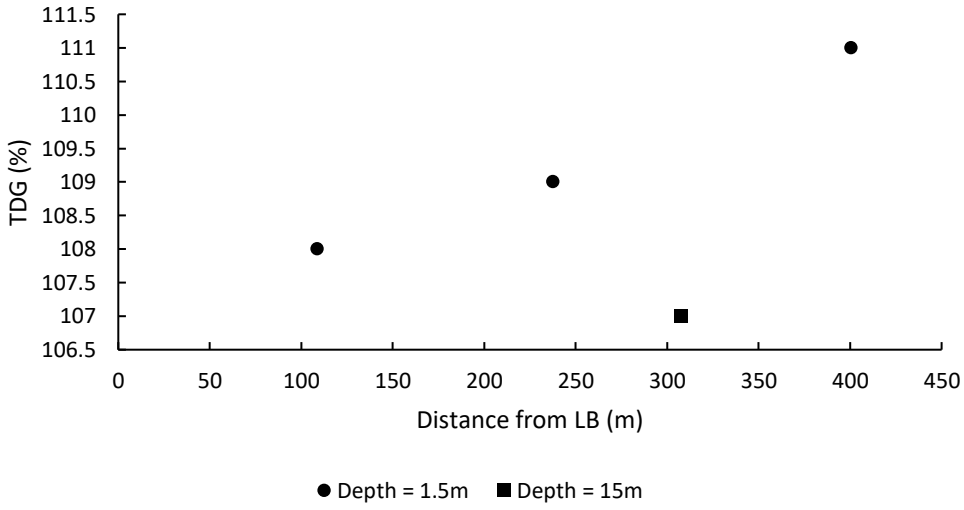

Figure 10: Forebay TDG spot measurements

Figure 11: HLK dam and downstream Columbia River

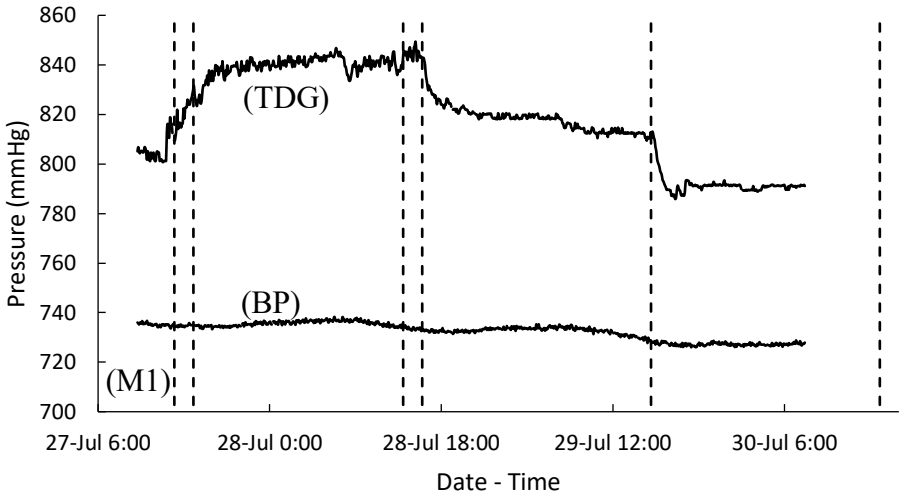
860
840
820
800
780
760
740
720
700
Pressure (mmHg)
(TDG)
(BP)
(M1)
27-Jul 6:00
28-Jul 0:00
28-Jul 18:00
29-Jul 12:00
30-Jul 6:00
Date - Time

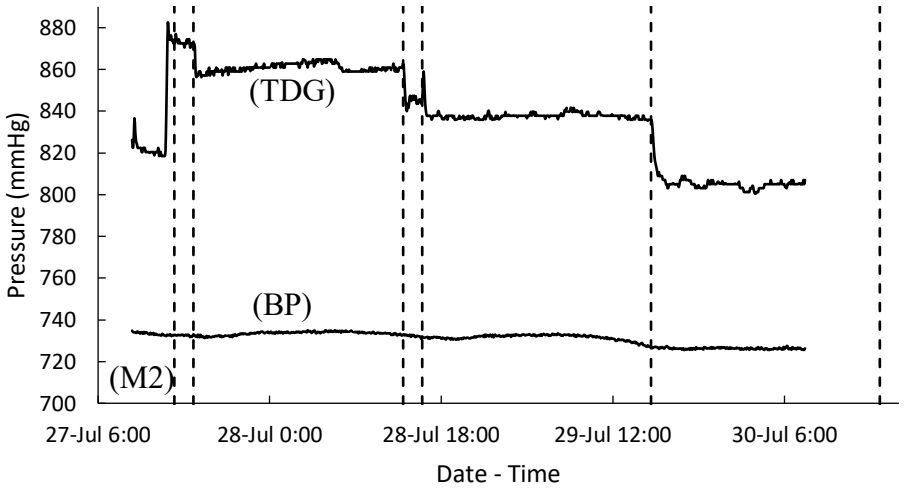
880
860
840
820
800
780
760
740
720
700
Pressure (mmHg)
(TDG)
(BP)
(M2)
27-Jul 6:00
28-Jul 0:00
28-Jul 18:00
29-Jul 12:00
30-Jul 6:00
Date - Time

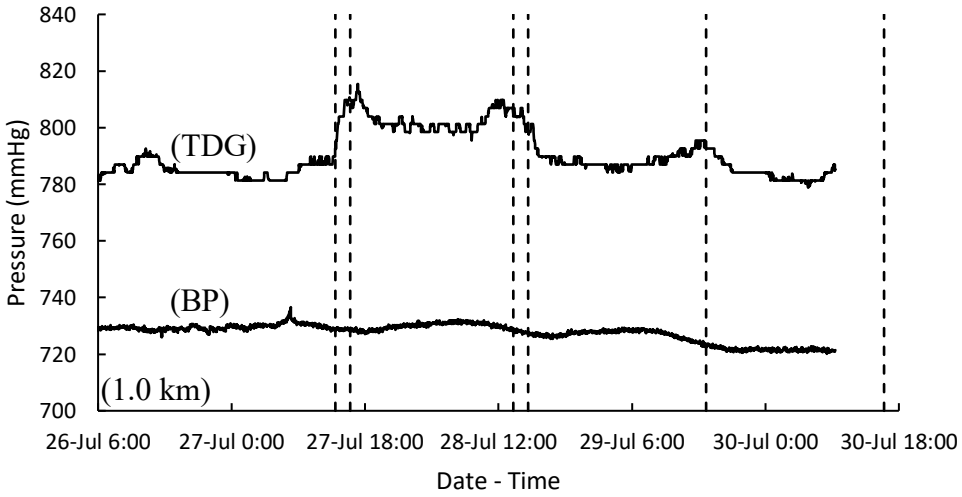
840
820
800
780
760
740
720
700
Pressure (mmHg)
(TDG)
(BP)
(1.0 km)
26-Jul 6:00
27-Jul 0:00
27-Jul 18:00
28-Jul 12:00
29-Jul 6:00
30-Jul 0:00
30-Jul 18:00
Date - Time

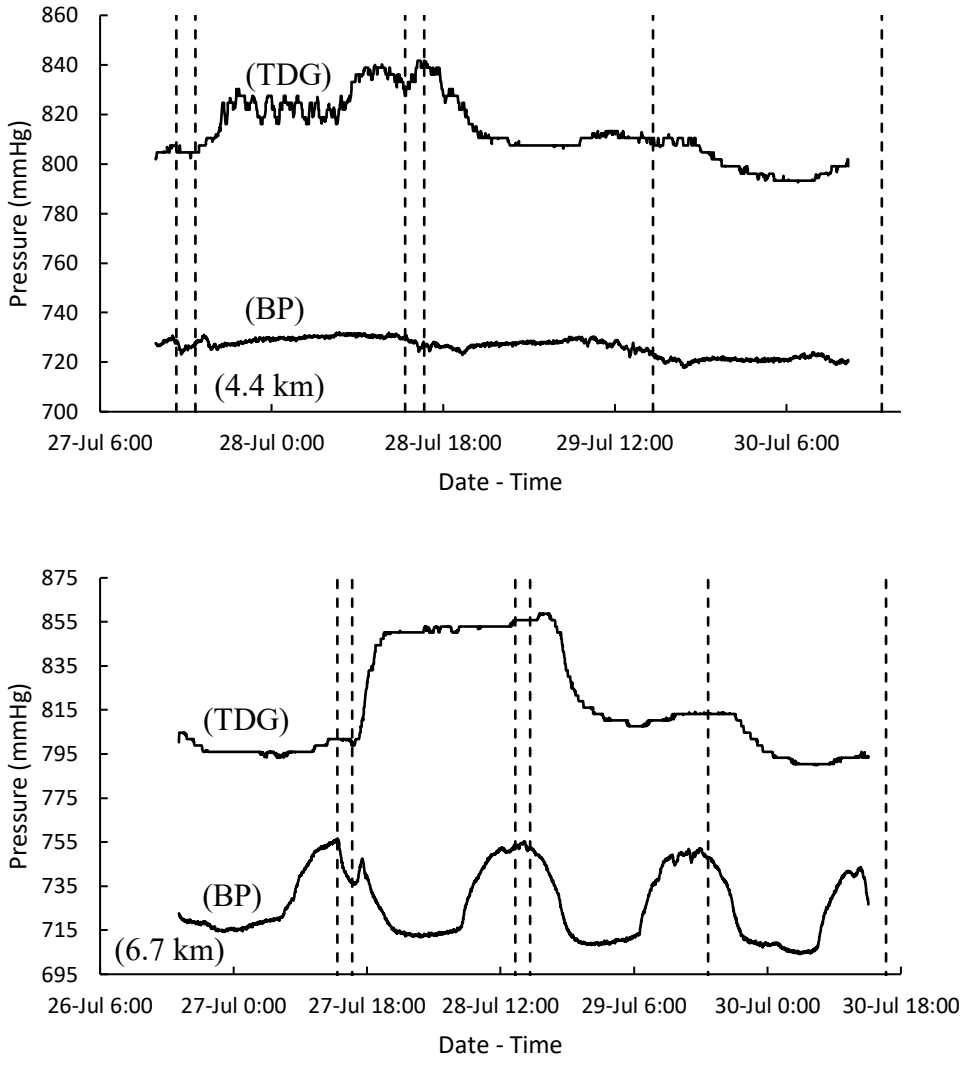

Figure 12: Total dissolve gas (TDG) and barometric pressure (BP) from continuous monitoring stations (vertical lines indicate end of scenarios, the first vertical line indicating the end of scenario 1)

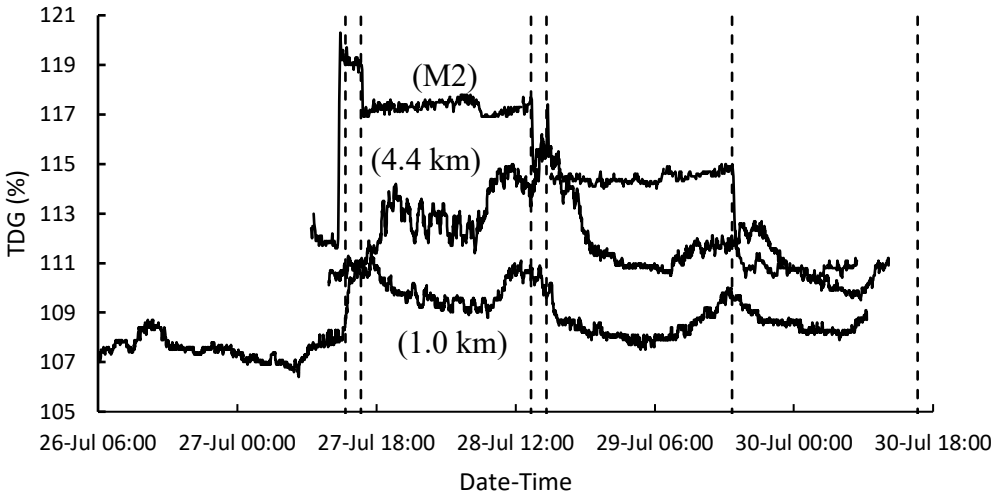

Figure 13: Continuous monitoring station TDG (vertical lines indicate end of scenarios, the first vertical line indicating the end of scenario 1), M2 in tailrace along rock berm, 1.0 km probe along left bank, and 4.4 km probe along right bank

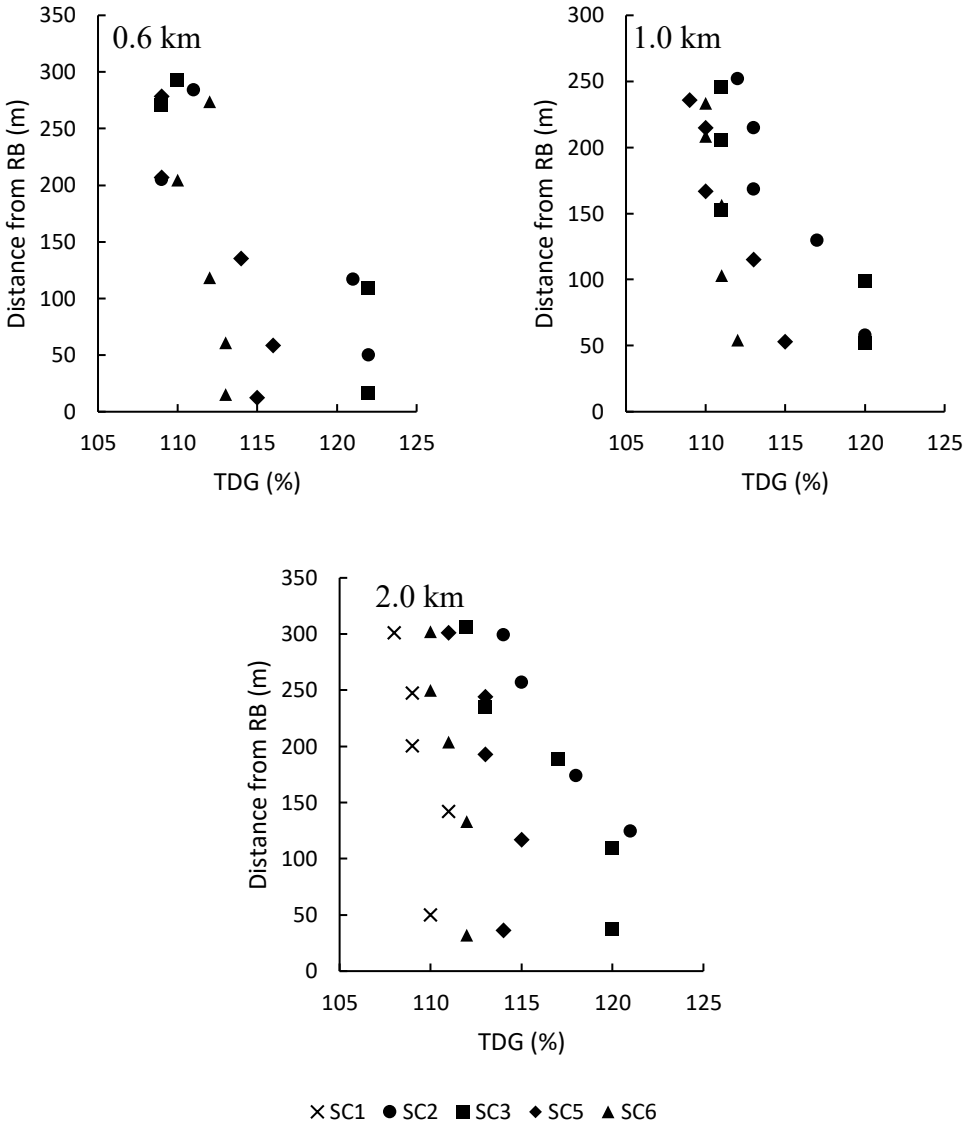

Figure 14: Transect spot measurements

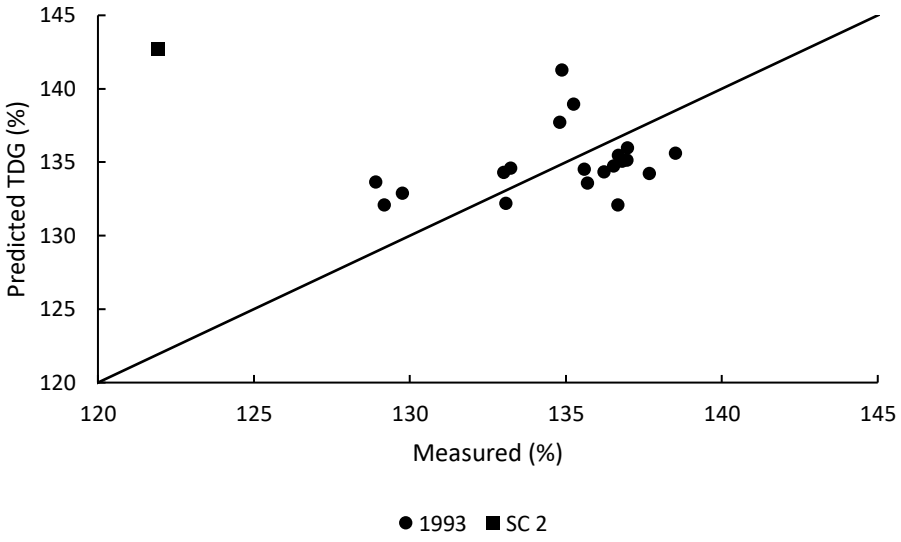

Figure 15: Johnson and King (1975) model prediction results for SC 2 and 1993 spillway data subset, RMSE = 2.9%

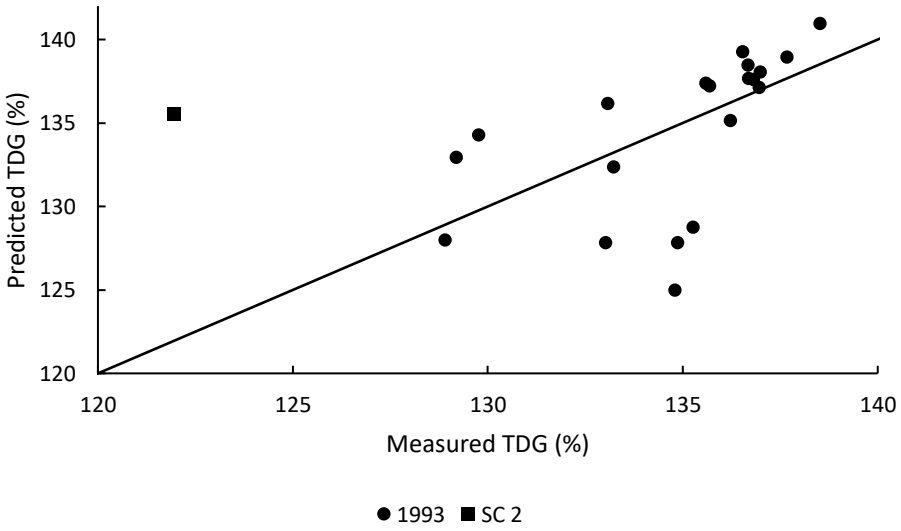

Figure 16: Geldert et al. (1998) model prediction results for SC 2 and 1993 spillway data subset, RMSE = 3.8%

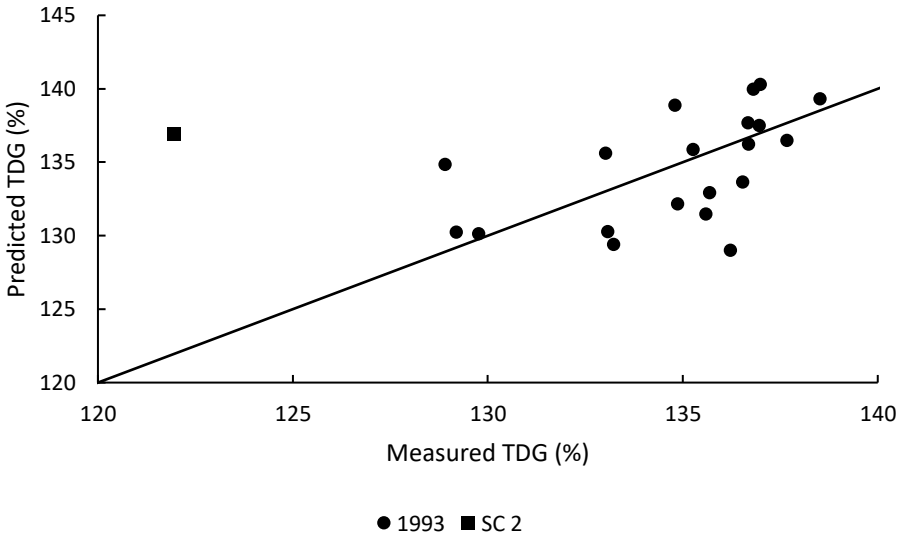

Figure 17: University of Washington (2000) model prediction results for SC 2 and 1993 spillway data subset, RMSE = 2.8%

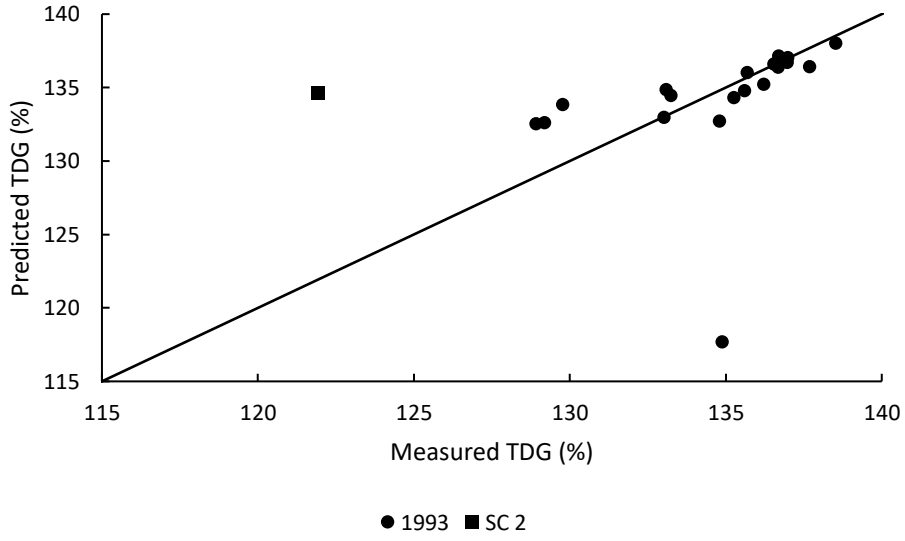

Figure 18: Bruce (2016) model prediction results for SC 2 and 1993 spillway data subset, RMSE = 4.2%

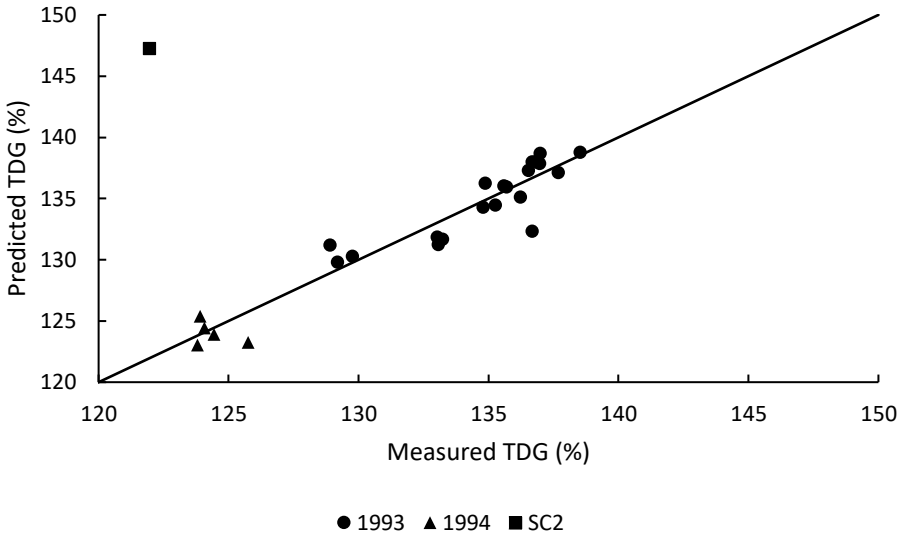

Figure 19: Urban et al. (1998) model prediction results for SC 2, 1993, and 1994 spillway data subsets, RMSE = 1.5%

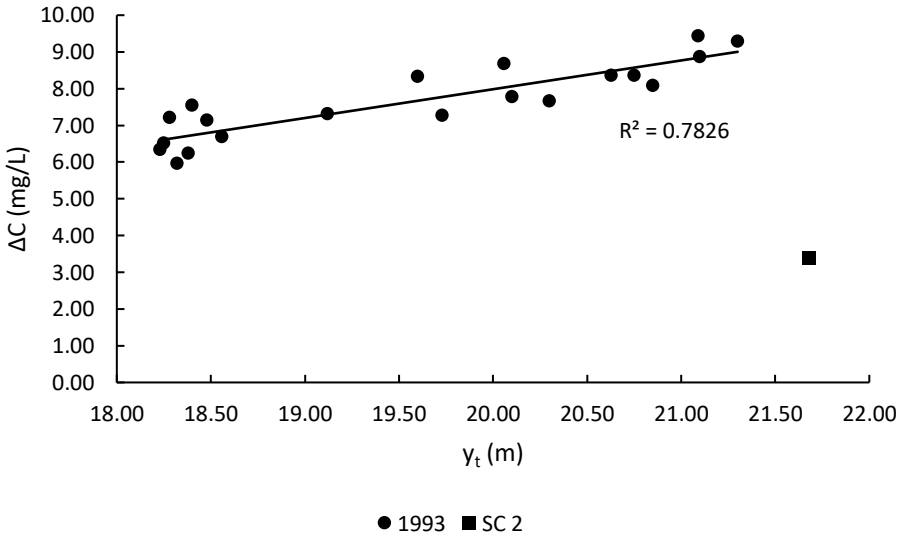

Figure 20: Measured TDG generation vs tailwater depth for spillway data, R-squared value is for 1993 data only

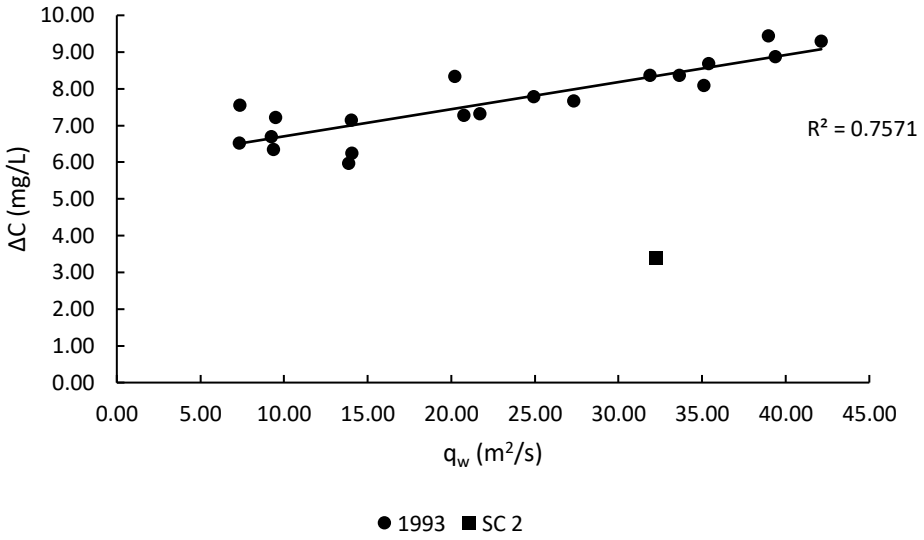

Figure 21: Measured TDG generation vs unit discharge for spillway data, R-squared value is for 1993 data only

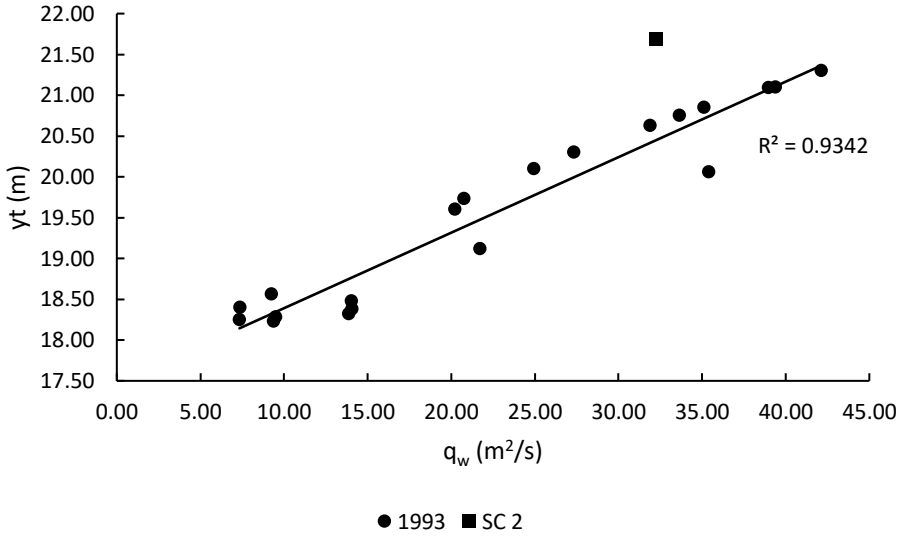

Figure 22: Tailwater vs unit discharge for spillway data, R-squared value is for 1993 data only

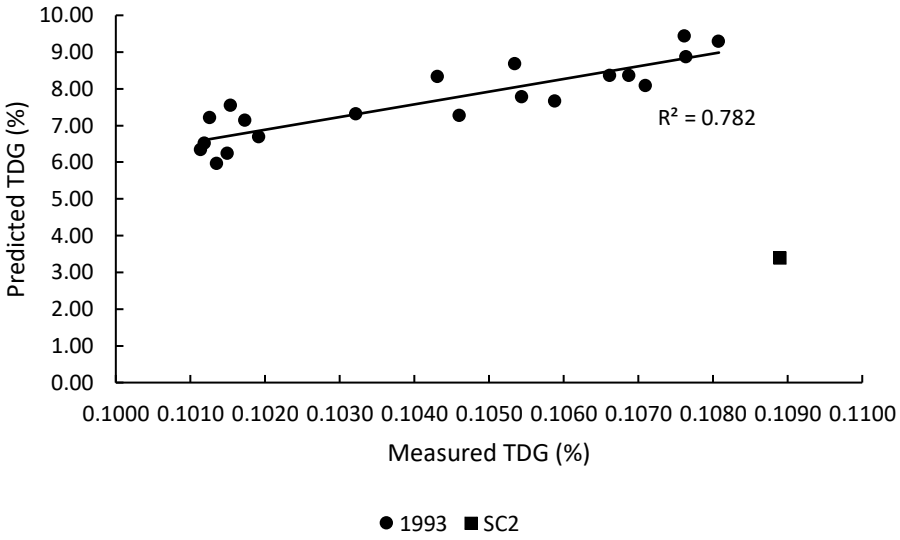

Figure 23: Measured TDG generation vs stilling basin bubble mass-transfer coefficient for spillway data, R-squared value is for 1993 data only

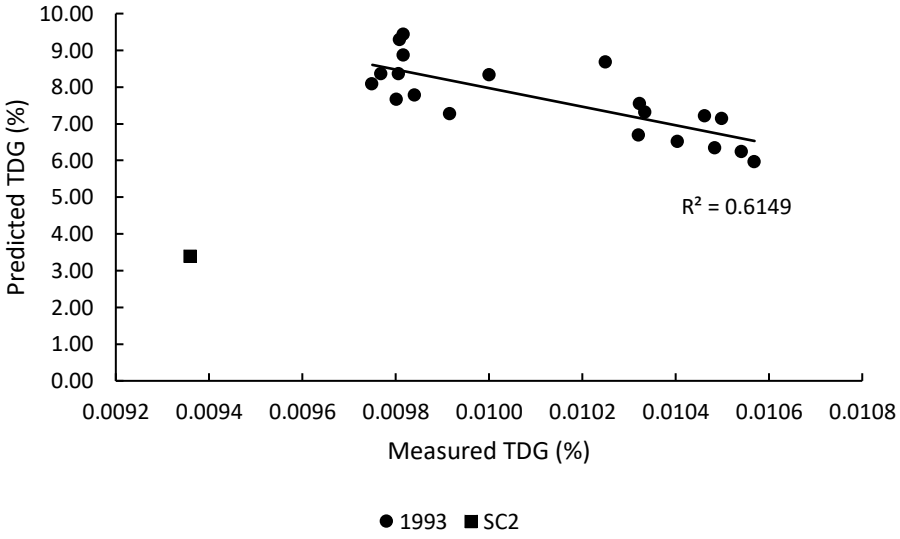

Figure 24: Measured TDG generation vs stilling basin surface mass-transfer for spillway data, R-squared value is for 1993 data only

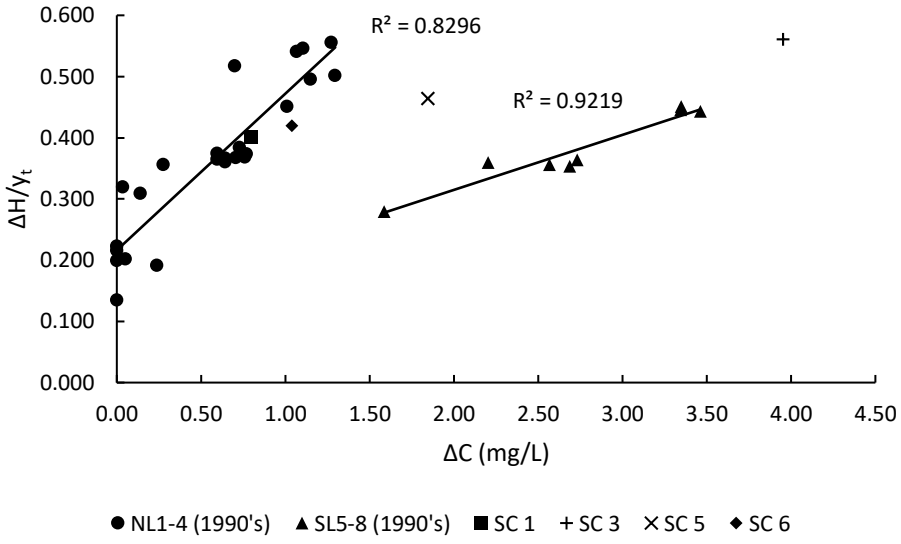

Figure 25: Π_1; Ratio of differential head to tailwater depth, $\Delta H/y_t$

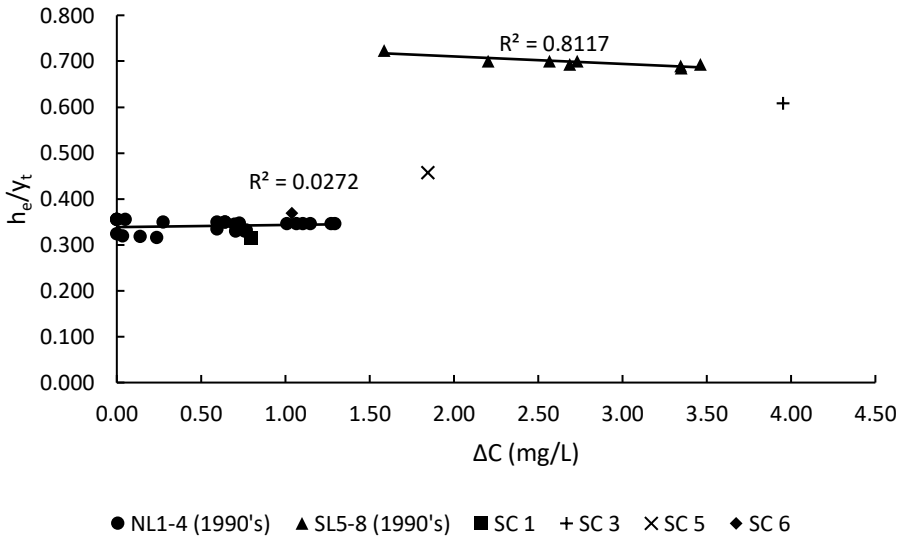

Figure 26: Π_2; Ratio of end sill height to tailwater depth, h_e/y_t

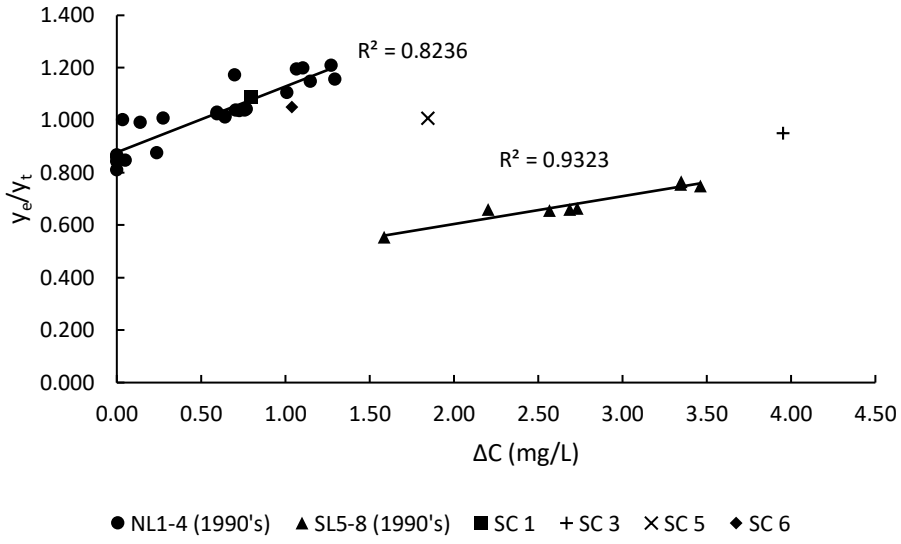

Figure 27: Π_3; Ratio of water depth above end sill to tailwater depth, y_e/y_t

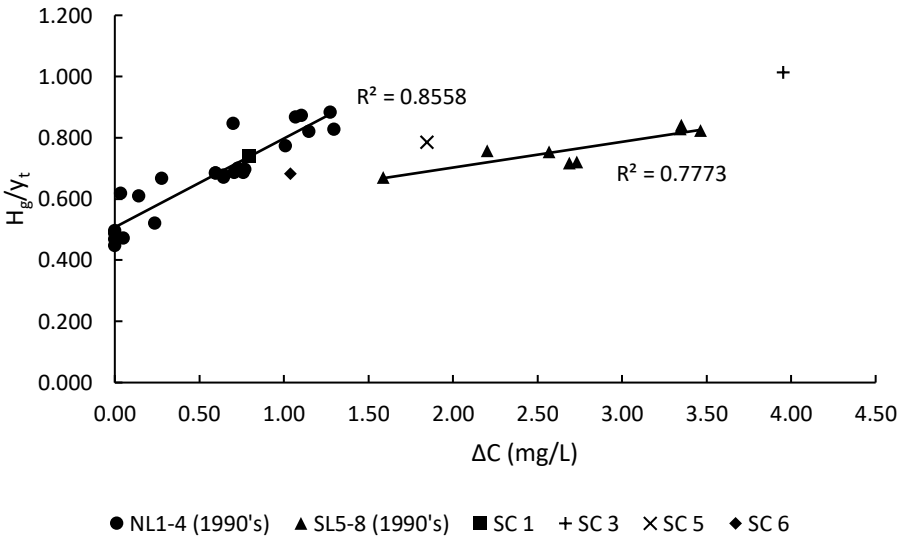

Figure 28: Π_4; Ratio of head above center of gate opening to tailwater depth, H_g/y_t

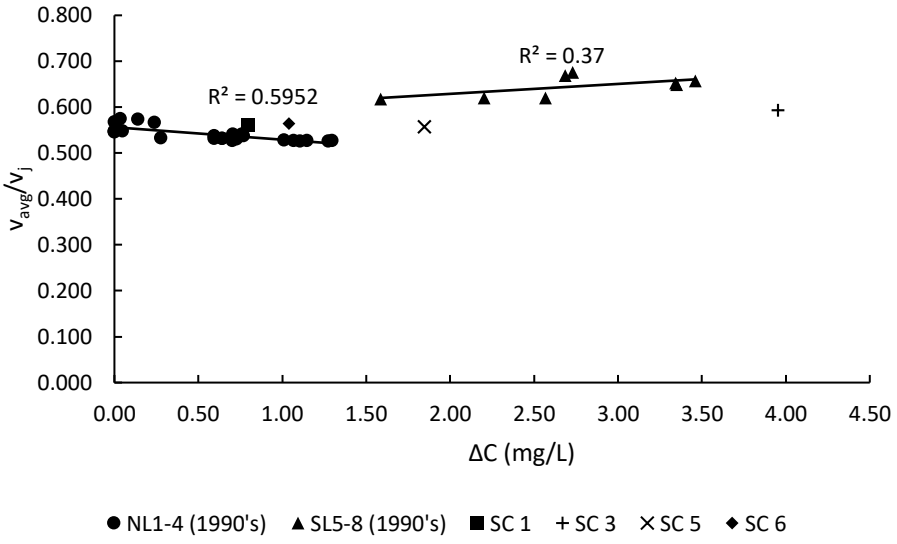

Figure 29: Π_5; Ratio of average stilling basin velocity to jet velocity, v_{avg}/v_j

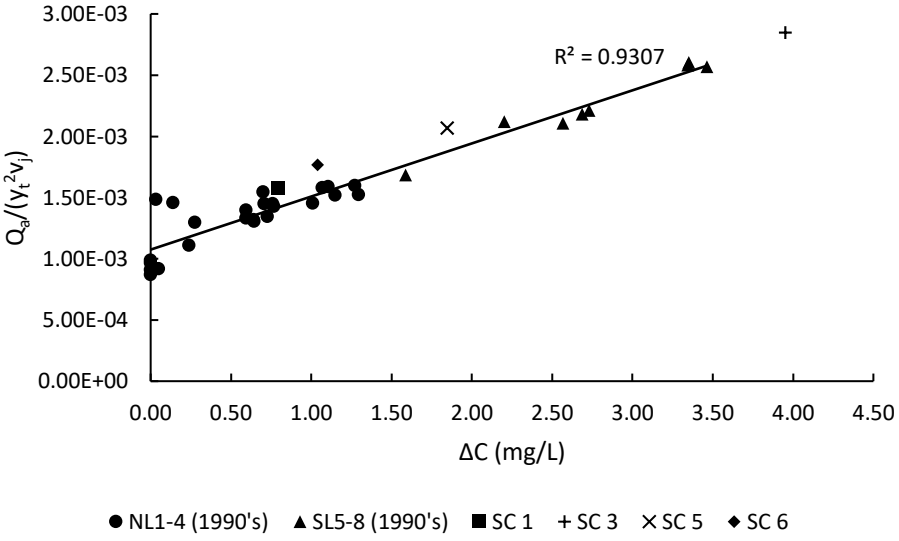

Figure 30: Π_6; Ratio of air flow rate to the product of the jet velocity and the tailwater depth squared, $Q_a/(y_t^2 v_j)$, R-squared value is for all 1990 data

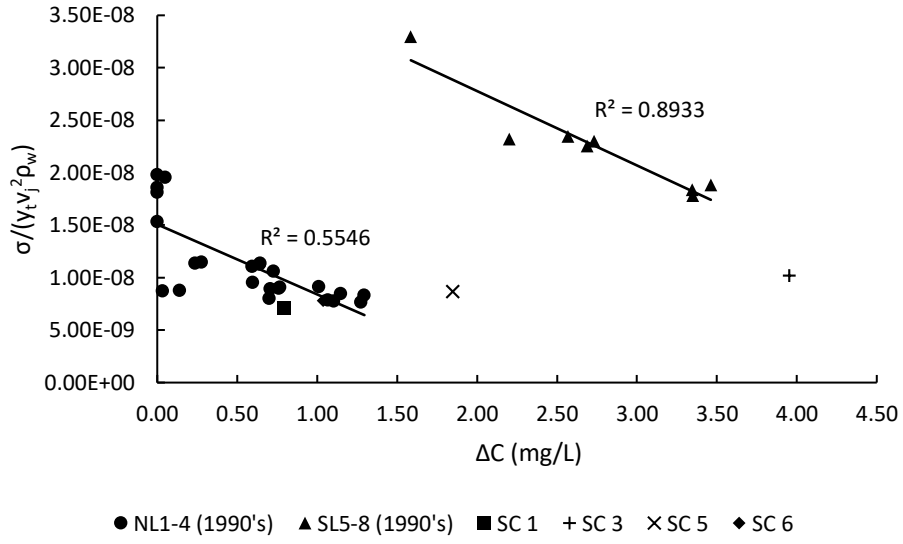

Figure 31: Π_7; Ratio of the surface tension of water to the product of the jet velocity squared, tailwater depth, and density of water, $\sigma/(y_t v_j^2 \rho_w)$

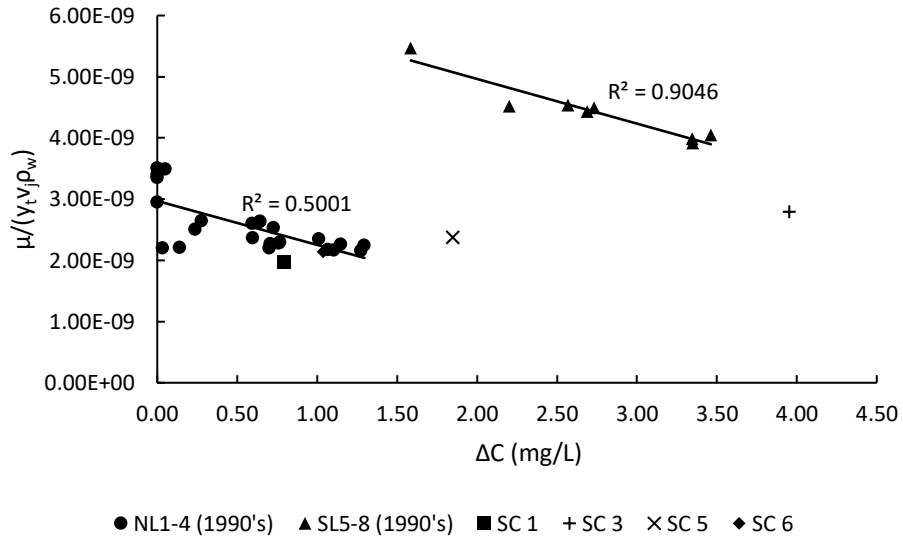

Figure 32: Π_8; Ratio of the dynamic viscosity of water to the product of the tailwater depth, jet velocity, and density of water, $\mu/(y_t v_j \rho_w)$

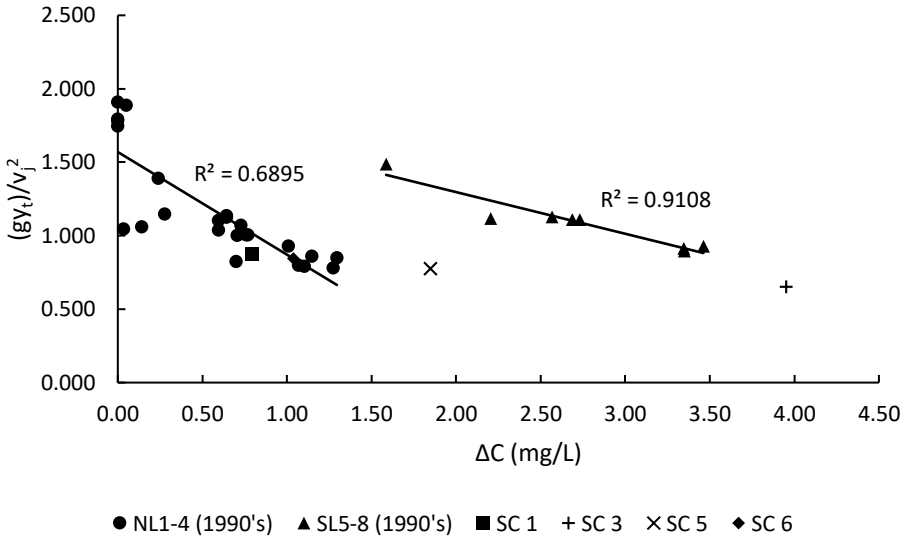

Figure 33: Π_9; Ratio of the product of the tailwater depth and acceleration due to gravity to the jet velocity squared, $(gy_t)/v_j^2$

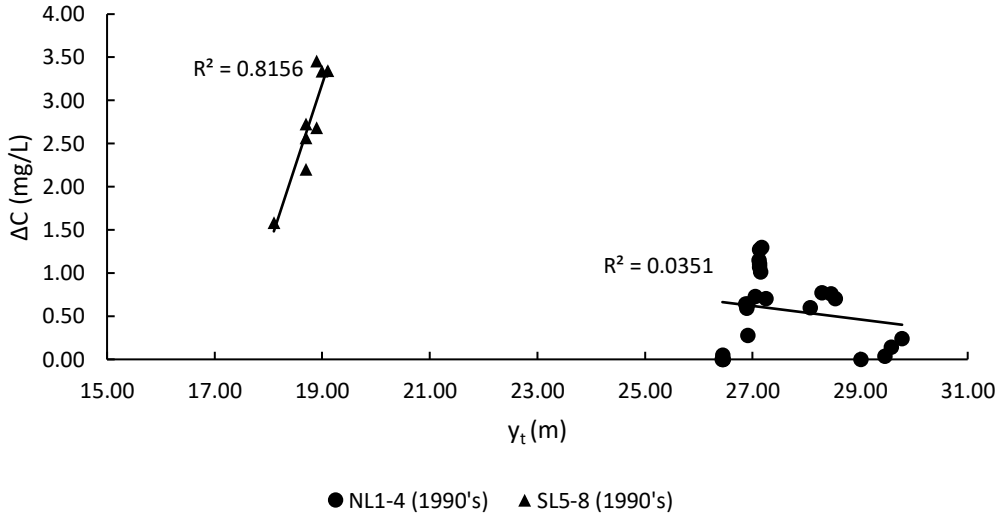

Figure 34: Total dissolved gas generation vs tailwater depth for low-level outlets (1990's)

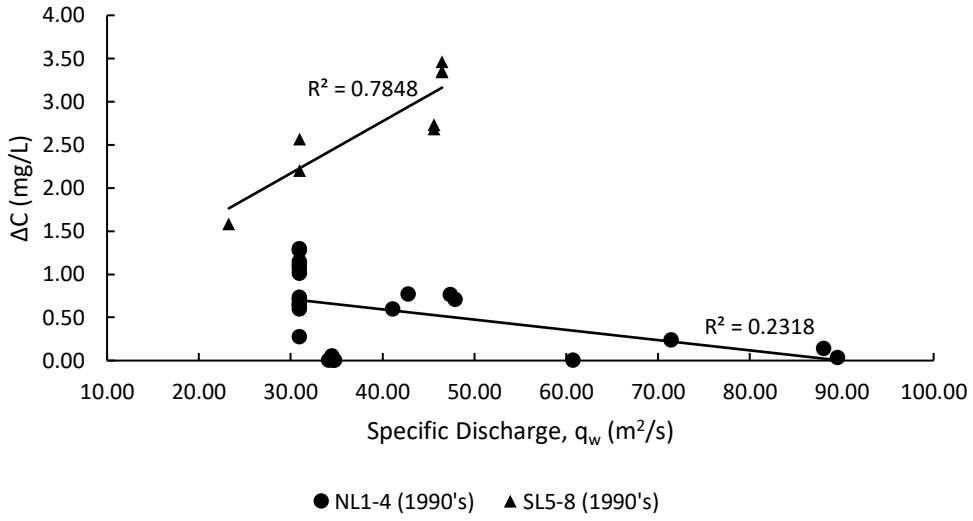

Figure 35: Total dissolved gas generation vs specific discharge for low-level outlets (1990's dataset)

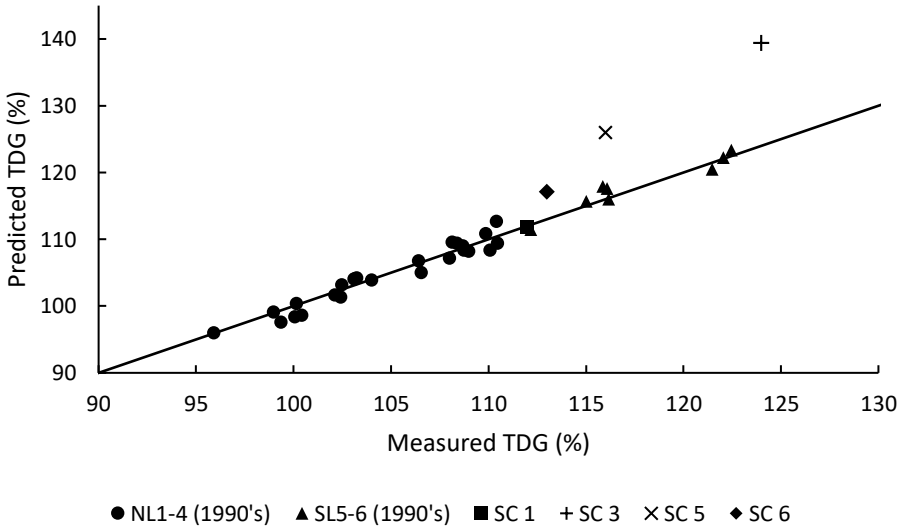

Figure 36: Bruce (2016) model prediction results for north and south low-level outlets, RMSE = 1.11%

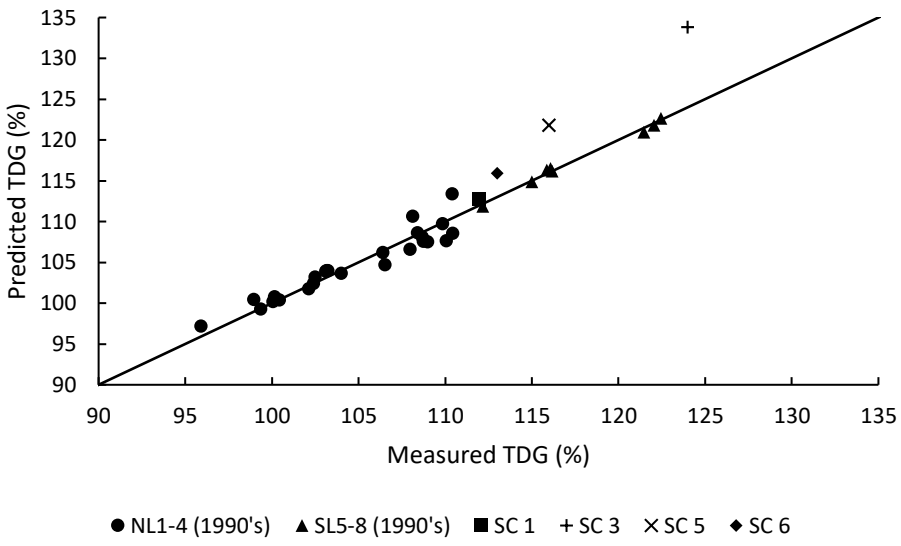

Figure 37: Geldert et al. (1998) model prediction results for north and south low-level outlets, RMSE = 1.13%

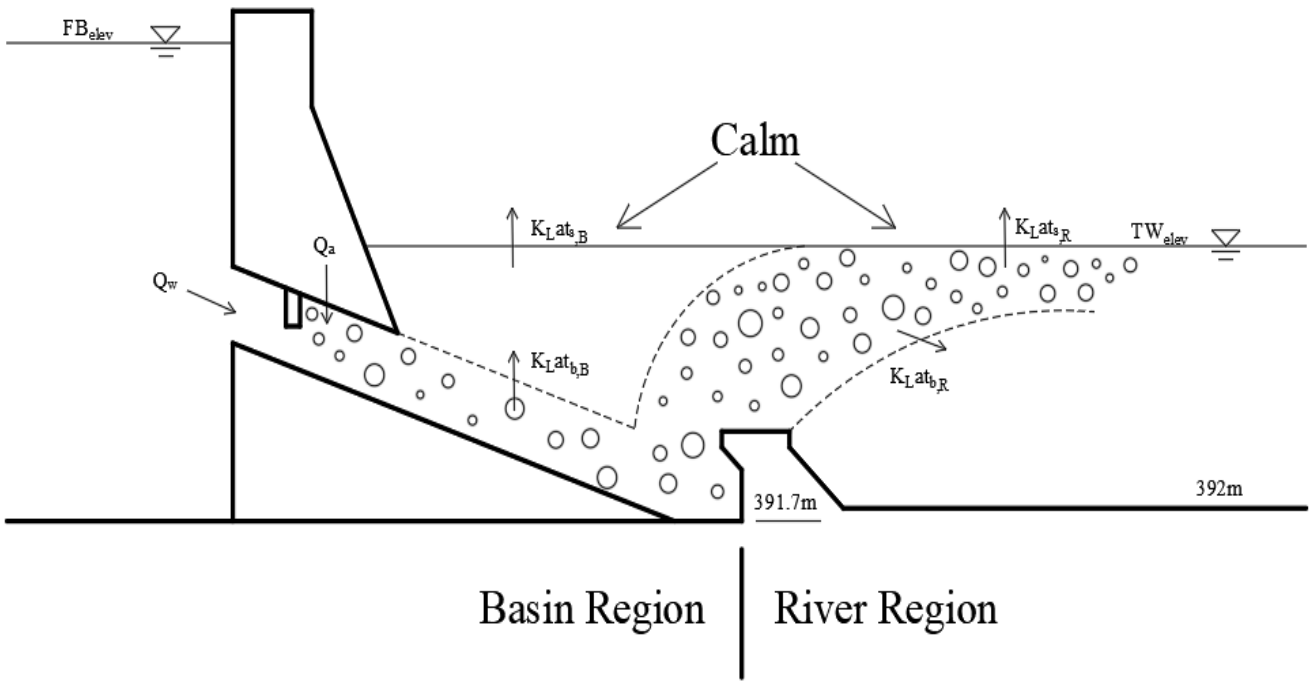

Figure 38: Proposed northern low-level outlet model schematic (NTS)

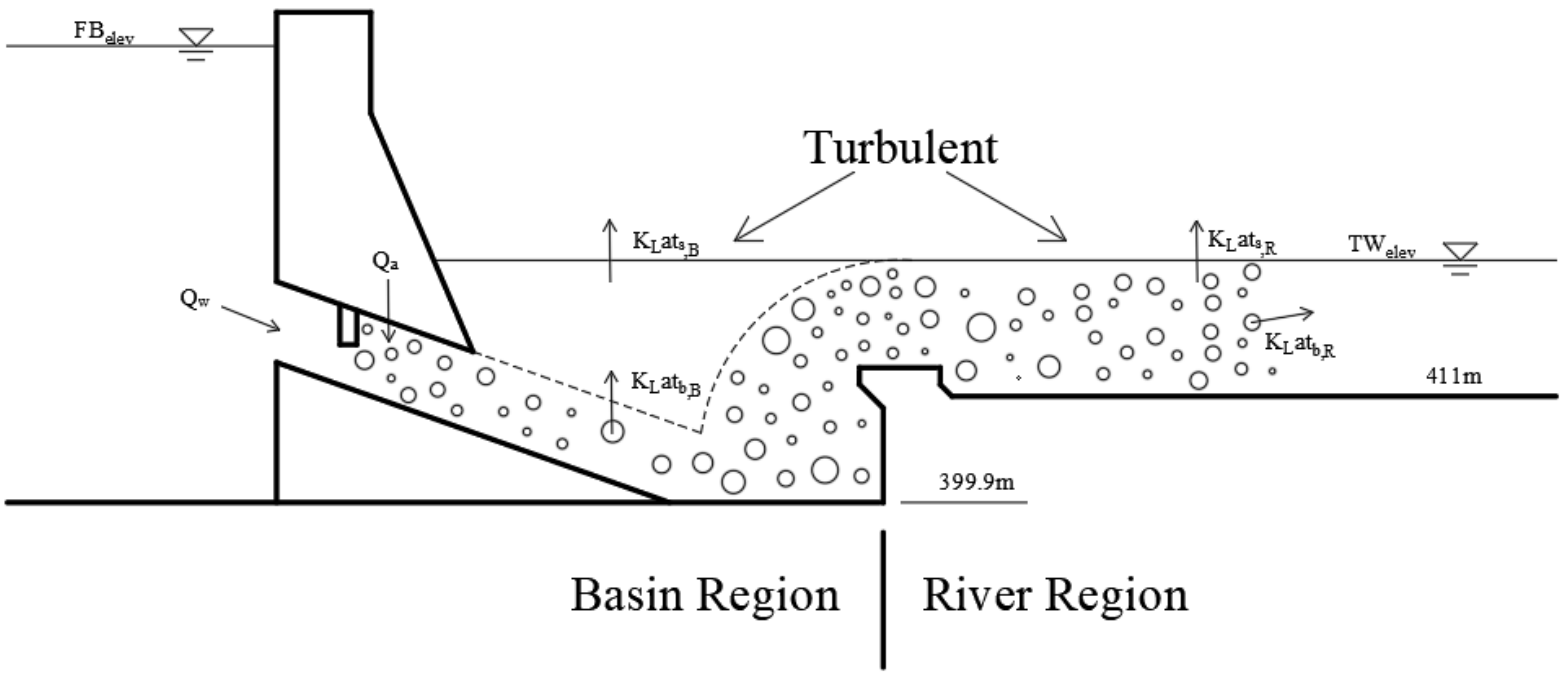

Figure 39: Proposed southern low-level outlet model schematic (NTS)

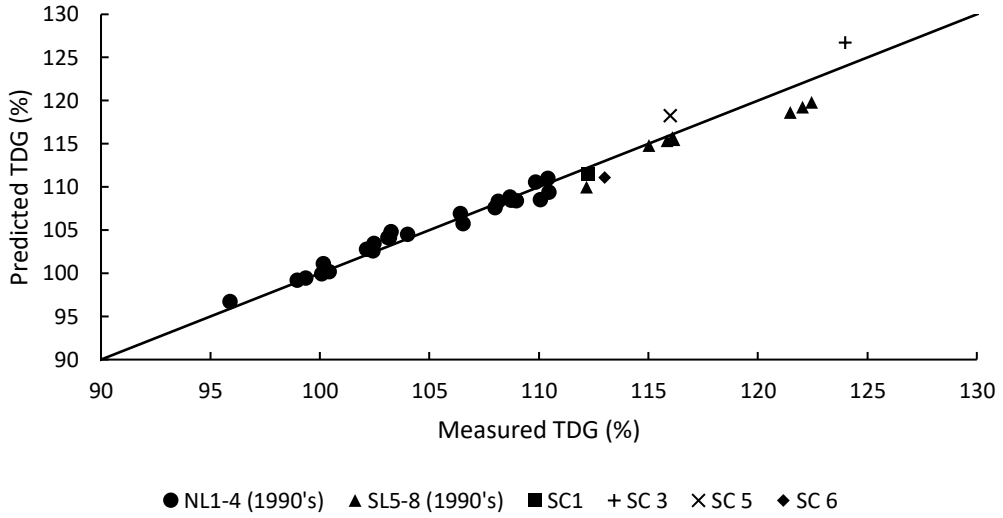

Figure 40: Modified Urban et al. (2008) model for predicting low-level outlet TDG, RMSE = 1.14%

Figure 41: SL5,6,7 in operation with typical surface turbulence

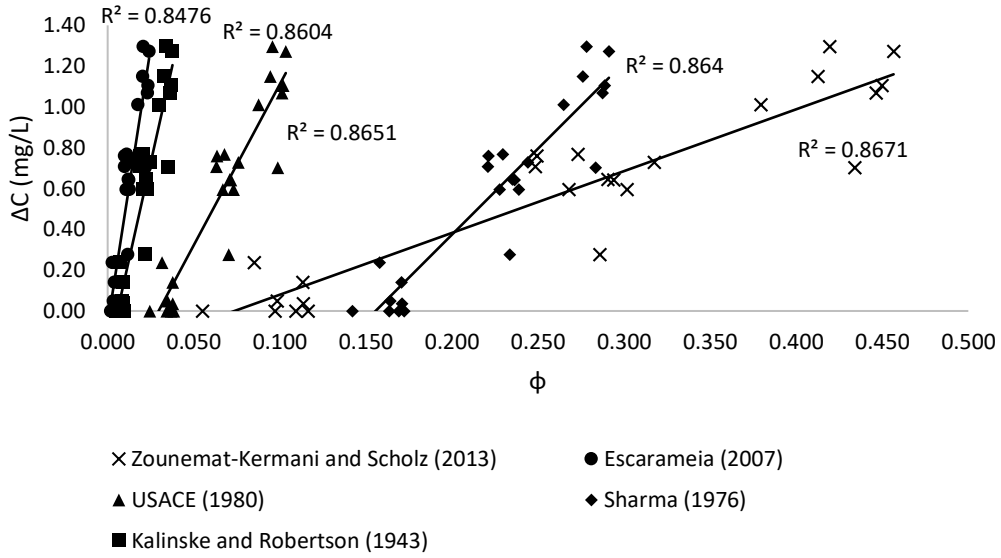

Figure 42: Measured dissolved gas concentration for northern low-level outlets vs air-void fraction where air demand is computed by various authors

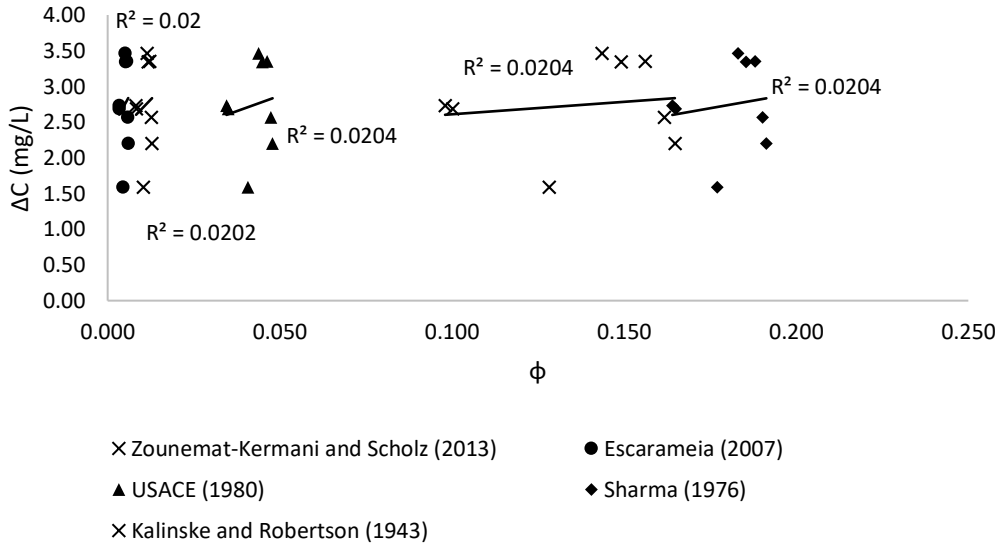

Figure 43: Measured dissolved gas concentration for southern low-level outlets vs air void fraction where air demand is computed by various authors

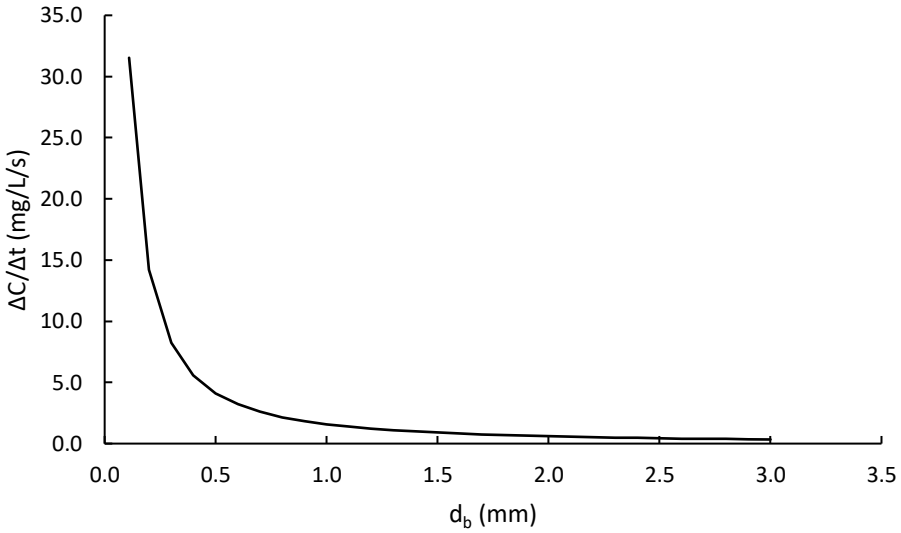

Figure 44: Gas dissolution rate vs bubble diameter for an air-void fraction of 0.0058

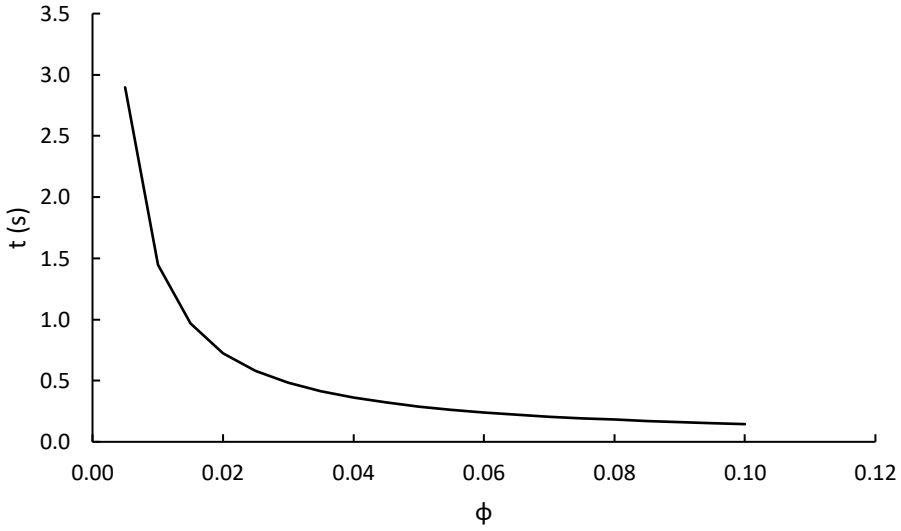

Figure 45: Time to dissolve 3.95mg/L of air vs air-void fraction for a bubble diameter of 1mm

References

Aspen Applied Sciences Ltd. 1995. Columbia River Total Dissolved Gas Pressure Reduction Study. Prepared for B.C. Hydro Safety and Environment, Castlegar, B.C.

Bruce, J. 2016. Fate Modeling of Air Supersaturated Waters in the Columbia River: Phase 1 – Model Development and Information Gap Analysis. Report Prepared for BC Hydro, Burnaby, BC, by Creekside Aquatic Sciences and LGL Limited. Report No. CAQ-017: 39 p + App.

Bruce, J. 2015. An Alternative Approach to Developing a Predictive Total Dissolved Gas Model Downstream of Hugh Keenleyside Dam. Report Prepared for BC Hydro, Burnaby, BC, by Creekside Aquatic Sciences and LGL Limited. Report No. CAQ-014: 26 p.

Bruce, J, and Plate, E. 2013. Total Dissolved Gas Supersaturation Downstream of Hugh Keenleyside Dam: A Model-Based TGP Risk Assessment of Facility Operations That Reduce on Low Level Ports for Water Conveyance. Report Prepared for BC Hydro, Burnaby BC. Creekside Aquatic Sciences. Report No. CAQ-001: 40 p + App.

Canadian Council of Ministers of the Environment. 1999. Canadian water quality guidelines for the protection of aquatic life: Dissolved gas supersaturation. In: Canadian environmental quality guidelines, 1999, Canadian Council of Ministers of the Environment, Winnipeg.

Chanson, H. 1996. Air Bubble Entrainment in Free-Surface Turbulent Shear Flows. Academic Press.

Colt, J. 2012. Dissolved Gas Concentration in Water. Computation of Dissolved Gas Concentration in Water as Functions of Temperature, Salinity and Pressure. Elsevier Inc.

Ervine, D. A. 1998. Air Entrainment in Hydraulic Structures: A Review. Proceedings of the ICE-Water Maritime and Energy, 142–53.

Escarameia, M. 2007. Investigating Hydraulic Removal of Air from Water

Pipelines. Proceedings of the ICE - Water Management 160 (1): 25–34.

Geldert, D. A., Gulliver, J. S., and Wilhelms, S. C. 1998. Modeling Dissolved Gas Supersaturation below Spillway Plunge Pools. Journal of Hydraulic Engineering 124 (5): 513–21.

Gulliver, J. S., Wilhelms, S. C., and Parkhill, K. L. 1998. Predictive Capabilities in Oxygen Transfer at Hydraulic Structures. Journal of Hydraulic Engineering-ASCE 124 (7): 664–71.

Gulliver, J. S., Hibbs, D. E., and McDonald, J. P. 1997. Measurement of Effective Saturation Concentration for Gas Transfer. Journal of Hydraulic Engineering 123 (2): 86–97.

Gulliver, J. S., Thene, J. R., and Rindels, A. J. 1990. Indexing Gas Transfer in Self-Aerated Flows. Journal of Environmental Engineering 116 (3): 503–23.

Hibbs, D. E., and Gulliver, J. S. 1997. Prediction of Effective Saturation Concentration at Spillway Plunge Pools. Journal of Hydraulic Engineering 123 (11): 940–49.

Johnson, P. L., and King, D. L. 1975. Prediction of Dissolved Gas at Hydraulic Structures. Symp. on Reaeration Research, ASCE, New York, N.Y.

Kamal, R., Zhu, D. Z., Leake, A., and Crossman, J. 2018. Dissipation of Supersaturated Total Dissolved Gases in the Intermediate Mixing Zone of a Regulated River. ASCE Journal of Environmental Engineering, in Press.

Kawase, Y, Halard, B. and Moo-Young, M. 1992. Liquid-Phase Mass Transfer Coefficients in Bioreactors. Biotechnology and Bioengineering 39 (11): 1133–40.

Klohn-Crippen Integ. 1994. Total Gas Pressure (TGP) Reduction Study 1994 Status Report. Prepared for BC Hydro. Report No. KCI-173.

Klohn Crippen. 2001. Preliminary Review of Operational and Structural Alternatives to Reduce Total Gas Pressure. Prepared for BC Hydro. Report No. KC-143 (PP1287).

Lamont, J. C., and Scott, D. S. 1970. Eddy Cell Model of Mass Transfer Into the Surface of a Turbulent Liquid. AIChE Journal 16 (4): 513–19.

Li, R., Li, J., Feng, L. K., Deng, Y., and Feng, J. 2009. Prediction for Supersaturated Total Dissolved Gas in High-Dam Hydropower Projects. Science in China, Series E: Technological Sciences 52 (12): 3661–67.

Ma, Q., Li, R., Zhang, Q., Hodges, B. R., Feng, J., and Yang, H. 2016. Two-phase flow simulation of supersaturated total dissolved gas in the plunge pool of a high dam. Environmental Progress & Sustainable Energy 35 (4): 1139-48

Mortensen, J. D., Barfuss, S. L., and Johnson, M. C. 2011. Scale Effects of Air Entrained by Hydraulic Jumps within Closed Conduits. Journal of Hydraulic Research 49 (1): 90–95.

Mortensen, J. D., Barfuss, S. L., and Tullis, B. P. 2012. Effects of Hydraulic Jump Location on Air Entrainment in Closed Conduits. Journal of Hydraulic Research 50 (3): 298–303.

Ozkan, F., Baylar, A., and Ozturk, M. 2006. Air Entrainment and Oxygen Transfer in High-Head Gated Conduits. Water Management 159 (WM2): 139–43.

Ozkan, F., Tuna, M. C., Baylar, A., and Ozturk, M. 2014. Optimum Air-Demand Ratio for Maximum Aeration Efficiency in High-Head Gated Circular Conduits. Water Science and Technology 70 (5): 871–77.

Politano, M., Carrica, P., and Weber, L. 2005. Prediction of total dissolved gas downstream of spillways using a multidimensional two-phase flow model. Mecánica Computacioinal XXIV: 285-295.

Politano, M., Amado, A. A., Bickford, S., Murauskas, J., and Hay, D. 2011. Investigation into the Total Dissolved Gas Dynamics of Wells Dam Using a Two-Phase Flow Model. Journal of Hydraulic Engineering 137 (10): 1257–68.

Politano, M., Carrica, P., and Weber, L. 2009. A Multiphase Model for the Hydrodynamics and Total Dissolved Gas in Tailraces. International Journal of Multiphase Flo*w* 35 (11): 1036–50.

Politano, M., Castro, A., and Hadjerioua, B. 2017. Modeling Total Dissolved Gas for Optimal Operation of Multireservoir Systems. Journal of Hydraulic

Engineering 143 (6): 04017007.

Qu, L., Li, R., Li, J., Li, K., and Wang, L. 2011a. Experimental Study on Total Dissolved Gas Supersaturation in Water. Water Science and Engineering 4 (4): 396–404.

Qu, L., Li, R., Li, J., Li, K., and Deng, Y. 2011b. Field Observation of Total Dissolved Gas Supersaturation of High-Dams. Science China Technological Sciences 54 (1): 156–62.

Roesner, L. A., and Norton, W. R. 1971. A nitrogen gas model for the lower columbia river. Rep. No.1-350, Water Resources Engineers, Inc., Walnut Creek, Calif.

Sharma, H. R. 1976. Air-entrainment in high head gated conduits. J. Hydraul. Div 102: 1629-1646.

Takemura, F., and Yabe, A. 1998. Gas Dissolution Process of Spherical Rising Gas Bubbles. Chemical Engineering Science 53 (15): 2691–99.

Thompson, E. J., and Gulliver, J. S. 1997. Oxygen Transfer Similitude for Vented Hydroturbine. Journal of Hydraulic Engineering 123 (6): 529–38.

University of Washington, Columbia Basin Research School of Aquatic and Fishery Sciences. 2000. Columbia River Salmon Passage Model.

Urban, A. L., Gulliver, J. S., and Johnson. D. W. 2008. Modeling Total Dissolved Gas Concentration Downstream of Spillways. Journal of Hydraulic Engineering 134 (5): 550–61.

US Army Corps of Engineers. 1980. Hydraulic Design of Reservoir Outlet Works. Engineer Manual EM 1110-2-1602.

US Army Corps of Engineers. 1996. Dissolved Gas Abatement Phase I.

US Army Corps of Engineers. 2005. Technical analysis of TDG precesses.

Wang, T., Politano, M., and Weber, L. 2018. Spillway jet regime and total dissolved gas prediction with a multiphase flow model. Journal of Hydraulic Research.

Weitkamp, D. E., and Katz, M. 1980. A Review of Dissolved Gas Supersaturation Literature. Transactions of the American Fisheries Society 109 (6): 659-702.

Yang, H., Li, R., and Wei, J. 2017. Analysis on Sensitivity of Parameters in Numerical Simulation of Dissolved Gas Supersaturated in Spillway Discharges. Nature Environment and Pollution Technology 16 (4): 1261-1266.

Zounemat-Kermani, M., and Scholz, M. 2013. Computing Air Demand Using the Takagi-Sugeno Model for Dam Outlets. Water (Switzerland) 5 (3): 1441–56.

Appendix A: Supplementary Data

The data listed in the tables below is a collation of scenario parameters at Hugh L. Keenleyside Dam pulled primarily from the reports of Bruce (2016), Klohn-Crippen Integ (1994), and Aspen Applied Sciences Ltd. (1995).

Table 1: Spillway operating gate data, 1993 - 1994

Year	Date	Gate #'s (SP)	Gate Opening (m)	Q (m3/s)	Qi (m3/s)	TW Elev (m)	FB Elev (m)	Head (m)	TWD (m)	FB TGP (mmHg)	TGP TW (mmHg)	ΔP (TW-FB) (mmHg)	BP (kPa)	BP (mmHg)	Water Temp. (°C)
1993	20-May	2,3	1.1	224	112.00	418.3	431.75	6.31	18.400	780	970	190	95.93	720	12.1
1993	23-May	2,3	1.58	281	140.50	418.46	430.15	4.47	18.560	800	970	170	95.88	719	12.5
1993	10-Jun	2,3	1.25	289	144.50	418.18	433.7	8.185	18.280	766	954	188	95.61	717	13.8
1993	14-Jun	2,3	1.19	285	142.50	418.13	434.24	8.755	18.230	767	927	160	95.87	719	12.2
1993	21-Jun	2,3	1.71	427	213.50	418.38	434.07	8.325	18.480	762	947	185	94.76	711	13.5
1993	28-Jun	2,3	2.5	660	330.00	419.02	435.94	9.8	19.120	750	950	200	95.17	714	16.2
1993	3-Jul	2,3	4.27	1076	538.00	419.96	435.92	8.895	20.060	740	975	235	95.1	713	15.7
1993	5-Jul	2,3,4	3.9	1535	511.67	420.65	435.51	8.67	20.750	752	977	225	95.29	715	15.4
1993	11-ju	2,3,4	4.66	1797	599.00	421	435.48	8.26	21.100	750	983	233	95.79	718	14.2
1993	13-Jul	2,3,4	5	1921	640.33	421.2	435.4	8.01	21.300	755	986	231	95.96	720	11.5
1993	17-Jul	2,3,4	4.66	1778	592.67	420.99	435.28	8.06	21.090	751	986	235	95.97	720	11.6
1993	22-Jul	2,3,4	2.41	922	307.33	419.5	435.44	9.345	19.600	759	975	216	95.42	716	13.5
1993	25-Jul	2,4	1.65	428	214.00	418.28	435.63	9.915	18.380	765	930	165	95.97	720	14.5
1993	28-Jul	2,4	1.58	422	211.00	418.22	436.03	10.35	18.320	765	925	160	95.03	713	15.2
1993	7-Aug	2,3,4	3.84	1601	533.67	420.75	436.87	10.06	20.850	757	985	228	94.8	711	17.9
1993	12-Aug	2,3,4	3.51	1455	485.00	420.53	436.79	10.145	20.630	754	988	234	95.67	718	17.5
1993	15-Aug	2,3,4	2.74	1138	379.33	420	436.68	10.42	20.100	751	971	220	95.4	716	18.0
1993	6-Jun	2,3	1.01	223	111.50	418.15	433.12	7.725	18.250	790	960	170	94.62	710	13.8
1993	4-Aug	2,3,4	2.29	947	315.67	419.63	436.72	10.685	19.730	770	975	205	95.86	719	17.8
1993	17-Aug	2,3,4	2.99	1247	415.67	420.2	436.87	10.485	20.300	760	975	215	95.2	714	17.6
1994	22-Oct	2	4.48	430	430.00	418.4	432.4	5.27	18.500	723.7	898	174.3	96.21	722	13.7
1994	23-Oct	2	6.53	559	559.00	418.6	432.4	4.245	18.700	723.1	894	170.9	96.27	722	13.7

Year	Date	Gate #'s (SP)	Gate Opening (m)	Q (m3/s)	Qi (m3/s)	TW Elev (m)	FB Elev (m)	Head (m)	TWD (m)	FB TGP (mmHg)	TGP TW (mmHg)	ΔP (TW-FB) (mmHg)	BP (kPa)	BP (mmHg)	Water Temp. (°C)
1994	26-Oct	3	7.4	577	577.00	418.6	432.3	3.71	18.700	720.5	879	158.5	94.46	709	13.7
1994	27-Oct	3	7.4	578	578.00	418.6	432.3	3.71	18.700	730.2	878	147.8	94.47	709	13.7
1994	28-Oct	4	7.4	578	578.00	418.6	432.3	3.71	18.700	721.8	903	181.2	95.74	718	13.7

Table 2: Northern low-level operating gate data, 1992 - 1994

Year	Date	Gate #'s (NL)	Gate Opening (m)	Q (m3/s)	Qi (m3/s)	TW Elev (m)	FB Elev (m)	Head (m)	TWD (m)	FB TGP (mmHg)	TGP TW (mmHg)	ΔP (TW-FB) (mmHg)	BP (kPa)	BP (mmHg)	Water Temp. (°C)
1992	29-Nov	1,2,3,4	4.85	1167.91	291.98	420.24	430.72	16.795	28.54	711	727	16	96.84	726	7.3
1992	2-Dec	1,2,3,4	4.79	1155.63	288.91	420.16	430.65	16.755	28.46	708	725	17	96.23	722	6.8
1992	4-Dec	1,2,3,4	4.27	1043.6	260.9	420	430.57	16.935	28.3	707	724	17	97.14	729	6.3
1992	1-Aug	2,3,4	7.32	1636.87	545.62	421.17	430.59	15.43	29.47	791	792	1	95.63	717	19.5
1992	13-Aug	2,3,4	7.32	1609.49	536.50	421.28	430.42	15.26	29.58	774	778	4	95.91	719	18.4
1992	13-Oct	1,2,3,4	4.21	1002.54	250.64	419.78	430.01	16.405	28.08	720	735	15	95.67	718	12.1
1992	29-Dec	1,2,3,4	5.89	1740.35	435.09	421.48	427.18	12.735	29.78	700	705	5	94.97	712	4.2
1993	13-Jan	1,2,3,4	5.89	1480.29	370.07	420.72	424.62	10.175	29.02	690	690	0	95.92	719	2.8
1993	21-Mar	2,4	4.6	420.4	210.2	418.15	423.48	9.68	26.45	722	723	1	96.23	722	2.5
1993	14-Apr	2,4	4.51	424.13	212.07	418.16	423.86	10.105	26.46	740	740	0	95.62	717	4.0
1993	1-Apr	2,4	4.6	416.44	208.22	418.14	423.4	9.6	26.44	730	730	0	94.96	712	2.9
1993	19-Apr	2,4	4.39	421.93	210.97	418.15	424.05	10.355	26.45	745	745	0	96.33	723	4.1
1994	2-May	1,2,4	3.1	566.3	188.77	418.62	428.2	15.15	26.92	734	740	6	95.55	717	5.4
1994	3-May	1,2,4	3.1	566.3	188.77	418.62	428.33	15.28	26.92	719	733	14	95.68	718	5.6
1994	4-May	1,2,4	3.05	566.3	188.77	418.58	428.43	15.405	26.88	733	747	14	95.74	718	5.7

Year	Date	Gate #'s (NL)	Gate Opening (m)	Q (m3/s)	Qi (m3/s)	TW Elev (m)	FB Elev (m)	Head (m)	TWD (m)	FB TGP (mmHg)	TGP TW (mmHg)	ΔP (TW-FB) (mmHg)	BP (kPa)	BP (mmHg)	Water Temp. (°C)
1994	6-May	1,2,3	3.05	566.3	188.77	418.6	428.66	15.635	26.9	752	765	13	95.84	719	5.8
1994	9-May	1,2,3	3	566.3	188.77	418.76	429.14	16.14	27.06	762	778	16	95.44	716	6.0
1994	17-May	1,2,3	2.77	566.3	188.77	418.86	431.12	18.235	27.16	752	777	25	95.05	713	11.3
1994	24-May	1,2,3	2.6	566.3	188.77	418.83	432.27	19.47	27.13	736	766	30	95.85	719	13.9
1994	25-May	1,2,3	2.6	566.3	188.77	418.88	432.51	19.71	27.18	753	787	34	95.31	715	14.1
1994	27-May	1,2,3	2.55	566.3	188.77	418.95	433.05	20.275	27.25	767	785	18	95.26	715	13.0
1994	31-May	1,2,3	2.5	566.3	188.77	418.84	433.52	20.77	27.14	752	778	26	95.38	715	10.5
1994	1-Jun	1,2,3	2.5	566.3	188.77	418.84	433.66	20.91	27.14	749	777	28	95.92	719	12.4
1994	3-Jun	1,2,3	2.47	566.3	188.77	418.84	433.92	21.185	27.14	757	789	32	95.23	714	12.0

Table 3: Southern low-level operating gate data, 1994

Year	Date	Gate #'s (SL)	Gate Opening (m)	Q (m3/s)	Qi (m3/s)	TW Elev (m)	FB Elev (m)	Head (m)	TWD (m)	FB TGP (mmHg)	TGP TW (mmHg)	ΔP (TW-FB) (mmHg)	BP (kPa)	BP (mmHg)	Water Temp. (°C)
1994	4-Apr	6,7,8	3	425	141.67	418	423.05	10.05	18.1	772.5	807	34.5	95.92	719	5.6
1994	22-Apr	5,7,8	3.5	566.3	188.77	418.6	425.25	12	18.7	763	821	58	95.17	714	7.2
1994	23-Apr	5,7,8	3.5	566.3	188.77	418.6	425.33	12.08	18.7	774	824	50	94.82	711	7.4
1994	24-Apr	5,6	5	555.9	277.95	418.6	425.4	11.4	18.7	761	823	62	94.45	708	7.4
1994	25-Apr	5,6	5	555.5	277.75	418.8	425.48	11.48	18.9	765	826	61	94.86	712	7.4
1994	10-May	5,6	4.4	566.3	283.15	418.8	427.17	13.47	18.9	788	873	85	95.82	719	10.9
1994	11-May	5,6	4.4	566.3	283.15	418.9	427.37	13.67	19	794	877	83	95.8	719	11.4
1994	12-May	5,6	4.3	566.3	283.15	419	427.62	13.97	19.1	791	875	84	95.27	715	11.9